

SCUOLA DI SCIENZE

Corso di Laurea Magistrale in Geologia e Territorio

Dipartimento di Scienze Biologiche, Geologiche ed Ambientali

Tesi di Laurea Magistrale

Debris flow susceptibility mapping for initiation
areas at medium scale: a case study in Western
Norway

Candidato:
Davide Festa

Relatore:
Prof. Matteo Berti

Contents

1. Introduction	
1.1 Motivation	1
1.2 Aims and objectives	2
1.3 Work steps	2
1.4 Study area	4
2. State of the art	
2.1 Mass movement	6
2.1.1 Classification	6
2.1.2 Debris flow	7
2.1.3 Debris flow initiation conditions	11
2.2 Landslide susceptibility assessment	13
2.2.1 Mass movement inventory	13
2.2.2 Susceptibility mapping	14
3. Regional setting of the study area	
3.1 Climate	20
3.2 Geology	21
3.3 Geomorphology and landslide activity	22
4. Field survey and statistical data analysis	
4.1 Methods	
4.1.1 Baseline data analysis	25
4.1.1.1 National database of slides for Norway	25
4.1.1.2 Geological and geomorphological setting of Førde and Jølster Municipalities	26
4.1.2 Field survey	28
4.1.2.1 Field methods	28
4.1.2.2 Debris flow categories and detected features	30
4.1.3 Debris flow inventory	34
4.1.4 Statistical evaluation of terrain data	35

4.2	Results	
4.2.1	Statistical comparison between source areas categories	38
4.2.2	Statistical comparison between source areas categories	40
4.2.3	Discussion	43
5.	Susceptibility modelling	
5.1	Methods	
5.1.1	Terrain data and thematic layers	46
5.1.2	D.F. initiation susceptibility	49
5.1.2.1	Weights of evidence	49
5.1.2.2	Model performance	53
5.2	Results	
5.2.1	Weights of the predictor variables	56
5.2.2	Models performances for different combinations of predictors	58
5.2.3	Discussion	62
	References	70

Abstract

In recent years, rapid mass movements such as debris flow and debris avalanches resulted in a significant impact on Norwegian society and economy. The need for dispelling the uncertainty inherent in landslide risk assessment has encouraged the development of hazard and susceptibility maps. Different statistically-based modelling methods, in combination with geographic information systems (GIS), have been extensively used to ascertain landslide susceptibility in quantitative terms. This thesis proposes a bivariate statistical method (Weights of Evidence) for assessing the spatial proneness of debris flows within *Førde* and *Jølster* municipalities (Western Norway), where emphasis is put on the critical conditions of initiation.

Since no feasible landslide database could be exploited for susceptibility mapping at medium scale, this thesis addressed the realisation of a new inventory. By coupling pre-existing data from remote sensing and field observations, circa 1100 debris flow initiation areas were outlined and differentiated in four categories with geomorphological repeatable features. Simple topography-based parameters such as slope, upslope contributing area, curvature and roughness were used to find significant statistical differences between the initiation area-types. Moreover, they were employed together with other thematic maps as informative layers for landslide modelling. In order to test the model fitting performance, the ROC curves method is used in this thesis.

The evaluation of different discretization schemes and combinations of the above-mentioned variables led to individuate models with different performances in terms of success rates. The best model is obtained by using only a combination of slope, flow accumulation and elevation (82% true positive rate), while the manual adjustment of the classification scheme did not lead to significant improvements.

1. Introduction

1.1. Motivation

As the world population has reached the highest growth rate in history during the last decade, the need for space has been pushing cities to sprawl (such as in mountainous areas). Exposure to areas more likely to be affected by landslides combined with an unwise land use is resulting in an increasing of vulnerability of human lives, public and private assets (McCall & Laming, 1990). This, in combination with the rising incidence of extreme weather and climate events, is putting human and natural systems at considerable risk (IPCC, 2012).

Due to their destructive strength and difficult predictability, rapid landslides such as debris flows are among the geo-hazards which hit the collective consciousness the most. They can be generically defined as a mixture of loose soil, rock, organic matter and water that flows downward at high velocities (Iverson, 1997). These phenomena are widespread where both favourable topographic and climatic conditions are present and they typically lead to severe economic and social damages.

Future projections for climate in Norway up to year 2100 (Hanssen-Bauer et al., 2009) have been made: annual temperature is estimated to increase by ca. 4.5 °C and annual precipitation will increase by ca. 18%. This tendency is likely to further produce intense and frequent rain floods, rapid snowmelt (thus enhanced run-off) and higher ground-water levels; therefore, the Norwegian territory will probably face more weather-triggered landslides. Especially debris flows will be threatening transport infrastructures, constructed facilities and people in a more severe way than happened in the past (Kalsnes et al., 2016). The Norwegian transport network has already experienced this trend in the last years, with a recorded 12 million € damage per year due to landslides (Bjordal & Helle, 2011).

The recent and urgent need for effective strategies for landslides risk management has led Norwegians public administrations and governmental agencies to investigate debris flows in more detail (Meyer et al., 2013). Along these lines, the Norwegian Geotechnical Institute have been involved with its projects in the above-mentioned topics since the end of the last century, providing remarkable assistance to this thesis.

The concept of risk is strictly linked to the evaluation of the spatial and temporal occurrence of a certain damaging event. The assessment of susceptible areas is an essential step for the spatial evaluation of landslide risk and, therefore, for the identification of appropriate structural and/or non-structural mitigation measures (Guinau et al, 2007; Stancanelli et al, 2017). Given that future landslides are likely to be produced by the same conditioning factors as landslides in the past and the present (Varnes, 1984), it's easy to understand the importance of mapping previous events. The actual national Norwegian database for all types of mass movements (Jaedicke et al., 2009) consists of more than 33 000 point locations from the last five hundred years covering the whole Norway. Although this dataset can be useful for large scale landslide susceptibility assessment (Meyer et al., 2013), it cannot be regarded sufficient when it comes to making accurate evaluation at smaller scales.

Over the last years, many qualitative and quantitative methods have been proposed for landslide susceptibility assessment: this kind of map can be elaborated by heuristic, statistical, deterministic and multidisciplinary approaches (Dai et al., 2002; Hürlimann et al., 2006; Yalcin et al., 2011). Nevertheless, intrinsic and extrinsic parameters used for these analyses, such as soil depth and soil mechanical features, usually have limitation of availability (Paudel et al, 2016). Increased availability of high resolution global digital

elevation models (DEM) and the prospect of using accessible and precise topography-based parameters has encouraged the development of statistical and GIS-based prediction models.

1.2. Aims and objectives

The aim of this thesis is to develop a medium-scale debris flow susceptibility map (for what concerns the only initiation areas) for *Førde* and *Jølster* Municipalities, which are located in the central-western part of Norway. This product can be regarded as a preliminary step for the future accomplishment of a comprehensive hazard and risk assessment and as a touchstone for further studies in regions with similar conditions.

The main interest is to investigate active and older debris flow, in order to locate potential initiation areas in the concerned territories. Since the only available national landslide database (Jaedicke et al., 2009) is not a feasible mean for the above-mentioned scope, this thesis firstly addresses the data gaps by compiling a new and precise inventory. Emphasis is put on:

- The definition of the spatial extent of those areas prone to trigger debris flows.
- The description of the triggering mechanism and the geomorphological repeatable features that can be observed, in order to classify the detected initiation areas into distinct categories.

Since the acquisition of a chronological record for each occurrence could not be fulfilled, temporal probability analysis is neglected.

A statistical GIS-based approach is preferred to obviate the lack of quantitative field information and to significantly manage pertinent terrain parameters extractable from digital elevation models (DEM). From this perspective, besides the realization of the susceptibility map, another object is the evaluation of the data distribution frequencies of the extracted terrain parameters within the mapped release areas and the related upper catchment.

As the quality of a statistically-based landslide susceptibility map depends on the predictor variables, the last aim of this thesis is to evaluate different combinations and different classification schemes of the used information layers. The knowledgeable use of these two aspects is able to provide the model with the best performance.

This thesis is based on the hypothesis that the assessment of the spatial propensity for debris flows initiation areas can be realised with already existing statistical methods that relies on accessible terrain parameters and pertinent thematic maps. Here, Weights of Evidence (WofE) method is used. The main belief is that the performance of the newest and automatic probabilistic models is vain when they are not coupled with data accuracy and expert opinion.

1.3. Work steps

This thesis took advantage from the readily available DEMs, aerial photographs, terrain data extracted from surface models, quaternary maps and the mass movement database of the Norwegian territory (Jaedicke et al., 2009). Starting from these indispensable resources, it was possible to map a remarkable number of debris flow throughout the study

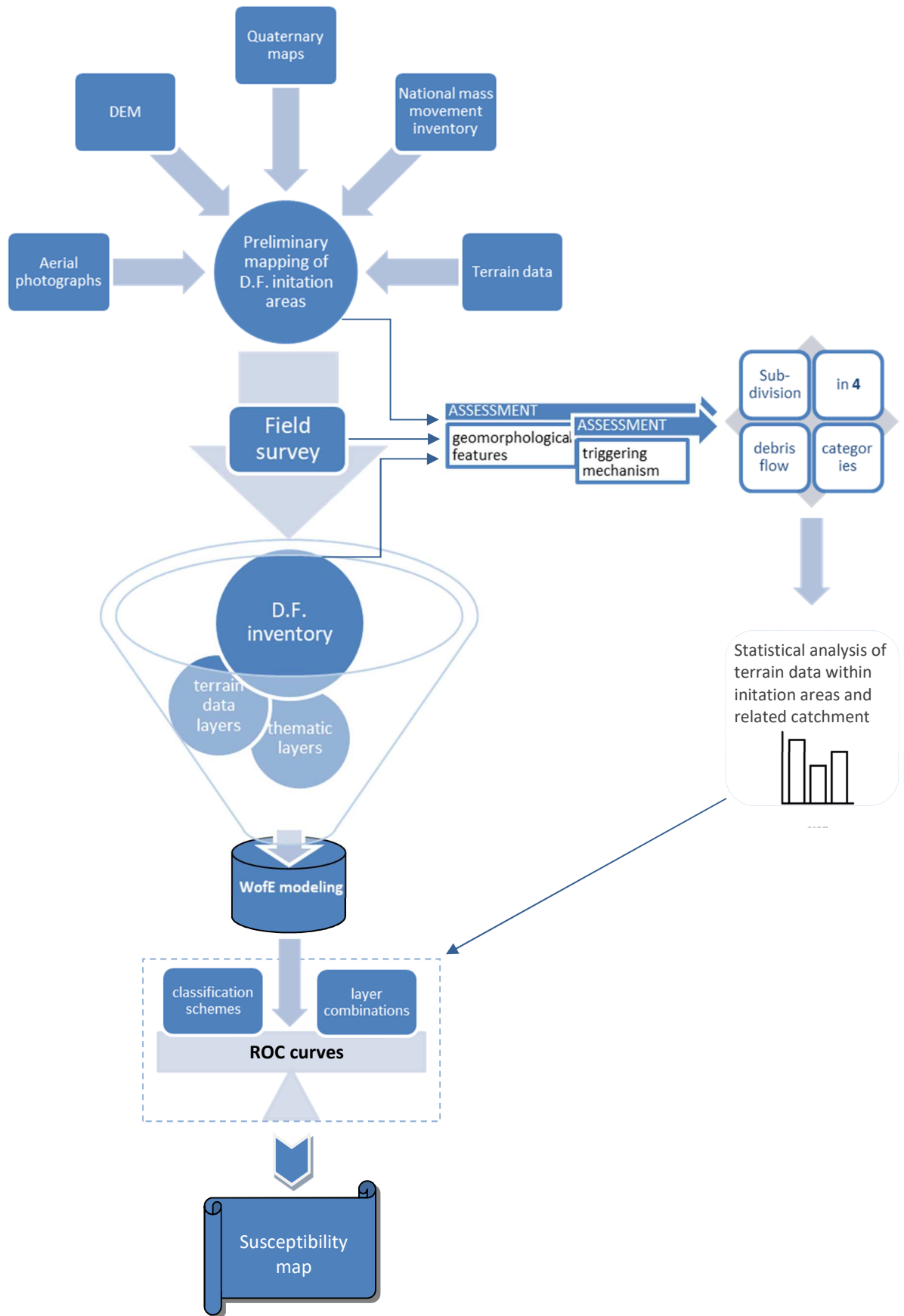


Figure 1. Workflow of the thesis study.

area and, then, to realize an inventory restricted to the object of this research: the initiation areas.

Two essential steps were carried out in order to fulfil the above-mentioned goal:

- Preliminary observation and detection of the geomorphological evidences suggesting recent landslide activity.
- Field validation, refinement of the previous mapping results and visual description and interpretation of the repeatable qualitative features encountered.

According to geomorphological aspects and triggering mechanism, four different categories were conceived to separate the mapped events.

In order to better investigate all the possible preparatory variables which make the slope susceptible to failure, the next step addressed the delineation of the upper portion of those catchments related to the detected release areas. The outer limit of each initiation area and corresponding catchment served as a mask for the extraction of different layers of data from the available terrain models: areal extension, slope, curvature and roughness. These are among the most pertinent terrain parameters involved in the occurrence of debris flows and they can be used in statistical determination when assessing the probability of landsliding. As a consequence, the analysis focused on the distribution frequencies performed for each kind of variable within both initiation areas and catchment. Evaluations were made considering every debris flow category, carrying out statistical tests such as *F* tests and *T-student's* tests. This enabled the quantification of average values of those parameters linked to the debris flow triggering and the comparison between the categories, as well as with literature thresholds.

The new debris flow inventory, the terrain data layers (as well as the related data distribution frequencies) and other thematic layers served as input data for modelling and for the computation of the debris flow susceptibility map. This was accomplished using the Weights of Evidence technique. As the output of such statistical models is conditioned by different combinations of the employed information layers, the last step addressed the evaluation, in terms of success rate, of different susceptibility maps produced by varying the input; the receiving operating characteristic (ROC) curves were used for this purpose. The overall workflow is shown in *Figure 1*.

1.4. Study area

Norway is located in Northern Europe and it includes part of the Scandinavian Peninsula. The country has land borders only to the east with Sweden, Finland and, for a shorter distance, also with Russia. The rest of Norway is surrounded by the sea, with the Barents Sea bordering the northern part, the Norwegian Sea and the North Sea lapping the west coast and the Skagerrak inlet limiting the South side. Including Svalbard islands and Jan Mayen in the north, the country encompass a total area of 385,199 km², while the mainland Norway covers 13° latitude, from 58°N to more than 71°N, and covers the longitude from 5°E to 31°E. The coast is extremely rugged and indented as it was carved by the movement of the glaciers of the past Ice ages, originating the actual fjords. The land is still rebounding because of the enormous weight of the thick ice sheet that was covering all Scandinavia. The isostatic rebound is still active today, causing an increase in elevation in different regions of the country, with the Eastern ones lifting up at greater rates. About two third of Norway is mountainous; approximately 50% of the country lies above an elevation of 500 meters, while 25% above 1 000 meters. The Scandinavian Mountains is the mountain range that runs

through the Peninsula; *Galdhøpiggen* is located in south Norway and with its 2 469 meters is the highest peak in mainland Northern Europe.

The two municipalities of *Førde* (586 km²) and *Jølster* (671 km²) are part of *Sogn og Fjordane* county which is seated in western Norway (*Figure 2*). The county is characterized by the physical variability of the terrain: mountains elevation tends to increase from the coastline to the inland. This can be regarded as the main reason for the high amount of precipitations usually registered in this region. *Sogn og Fjordane* district includes the largest glacier in continental Norway, *Jostedalsbreen*, and Europe's deepest lake, *Hornindalsvatnet*.

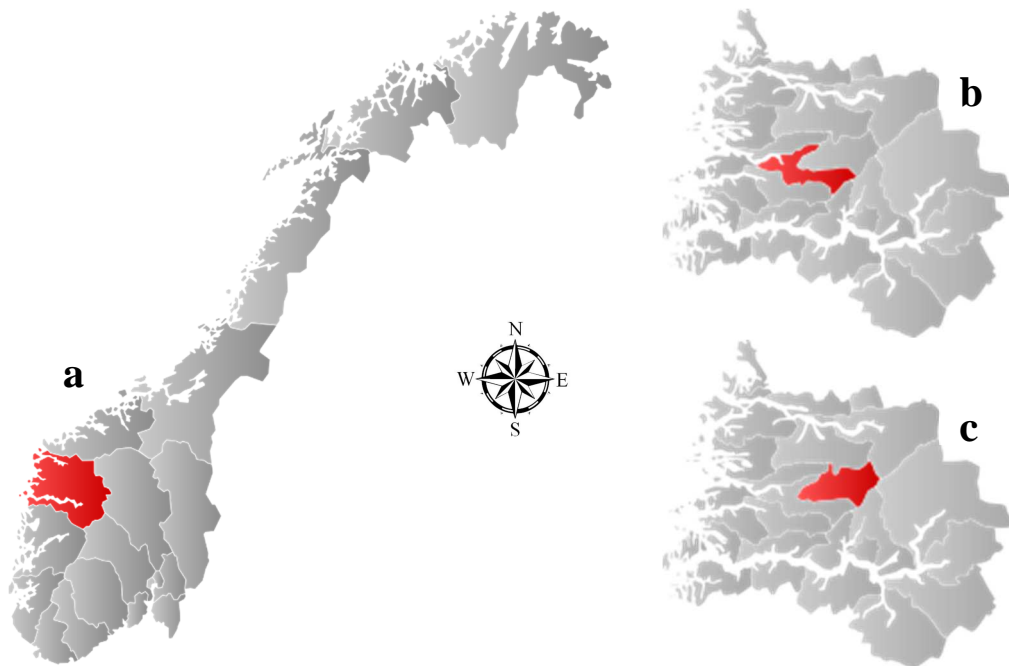


Figure 2. (a) Norway overview and location of (b) *Førde* and (c) *Jølster* municipalities. (source: Wikipedia)

2. State of the art

2.1. Mass movement

2.1.1. Classification

Cruden (1991) stated that a landslide is <<the movement of a mass of rock, debris or earth down a slope>>. As landslide processes can include also snow and ice, the most general term mass movement is sometimes preferred to include the whole variability of those phenomena. According to the nomenclature proposed by Varnes (1984) and expanded upon by Hungr et al. (2013), besides the nature of the mass involved, there are six types of movement: fall, topple, slide, spread, flow and slope deformation (*Figure 3*). Varnes (1984) enriched the classification scheme with other important terms such as: state of activity, which indicates the timing of movements; distribution of activity, which describes where the landslide is moving; style of activity, which describes the manner how different movements contribute to the landslide; rate of movement; water content of landslide materials.

Type of movement	Rock	Soil
Fall	1. <i>Rock/ice fall</i> ^a	2. <i>Boulder/debris/silt fall</i> ^a
Topple	3. <i>Rock block topple</i> ^a	5. <i>Gravel/sand/silt topple</i> ^a
	4. <i>Rock flexural topple</i>	
Slide	6. <i>Rock rotational slide</i>	11. <i>Clay/silt rotational slide</i>
	7. <i>Rock planar slide</i> ^a	12. <i>Clay/silt planar slide</i>
	8. <i>Rock wedge slide</i> ^a	13. <i>Gravel/sand/debris slide</i> ^a
	9. <i>Rock compound slide</i>	14. <i>Clay/silt compound slide</i>
	10. <i>Rock irregular slide</i> ^a	
Spread	15. <i>Rock slope spread</i>	16. <i>Sand/silt liquefaction spread</i> ^a
		17. <i>Sensitive clay spread</i> ^a
Flow	18. <i>Rock/ice avalanche</i> ^a	19. <i>Sand/silt/debris dry flow</i>
		20. <i>Sand/silt/debris flowslide</i> ^a
		21. <i>Sensitive clay flowslide</i> ^a
		22. <i>Debris flow</i> ^a
		23. <i>Mud flow</i> ^a
		24. <i>Debris flood</i>
		25. <i>Debris avalanche</i> ^a
Slope deformation	28. <i>Mountain slope deformation</i>	30. <i>Soil slope deformation</i>
		31. <i>Soil creep</i>
		32. <i>Solifluction</i>
		29. <i>Rock slope deformation</i>

Figure 3. Mass movement classification system proposed by Hungr et al. (2013) along the lines drawn by Varnes (1974).

a denotes movement types which usually reach extremely rapid velocities (Hungr et al., 2013).

2.1.2. Debris flows



Figure 4. Debris flow channel in *Førde* municipality showing recent activity. It is noticeable the poorly sorted mixture of clastic material and wood forming a temporary blockade.



Figure 5. Debris avalanche in Romsdalen, in 2011. (photo: Knut Stalsberg)

The lack of precise use of existing terminology has led to create a cloud of vagueness around the term debris flow (Meyer et al., 2013). Varnes (1978) and then Hutchinson (1988) proposed the most commonly accepted systems of landslide classification and definition. The first one suggested the movement mechanism and the material type as the main discriminating factors, the latter gathers landslides in different categories with similar kinematic patterns. Flow-type landslides can be regarded as the ones hardly classifiable, because of the number of factors affecting the mass behaviour during motion. Cruden & Varnes (1996) stated that <<a flow is a spatially continuous movement in which surfaces of shear are short-lived, closely spaced, and usually not preserved. The distribution of velocities in the displacing mass resembles that in a viscous liquid>>. Iverson (1997) defines debris flows as gravity-driven flows of poorly sorted, water-saturated sediment with a transition between solid and liquid phases while undergoing irreversible deformation. Debris flows have properties of both dry and granular mixtures such as avalanches and water floods and therefore are incredibly destructive (Iverson, 1997). The rate of movement associated with those flows is usually rapid and very rapid, with velocities usually comprised between 0.5 *m/s* and 20 *m/s* (Costa, 1984). One of the main feature of debris flow is its pulsating character due to temporary blockades that form along the steep path (*Figure 4*). Beside the movement mechanism, the kind of sediment involved in those flows has to be cleared: according to Varnes (1978) debris is typically a coarse material which holds 20% to 80% of particles larger than 2 mm. The texture is unsorted and consists mainly of gravel, sand, cobbles and boulders with varying proportion of silt, traces of clay and organic material, including tree trunks (*Figure 4*). The fraction with particle diameters smaller than 2 mm can be regarded as the matrix surrounding the coarse clasts. As a result, debris is mostly a non-plastic material (Jakob & Hungr, 2005) or, at least, weakly plastic.

Another strong controlling factor which affects the flow mobility is the water content. Lorenzini & Mazza (2004) assert that 20% to 40% of water is contained in debris flows mass, although it is reported that in Norway the percentage might be superior (Norem & Sandersen, 2012). Because of the extreme variability of the materials, the water contents and behaviour that concern the downward debris motion, many different terms were coined throughout literature in order to better distinguish different behaviours or different phases of the same phenomenon: mud flow, debris flood and debris torrent are some examples (*Figure*

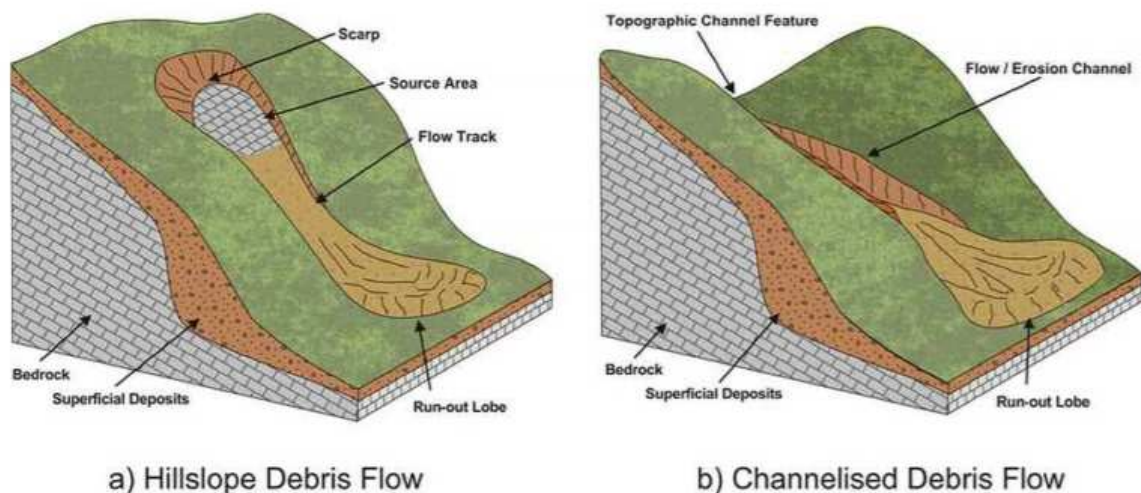


Figure 6. Schematic depiction of (a) hillslope debris flow (unconfined at early stages) and (b) channelised debris flow (confined).

3). For the purpose of this study, distinctions of this kind are considered pointless except for the one which Hutchinson (1988) came up with: channelised (confined) and hillslope (unconfined) debris flow (*Figure 6*). The latter type initiate as a debris slide and can turn into the first one when the flow seizes on already existing gullies. Otherwise, a small debris slide can pick up speed and incorporate vegetation, soils and all kinds of debris on steep and convex slopes where the affected area is wider as the debris moves downward: this is typical of debris avalanches (*Figure 5*). All these discriminations are taken in account for this thesis as they are largely documented in Norway (Meyer et al., 2013). Debris flows can be spatially divided into 3 main geomorphological units (*Figure 7*) which

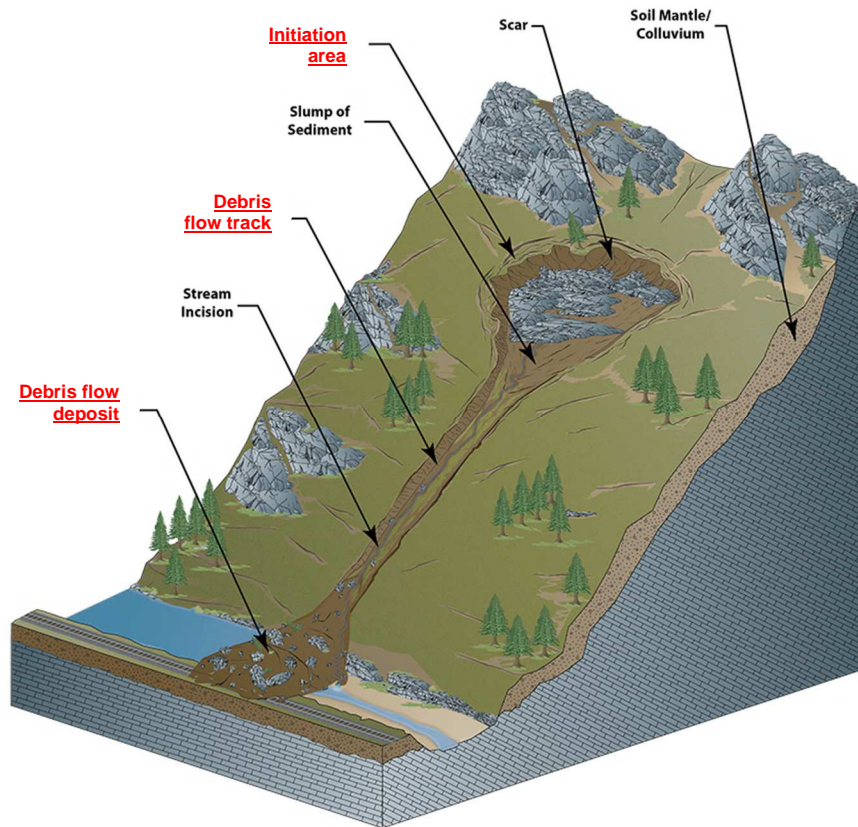


Figure 7. Representation of the 3 geomorphological units of a debris flow (image from the Wyoming Geologic Survey, modified).

are the initiation area, the flow track and the deposition zone:

- 1) The initiation area is the place where the initial volume of material starts its motion downslope. The material consists of weathered and weak bedrock, soil, *colluvium* or downfall deposits. The areas are usually located on steep slopes where the gradient limits are set between 20° and 45° (Jakob & Hungr, 2005), whereas the plant cover is scarce. As Fischer et al. (2012) stated, these source areas can be described as surface depressions, filled up with variable quantity of erodible material, which shrink and culminate in flow tracks (channelized debris flow); alternatively, they occur on hillslopes without previous incisions with abundant unconsolidated sediments (unconfined debris flow).
- 2) The flow track has an elongate shape that acts not only as a corridor for the passage of debris but also as a source zone itself; in fact, if the channel is erodible, debris

flow can entrain loose saturated material from the bed increasing the total volume. Sediment entrainment has been a constant factor in the definition of debris flows as the initial release volume is often quite small compared to the final volume. The transport zone of a debris flow extends from below the source area to the point where the rate of deposition exceeds that of erosion (Norem & Sandersen, 2012). On the channel sides terraced deposits are present and, outwardly, typical lateral levees can confine the paths of ensuing debris flows. In case of open-slope debris flow, the mass could flow downward without being confined in any channel. Transportation zones of debris flows are usually steeper than 10° (Jakob & Hungr, 2005), whereas at lower gradients deposition is more likely.

- 3) The deposition zone corresponds to the area where the moving mass of debris decreases its velocity and eventually halts. This happens at low slope gradients which can vary depending on the debris flow volume and rheology, size of debris flow snout and channel topography (Jakob and Hungr, 2005). Because of the lack of confinement, this zone usually displays lobate shapes; if more than one event occurs in correspondence with the same deposition zone, a fan can form. Boulders and large cobbles are the first to stop, while in the more distal part of the fan and further the finer mass of liquefied debris settles (Jakob & Hungr, 2005).

Two preparatory conditions and one triggering factor are needed for debris flow to happen: high slope degree ($>20^\circ$), availability of loose and unconsolidated material and adverse hydrogeological conditions. Whilst the first two aspects are the ones that make an area susceptible to failure, the third one is the variable which shifts the slope from a marginally stable to an unstable state (Dai et al., 2002). The latter is due to convergent topography, enhanced runoff, temporary stream blockade, rapid ice or snow melting. Once a debris flow occurs, sediment storages filled with weathered and loose material are sometimes totally evacuated; this is the case of weathering-limited catchments and as long as no erodible material is available no debris flow will take place (Meyer et al., 2013).

Two are the main mechanisms that trigger debris flows release areas: they can start as shallow landslides which typically involves the first meters of a thin and weathered soil covering the underlying bedrock; otherwise, enhanced water supply and run-off can gradually incorporate erodible and loose particles from an already existing channel bed.

The importance of recognizing the triggering mechanism has different implications in the spatial prediction of those phenomena. In fact, in the first case the only possible discrimination is between areas which are more or less susceptible to failure, while, for what concerns the second case, the active channels are usually acknowledged and monitored. It is even more complicated to assess the temporal predictability in terms of triggering conditions: intensity-duration (ID) thresholds and Magnitude-frequency relations can be empirically derived in order to quantify the critical circumstances of rainfall and earthquakes events which initiate landslides in a given region.

In using ID thresholds (*Figure 8*) it is common to assume that, for a given rain duration, there exists an intensity at which a debris flow is almost always triggered (the maximum ID threshold). The minimum ID threshold is the precipitation intensity duration under which a debris flow is very unlikely to be triggered (Meyer et al., 2012). For regions associated to high seismicity, it is of common sense to relate Magnitude to frequency density curves for

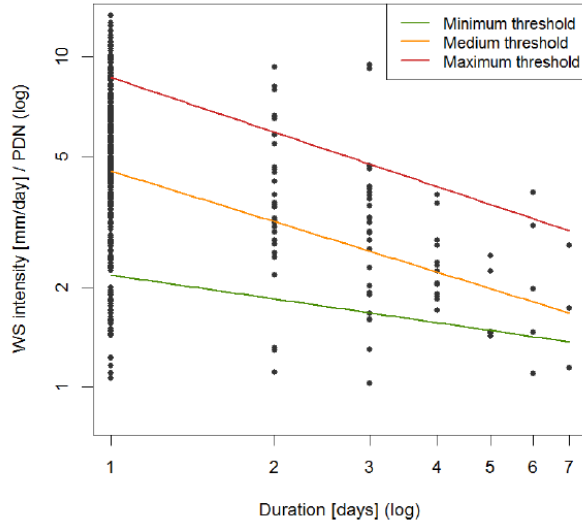


Figure 8. Example of rainfall ID thresholds for triggering debris flow. In particular, the figure is showing normalized ID thresholds curves for debris flow initiation in Norway (Meyer et al., 2012).

earthquake-induced landslides through power-law relationships derived for available inventories. One of the main aims is the calculation of the expected Magnitude of earthquake (or multiple earthquakes) required for landslides to trigger in a certain region (Crosta et al., 2014).

2.1.3. Debris flow initiation conditions

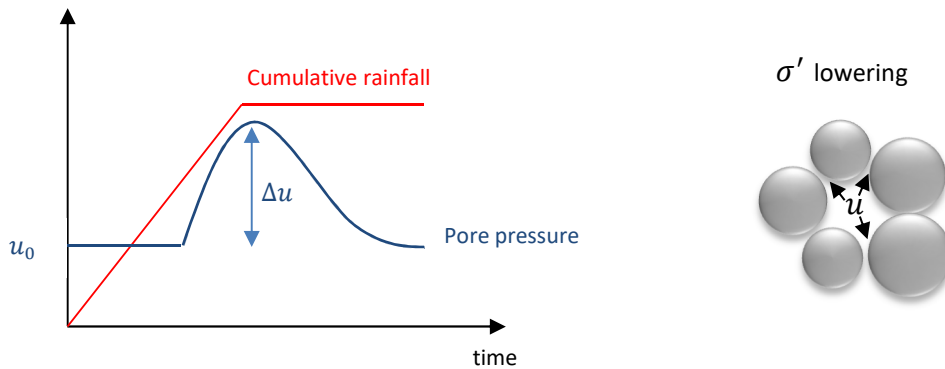


Figure 9. Simplified graph and image showing how an intense precipitation event can affect the pore pressure within soil particles. Initial value pore pressure (u_0) increase due to overpressures (Δu) resulting in the decrease of effective normal stress and the consequent decrease of resisting stress of the soil.

Debris flows are triggered by either flowing water mobilizing loose soil or rocks on a steep slope or channel, or by another slope movement process (fall, topple, or slide) over loading saturated sediments on a steep gradient (Highland et al., 2008). Hungr et al. (2001) underline the aspect that debris flows usually involves any kind of loose unsorted material of low plasticity produced by mass wasting, weathering, glacier transport, and explosive volcanism. The other key-aspect linked both to debris flow initiation and mobilization is the material saturation: this is most commonly provided by precipitation events, snow melt, *jökulhlaups*

(glacial lake outburst floods), or the failure of volcanic crater lakes (Costa, 1984). When debris flows are the result of slope failure, this can be explained as an imbalance between driving and resisting stress. This is described by the *Mohr-Coulomb* failure criterion:

$$\tau_r = c' + \sigma' * \tan\phi'$$

$$\sigma' = \sigma - (u + \Delta u)$$

where τ_r is the driving shear strength, while the resisting stress is composed by c' which is the inherent shear strength (or cohesion of soil particles), ϕ' which is the bulk friction angle and by σ' which is the effective normal stress that in turn is the difference between the total normal stress (σ) and the pore fluid pressure (u). Slope failure and debris flow depends on changes in pore pressure and in effective stress. The overpressures (Δu) leads to a decrease of the effective stress, and thus leading to a decrease of the resisting stress (*Figure 9*). This causes the failure of a slope along a rupture surface. An increase of the slope weight due to wetting and saturation of sediments creates instability as well (Cepeda, 2009).

The second main triggering mechanism is explained by Cepeda (2009) as progressive bulking of sediments entrained by run-off, where flows eventually reach a high enough concentration of solids that they exhibit non-Newtonian characteristics and have greatly increased erosive capacity. Headwater run-off usually develops on steep rock faces (catchments) enabling turbulent flows to erode channel bedload or loose and unsorted sediment covers tied to the catchment outlet (*Figure 10*)

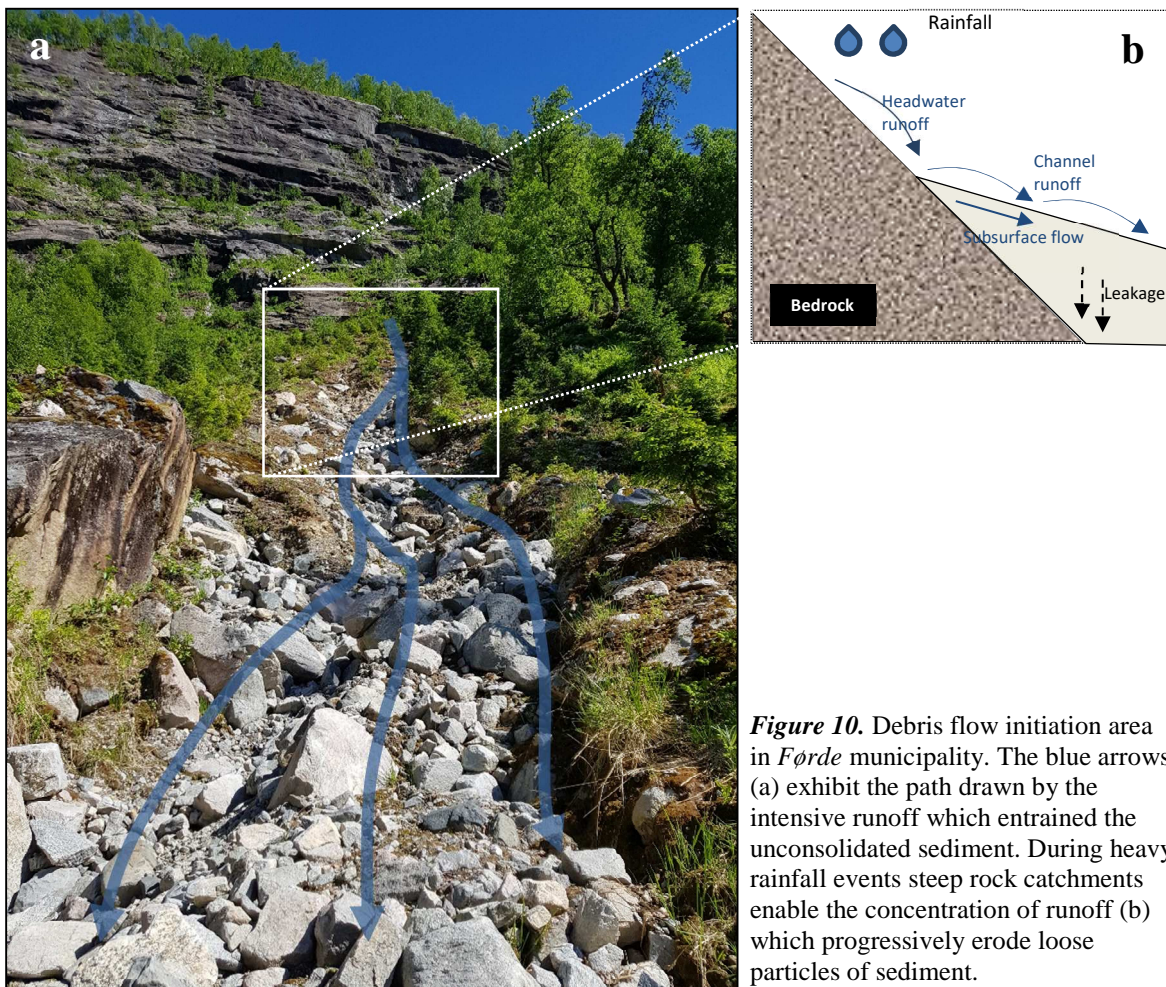


Figure 10. Debris flow initiation area in Førde municipality. The blue arrows (a) exhibit the path drawn by the intensive runoff which entrained the unconsolidated sediment. During heavy rainfall events steep rock catchments enable the concentration of runoff (b) which progressively erode loose particles of sediment.

Once in motion, debris flows have liquefied interiors ($\tau_r \sim 0$) where cohesive bonds are broken during failure ($c' = 0$) and the maintenance of the liquified debris flow core with pore fluid pressures that exceed static equilibrium occurs through the compressibility and limited permeability of debris (Iverson, 1997).

Besides the triggering mechanism, the factors that cause slope instability and lead to debris flow initiation can be both natural and anthropogenic. Erosion or excavation at the base of the slope increases the steepness and decrease the overall stability (Cepeda, 2009). Logging, wildfires and unwise land use are responsible for the removal of vegetation and the alteration of the drainage pattern, which are recognized as contributing factors to general slope instability.

2.2. Landslide susceptibility assessment

2.2.1. Mass movement inventory

The most straightforward initial approach to any study of landslide hazard is the compilation of a landslide inventory (*Figure 11*), and such inventories are the basis of most susceptibility mapping techniques (Dai et al., 2002). Landslide types are usually defined according to Varnes (1978) and usually classified as deep-seated or shallow, depending on the type of movement and the estimated landslide volume (Guzzetti et al., 2012). Inventories should be provided with different layers of information such as: spatial extents, type of movement, volumes involved, estimated thickness of material involved in landsliding and date of known activity (Dai et al., 2002). Although, this is not always easy to accomplish. This leads to the absence or incompleteness of landslide records, which is one of the major drawbacks in the assessment of landslide hazard risk (Van Westen et al., 2005). Visual interpretation of aerial photos and digital elevation models (DEM) coupled with field survey still remains the most used technique for landslide mapping and GIS still remains the best platform where to store landslide databases (Van Westen et al., 2008).

Guzzetti et al. (2012) and Reichenbach et al. (2018) state that there are four type of landslide inventories:

- Geomorphological inventories, where the visible physical features are examined throughout the study area in order to identify the mass movements.
- Event inventories, which collect data about landslides associated with a given rainfall or earthquake event.
- Multi-temporal inventories, which are prepared for the same area but for different time periods.
- Historical inventories.

For the compilation of the inventories, it often takes a lot of time and the involvement of expert opinion. Reichenbach et al. (2018) report all the possible techniques which can be used in realizing a landslide inventory:

- Visual interpretation of aerial photographs.
- Interpretation of optical satellite imagery.
- Field mapping.
- Interpretation of high resolution DEMs.
- Automatic or semi-automatic mapping using remote sensing imagery.
- Archive search.

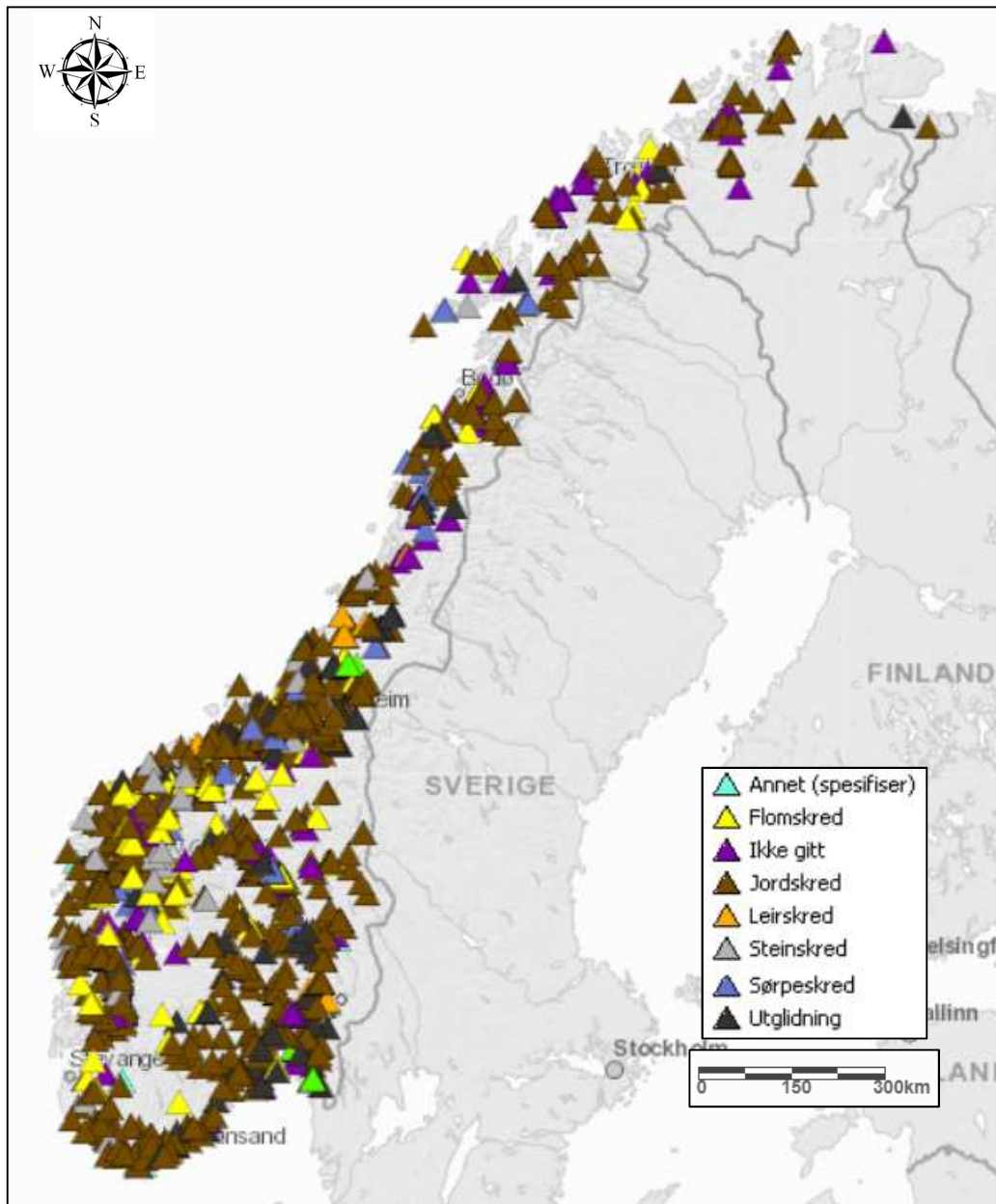


Figure 11. National landslide inventory map covering the whole Norwegian territory. In map are reported the registered landslide events within the last 10 000 days. Each entry features the timing and approximate coordinates of where debris flows (in legend indicated as *Flomskred*) and other type of mass movements had deposited or blocked a traffic line. (source: xGeo.no)

2.2.2. Susceptibility mapping

Over the last decades, many studies dealt with landslide hazard analysis and consequently with risk assessment. Two main reasons are ascribed to this recent trend: increasing socio-economic losses and the widely accepted uncertainty arising from landslide prediction (Dai et al., 2002; Van Westen et al., 2005). Many definitions of risk do exist in literature. Here is quoted the one expressed by Varnes (1984), where risk is explained as <<the expected number of lives lost, persons injured, damage to property and disruption of economic activity

due to a particular damaging phenomenon for a given area and reference period>>. This statement can be translated into the following formula:

$$R = H \times V \times E.$$

where total risk can be referred to as the product of Hazard (probability of occurrence of the event with a given magnitude within a reference period), Vulnerability (fraction of the value

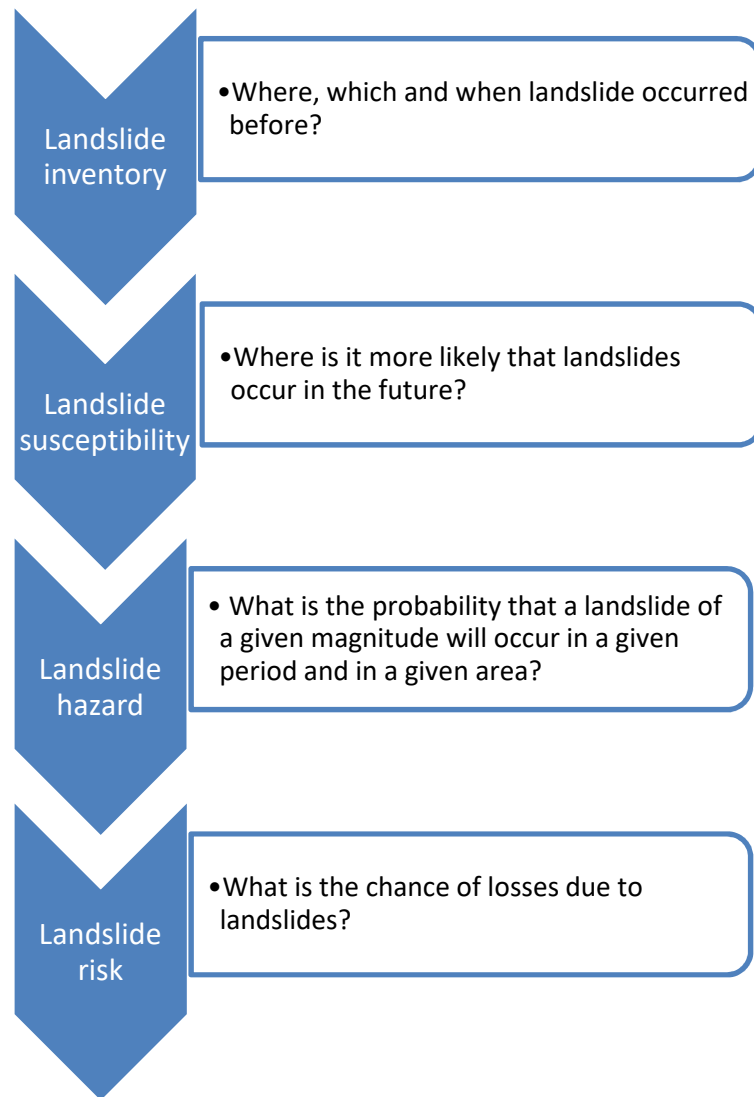


Figure 12. Simplified flow chart exhibiting the steps required to perform a landslide risk assessment. Landslide susceptibility can be regarded as the spatial component of the hazard assessment.

of a particular element at risk for a specific type of hazard) and Exposure (value of the element at risk). From these considerations, it can be derived that risk assessment strongly depends on hazard delineation. Hazard is a concept linked to both spatial and temporal probability (Figure 12). The latter is not always easy to obtain: historical records able to couple detected landslides with triggering-related events (such as storms, intense rainfalls or earthquakes) are often missing or cannot be regarded sufficient. Physical models, useful to relate magnitude and return period of the above-mentioned events with the occurrence of

landslide, are difficult to obtain, costly and time-consuming. As a result, it's easy to understand why most of the published studies deals only with landslide susceptibility assessment (example visible in *Figure 13*), which can be considered as a relative indication of spatial probability (Varnes, 1984; Van Westen et al., 2003; Van Westen et al., 2005). This is ascribable to the fact that susceptibility maps provide information on potentially unstable slope without supplying direct information on landslide magnitude and frequency (Guinau et al., 2007; Reichenbach et al., 2018).

Susceptibility mapping concerns the identification of the areas likely to produce landslides in a given region on the basis of local terrain and preparatory conditions (Paudel et al., 2016), while the spatio-temporal effect of triggering factors on landslide occurrence tends to be smoothed out in this kind of analysis (Dai et al., 2002). Landslide hazard is more difficult to ascertain than landslide susceptibility (*Figure 12*), as susceptibility is a component (the spatial component) of the hazard (Guzzetti, 2006b). The need for circumscribing the necessary conditions which lead to slope failures is regarded as the key for future events since they are assumed to be the same as of for past occurrences (Carrara et al., 1995). This is the reason why susceptibility assessment and, therefore, hazard and risk assessment require the preparation of a reliable landslide inventory, where different levels of information regarding past landslides should be collected and stored in national inventories, which are qualitatively and quantitatively scarce in most of the cases. Spatial landslide occurrence can be inferred from heuristic investigations, computed through the analysis of environmental or inferred from physical models. Thus, a territory can be zoned into susceptibility classes ranked according to different probabilities (Carrara et al., 1995; Reichenbach et al., 2018). Many recent studies have been using GIS for indirect mapping susceptibility approaches, which can be distinguished from the direct ones: the first methods use either statistical or deterministic models, the latter involves the knowledge of an expert who directly states the degree of susceptibility throughout the given area (Van Westen et al., 2003).

Statistical models are based on the known distribution of landslides, which is taken as the dependent model variable employed in finding statistical relationship with instability factors (geo-environmental variables). Many different statistic techniques have been used in literature. Therefore, statistical models can be classified in (Reichenbach et al., 2018):

- Classical statistics (which use methods like logistic regression, linear regression).
- Index-based (which use weight of evidence and heuristic analysis methods).
- Machine learning (fuzzy logic systems, forest trees).
- Neural networks.
- Multi criteria decision analysis.
- Other statistics.

Any landslide susceptibility maps created needs proper validation. Statistical models for landslide susceptibility zonation reconstruct the relationships between dependent and independent variables using training sets, and verify these relationships using validation sets (Guzzetti et al., 2006b). The quality (i.e., consistency, robustness, degree of fitting and prediction skill) of the proposed susceptibility estimate should be established by the same landslide data used to obtain the final map, or by using other pertinent landslide inventory maps not employed in the construction of the model (Yalcin et al., 2011). After a prediction image is obtained, the model prediction performance should be based on the comparison between the prediction results and the unknown target pattern, the areas affected by future landslides (Chung & Fabbri, 2003). Multi-temporal data are required so that they can be divided in two periods: in this way the training dataset should be referred to an earlier period

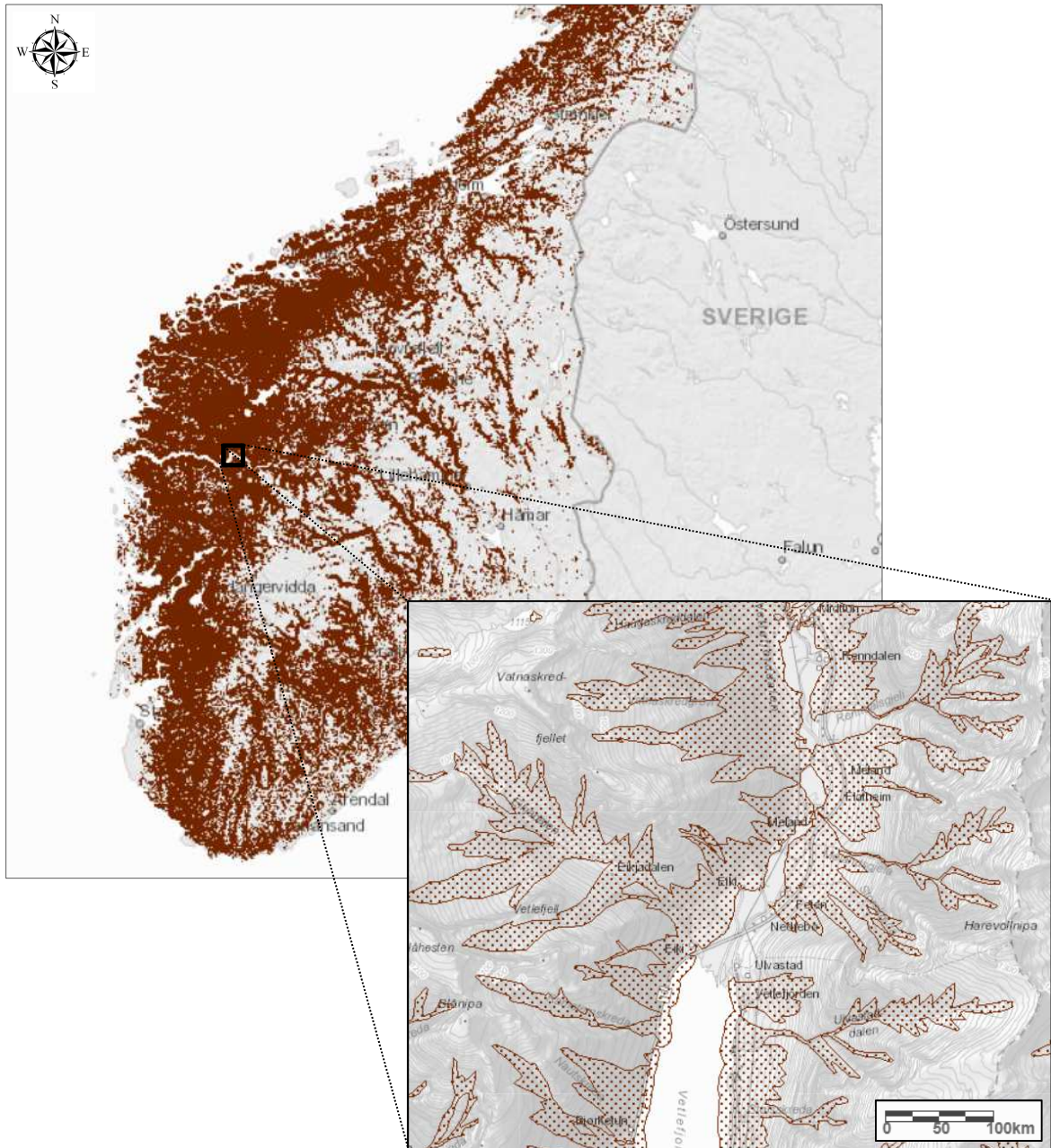


Figure 13. Example of susceptibility map. Different susceptibility classes are not considered. The map shows the potentially susceptible areas (starting and runout) for debris slides, debris avalanches and debris flows at 1:50 000 scale. (source: xGeo.no)

and are used to generate the prediction image, while validation dataset (which is referred to the occurrences of the last period) is used as the comparison term (Chung & Fabbri, 2003). Alternatively, it is possible to adopt a spatial or a random validation: the landslide information is segmented using spatial (geographical) criteria where the validation set is part of a different portion of the territory; otherwise random selection is used to obtain the validation set. In contrast to the model prediction performance, the model fitting performance is obtained by comparing the prediction image with the same dataset used to generate it. Different metrics are used in literature to evaluate the fitting rate (Reichenbach et al., 2018), where the most common are: i) success rate curves; ii) landslide density or frequency; iii) Receiving Operating Characteristics (ROC) curves. For what concerns the model prediction

performances, the most common metrics are: I) prediction rate curves; II) landslide density or frequency; III) ROC curves.

The aim of this study is to implement a statistical model using a bivariate technique (Weights of Evidence) based on the analysis of a landslide inventory. This is obtained preparing landslide density maps. The quality of the assessment usually depends on the reliability of the inventory (Reichenbach et al., 2018). The idea behind statistical models is to couple all possible instability factors with a landslide inventory. Thanks to GIS support, each continuous (such as slope angle) and discrete variable (such as lithology map) pertinent to slope stability can be both created and converted into different maps (Van Westen et al., 2008); then, each of them are overlaid on the landslide inventory map. The result of these kind of statistical methods is that each grid cell can be adjusted to new values representing the degree of probability, certainty, belief or plausibility that may be subject to a particular type of landslide in the future (Chung & Fabbri, 1993; Bonham-Carter, 1994; Van Westen et al., 2005). WofE (Weights of Evidence) is a bivariate statistical method which is widely used in landslide susceptibility assessment. It consists in adapting every intrinsic and extrinsic data map in a simple binary format (0,1) indicating, respectively, the presence or absence of a

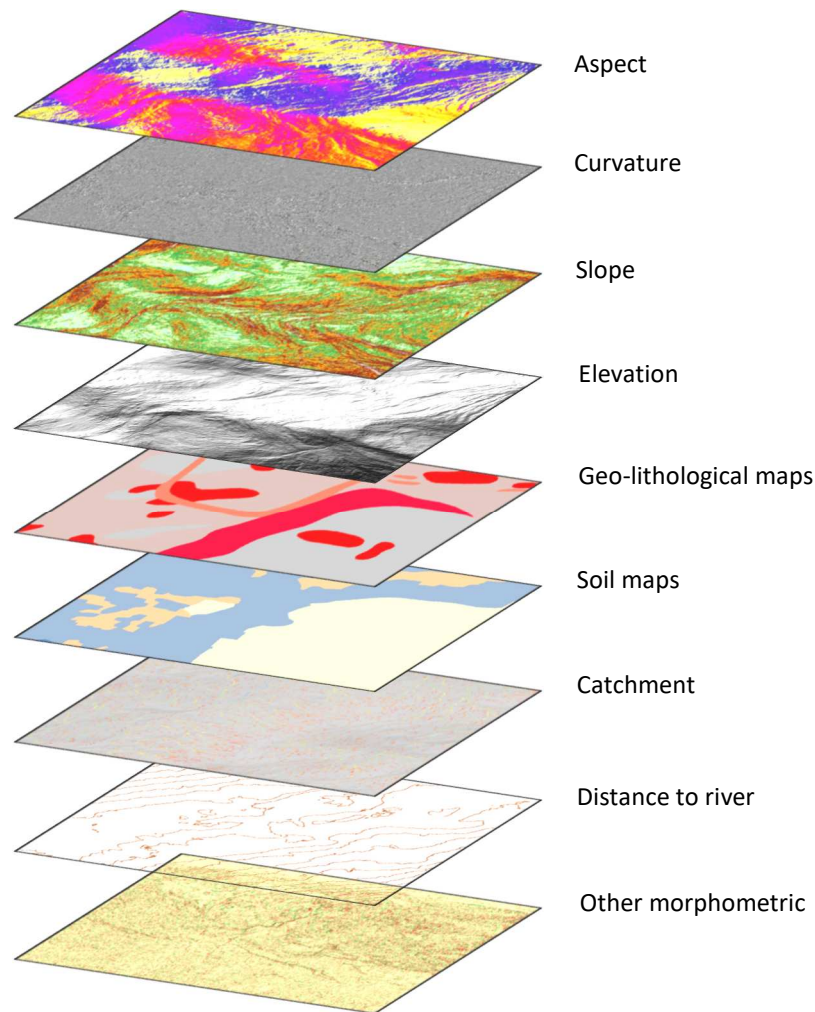


Figure 14. The most used parameters (continuous and categorical) in landslide susceptibility modelling according to Reichenbach et al. (2018).

certain class or interval of a determined parameter. In this way, it will be contemporary assessed, within each pixel, if the independent variable (every single class or interval of the considered layer of information) occurs in conjunction with the presence of the depend variable (landslide event). The influence of each variable is evaluated independently, which is done taking into consideration the density of landslide within each parameter class and comparing it with the landslide density in the entire area. The weights of all predictor variables are combined together resulting in a computed landslide susceptibility index, which can be described as a degree of probability. According to the literature review made by Reichenbach et al. (2018), there have been a number of input variables in producing susceptibility maps and they can be grouped in five thematic clusters: geological, hydrological, land cover, morphological and other. Among the most used there are slope, aspect, curvature, elevation, soil types, geo-lithological classes, river/catchment measures, distance to river and other morphometric variables (*Figure 14*).

Statistical techniques, such as WofE, can be regarded as the most suitable for landslide susceptibility mapping at medium scales of 1:10 000 – 1:50 000 (Dai et al., 2002; Van Westen et al., 2005), and moreover, GIS-based statistical methods have recently become very common because of the capacity to obviate the absence of information otherwise difficult to obtain, the easy data management and customization, the fast calculations and the output and prediction accuracy. However, several drawbacks are linked to the use of such techniques:

- Using multiple predictor variables may violate the assumption of conditional independence between these predictors, which is required for an unbiased susceptibility estimate (Bonham-Carter, 1994; Meyer, 2013).
- Statistical techniques might be used in a black-box manner with inadequate consideration of the mechanics of the physical processes involved, thus correlating non-pertinent predictor variables and giving misleading results (Dai et al., 2002).
- The simplification of the problem can lead to assume that landslides happen under the same combination of factors throughout the study area (Van Westen et al., 2003).
- Different types of landslide have different types of causal factors and many studies actually merge them together in order to develop generalized statistical relations (Van Westen et al., 2005).
- The use of expert opinion is more and more considered as subjective and sought to be replaced by objective computer algorithms, thus, giving more credits to the tool than to the significance of the input data (Van Westen et al., 2003; Van Westen et al., 2005).

3. Regional Setting of the study area

3.1. Climate

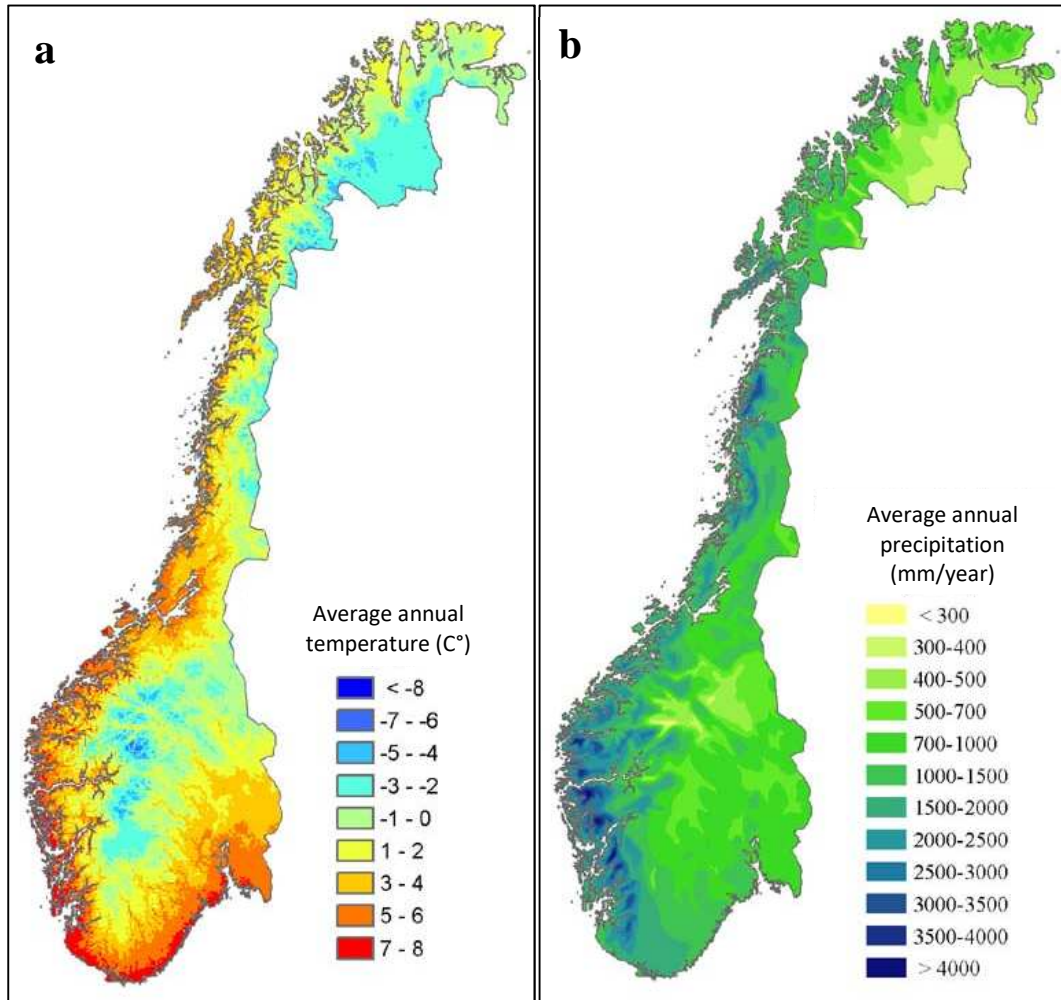


Figure 15. Maps of Norway showing (a) the average annual temperature and (b) the average annual precipitation within the reference period 1961-1990 (maps from *met.no*, modified).

Norway is a Nordic country and its climate shows large variations because of its large extension in latitude, the warming influences of the Northern Gulf Stream and the terrain physical variability. There are five distinct climate zones in Norway:

- I. Northwestern Norway extends above the Arctic Circle and has a subpolar oceanic climate.
- II. The southwestern coast has maritime mild temperate climate. This part of Norway is characterized by rapid changes in both weather patterns and temperature, with heavy precipitations dominating throughout all seasons.
- III. The southeastern coast has mainly humid continental climate with a smaller influence of the ocean than the west coast.
- IV. The inland areas show a continental subarctic climate and they typically experience snowy weathers during winters.
- V. The northern islands, which are Svalbard and Jan Mayen, have polar climate.

The mean annual temperature for the Norwegian mainland during the reference period 1971-2000, is calculated to be +1.3 °C. The highest annual temperatures, up to +7 °C, are found along the coast of southern Norway and the lowest in the high mountains with down to -4 °C (Hanssen-Bauer et al., 2017). For the reference period (1971-2000), the mean annual precipitation for the Norwegian mainland is estimated to be 1600 mm.

Annual precipitation is highest (>3500 mm) in central parts in western Norway and lowest (~300 mm) in the upper part of the valley *Gudbrandsdalen* (south-eastern Norway) and in interior parts of *Finnmark* county (Hanssen-Bauer et al., 2017). For visual representations, please refer to *Figure 15*.

It is widely acknowledged that an increasing temperature trend has been experienced over the last century across the whole world. From 1900 until 2014 the annual mean temperature for the Norwegian mainland increased by approximately 1 °C (IPCC, 2012). The same trend has been registered for what concerns precipitation rates. Annual precipitation over Norway has increased since 1900, and particularly from the late 1970s.

For the country, as a whole, the increase in annual precipitation is approximately 18 % (Hanssen-Bauer et al., 2017). High-intensity rainfalls are expected to increase both in intensity and frequency, with the consequence of putting human and natural systems in danger in a more severe way than observed before (IPCC, 2012).

3.2. Geology

Norway is part of the *Fennoscandinavian* Shield (or Baltic Shield). The geology consists mainly of granitic and gneissic rocks, while sedimentary rocks (sandstone, limestone and marine deposits) concentrate in few and small areas (*Figure 16*). The oldest rocks in Norway are 2.9 billion years old and are located in Finnmark and along the coast in *Troms* and *Vesterålen*, while, moving south and west the bedrock becomes gradually younger: in the Oslo region (*Figure 16*) there is evidence of volcanic activity during the Permian (250-300 Ma). With the exception of the Oslo Rift, which is a failed rift system that continues into the Skagerrak and the North Sea (Lidmar-Bergström et al., 2000), in the rest of Southern Norway the bedrock was formed in more ancient eras as it is the remnant of two important mountain chains: the *Gothian* (1700-1500 Ma) and the *Sveconorwegian* (about 1130-900 Ma). But the backbone of the whole country is the belt of the *Caledonides*. The Scandinavian Caledonides, are made up of Neoproterozoic to Silurian metasedimentary and metavolcanic rocks (700-400 Ma). Most of the limestones rocks in Norway are located in this mountain chain (more precisely in the north part of the country, between *Trondheim* and *Tromsø*) and have a long history of subduction, which caused alteration and transformation into metamorphic limestone, called marble, of a grey or blueish colour. The genesis of Caledonides has led to the closing of the *Iapetus* Ocean, where large rock sheets were then thrust from the Northwest to the Southeast. In the subsequent time, rifting processes and the warm climates during the Mesozoic and Tertiary forced the erosion of the orogen (Lidmar-Bergström et al., 2000). Western Norway is characterized by the *Transscandinavian* igneous belt. This area is comprised mostly out of granitic basement rocks that stretch along a 1500 km long zone from southern Sweden to the Lofoten Islands.

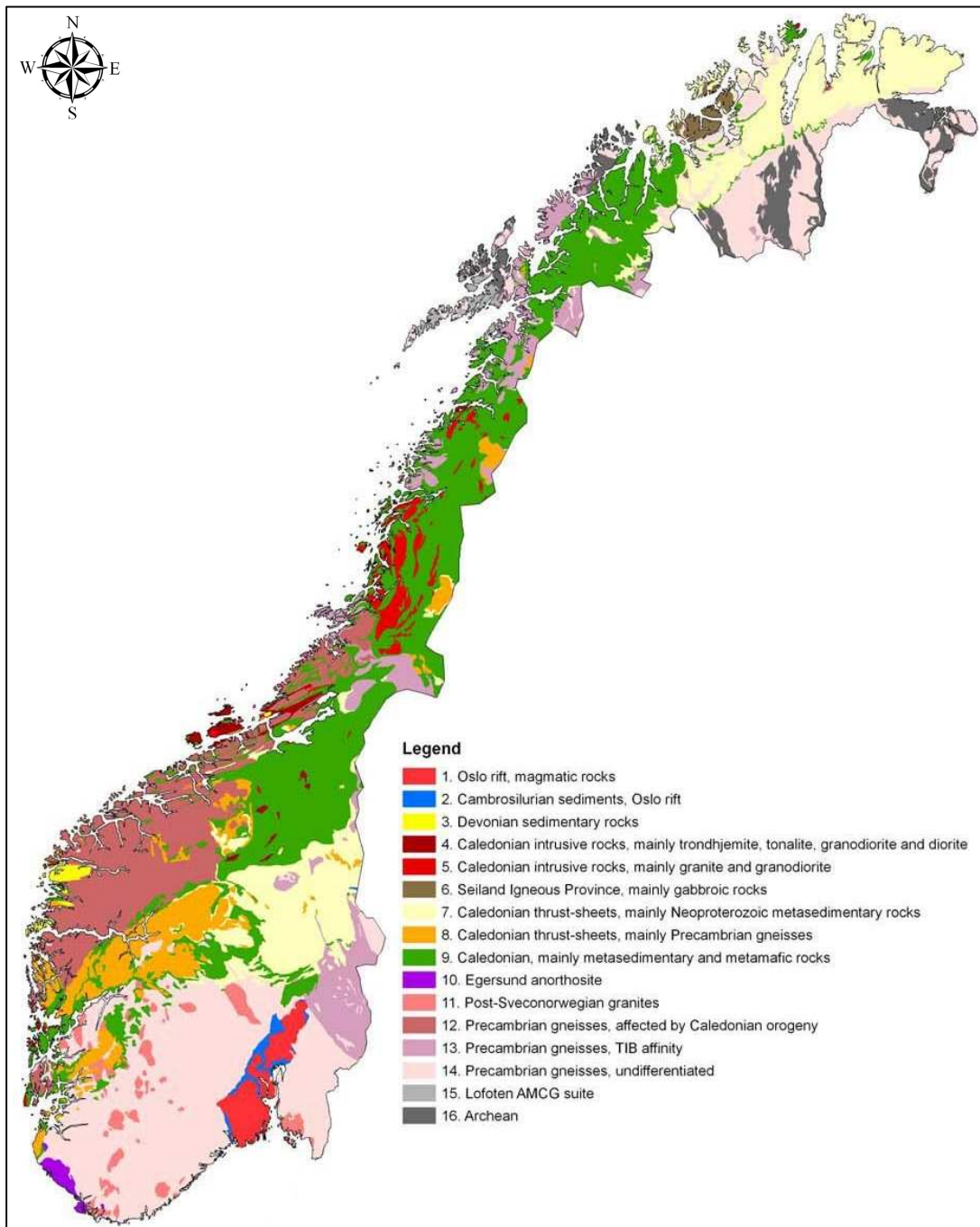


Figure 16. Geologic map of Norway (image from Sigmond (2002), modified).

3.3. Geomorphology and landslide activity

Most of today's landforms in Norway can be attributed to the latest phase of the glaciations, the *Weichselian* stadial, which took place between 117 and 11.7 ka, while the maximum extension of the ice sheet occurred between 22 and 19 ka (Olsen et al., 2002). Before the inland ice covered and modelled the Scandinavian peninsula throughout all the glacial stages, the pre-existing landscape was generally mild and characterized by gentle outlines:

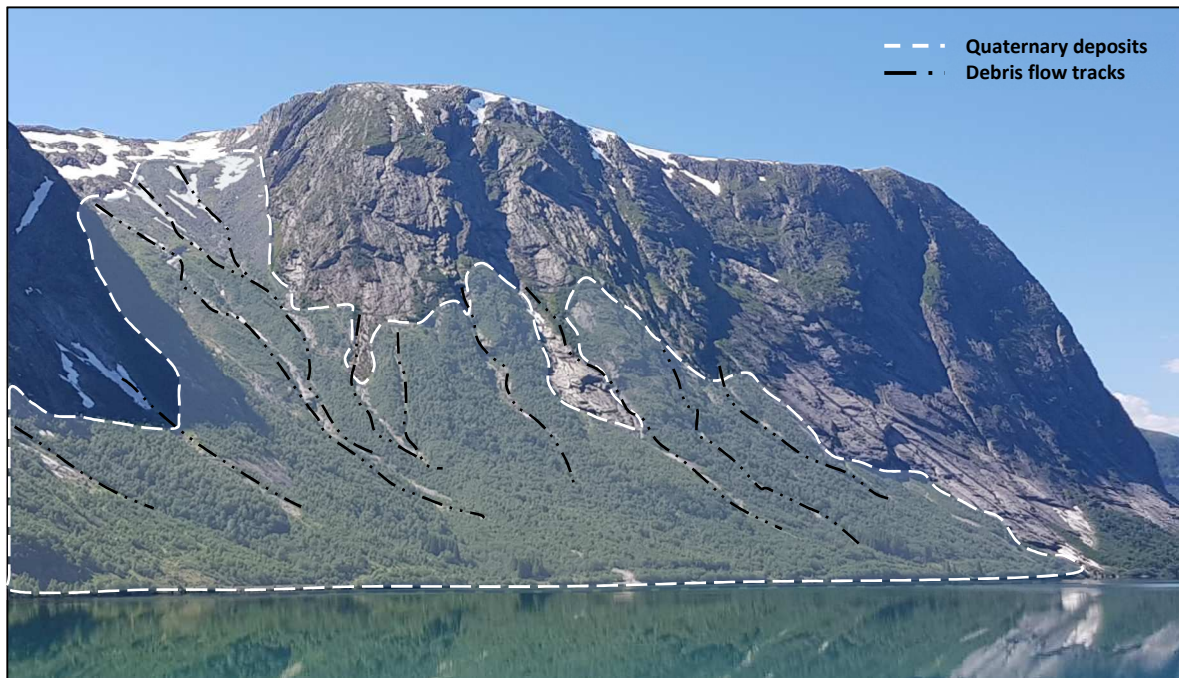


Figure 17. Example of quaternary deposits asset and debris flows disposition throughout Jølster municipality. It is noticeable the steep rock faces, the overlying shallow quaternary cover and the numerous and neighbouring debris flow tracks.

that surface was called the *Paleic* surface (Strom, 1948). Before the end of Tertiary there was a high rate of fluvial activity and during Pleistocene, outlet glaciers deriving from the ice sheet emphasized the erosion forming over-deepened valleys, fjords and lakes. While in Western Norway glaciers were widening and deepening existing pre-glacial valleys (it has reported a maximum vertical excavation of about 2000 meters in *Sognefjord*), the east of Norway kept its fluvial character with valley incisions not deeper than 250 meters (Strom, 1948; Lidmar-Bergström et al. 2000).

Since the end of Pleistocene about 11 ka, the Scandinavian peninsula have been experiencing a post-glacial rebound (or isostatic rebound), which consists of the rise of land masses after the lifting of the huge weight of ice sheets during the last glacial period.

This led to the formation of new coast lines and lower inland areas with a ground mainly made of maritime clays, which usually become sensitive in aerial conditions causing problematic quick clay slides.

Where erosion rates are high, there are also vast accumulations of loose material. mountainous area in Norway is covered by moraines. The latter consist of an unsorted mixture of all grain sizes, from small clay particles up to large boulders. The actual surface of Norway is characterized by very large morainic and glacialfluvial deposits, extensively present in those areas situated between the watershed and the wasting ice sheet (Strom, 1948). Weathered material after deglaciation is also common in Norwegian mountains. Peripheral morainic deposits along slopes covering the underlying bedrock are widely widespread, thus providing abundant and erodible debris involved in frequent slope activities since the beginning of Holocene (*Figure 17*).

Landslides, together with floods and snow avalanches, are one of the main natural hazards in Norway (Nadim et al., 2009). Western and Northern parts of the country are seriously affected by snow avalanches, which are the responsible for the main part of economic and life losses. Over the past 150 years, snow avalanches caused 1500 deaths (Kalsnes et al.,

2016). Western and Northern Norway have been experiencing also large rock slides and rock avalanches which caused devastating tsunamis in the fjords, lakes and reservoir (Kalsnes et al., 2016). About 5 000 km² of Norway is covered by maritime clays, where 20% of this area is made up of highly sensitive clay; quick-clay slides represent a particularly high hazard in Eastern and Central Norway (Kalsnes et al., 2016). None of the documented landslides in Norway have been triggered by earthquakes, given the moderate seismicity of the country. Landslides are frequently triggered by adverse hydrogeological conditions. In this sense, water plays an important role in affecting the slope instability. This is accomplished in two ways: 1) the increase of pore water pressure and the decline of the effective stress; 2) water enhanced erosion. In both cases, the abundance of water is related to the triggering mechanism, which is in turn linked to the weather conditions. Kalsnes et al. (2016) state that the main weather-related landslide triggering factors in Norway are:

- Heavy and/or prolonged rainfalls, which result in a large availability of water respectively for a short period or distributed over a longer period.
- Erosion, which take place during floods and may cause slope undercutting; in Norway, erosion is also observed to initiate in channel beds, where the entrainment of sediment may start debris flows.
- Rapid snowmelt, where water infiltrates into the ground and, in the presence of underlying impervious layers of frozen soil or rock, leads to a rather rapid increase of soil pore pressure.
- Weathering and frost weathering, which are processes that are generally responsible to produce regolith layers and materials frequently involved in landslide occurrence.

Today the debris flow activity is bound to the steep slopes found in small catchments characterized by short river lengths and steep longitudinal profiles: this landscape is dominant in the west and north of the country. Here, the morphology is in evolution with the recent increasing rate of extreme rainfall events, which seriously affect the slope balance. Human activities, such as clear cutting and intensive soil use, are responsible for producing an extra amount of sediment likely to be included in slope activities. The periglacial conditions prevailing in the south-central mountain range and in the north are decisive in making slopes susceptible to debris flows: the reduced infiltration capacity of permafrost can result in an increase of runoff or the layer detachment on slopes can frequently initiate debris flows and slides (Berthling & Etzelmüller, 2011). Debris flows can be explained both by short-term intensive precipitation events and rain accumulating over a longer period. This can explain the two geomechanical initiation processes which can be found in Norway: surface erosion during short and intense storm events, and slow build-up of pore pressure over long longer time periods with lower rainfall intensity (Kalsnes et al., 2016).

4. Field survey and statistical data analysis

4.1. Methods

The following sections are aiming to give an overview of the methods, the tools and the findings which were employed to collect and analyse the multiple aspects related to debris flow initiation areas.

4.1.1. Baseline data analysis

4.1.1.1. National database of slides for Norway

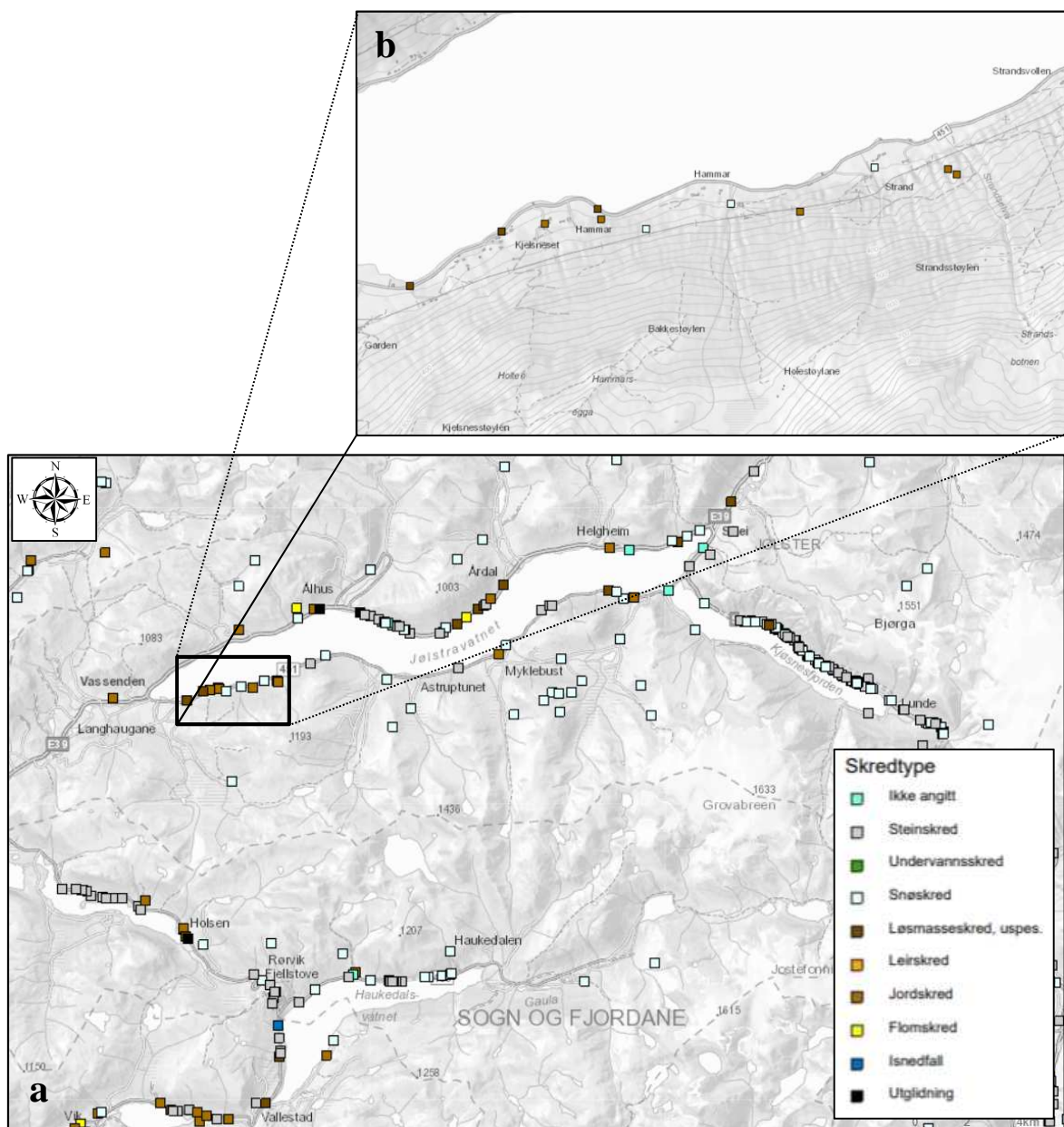


Figure 18. Example of the national database of rapid mass movements for Norway. The images (a, b) shows an overview of part of the *Sogn og Fjordane* county. It is noticeable that the recorded events lack of a definition of the area affected by the mass movement. The recorded slides concentrate next to the major traffic routes, while they are seldom reported in remote areas.

The present study strongly aimed at producing precise data in order to develop consistent results. As previously stated, the quantity, the quality and the type of information available address the choice of the analysis methods and the reliability of the output. All the existing datasets were stated unsuitable for the realization of a landslide susceptibility map at a medium scale. The national mass movement inventory (Jaedicke et al., 2009), with the joint use of terrain models and aerial photographs, was here considered as a helpful tool for the preliminary compilation of a new and reliable inventory, which is restricted to release zones of debris flows and of debris slides within the study area.

The national database of slides for Norway (*Figure 18*) integrates every registered event concerning all types of rapid mass movements (including snow avalanches and ice falls). Only time, location (which is stored as a point in projected geographical positions) and type of movement are the mandatory data; however, also other optional parameters like materials involved and damages caused are sometimes submitted. The national database contains more than 33 000 events where the road authorities and the Geological Survey of Norway provided the most part of the recordings which cover a time span of five decades (Jaedicke et al., 2009). The different nature of the sources employed in building the mass movement inventory is a considerable aspect when it comes to judge the quality and the quantity of the reported observations. Most of the recorded events are rock falls and snow avalanches and they are typically located close to the main roads. The spatial distribution of the events is biased towards the valleys with population and infrastructure and, in addition to that, the recorded slide events are not well distributed in time, so a frequency analysis of events is ruled out with this dataset (Jaedicke et al., 2009; Meyer et al., 2013). Other noticeable drawbacks of the national mass movement inventory are: events prior to the 1970s are few and they are mainly related to historical reported damages and losses; the amount and reliability of the data depends on the large variability of personnel which made the observations. In this way, the number of real and unreported landslides is most likely to exceed the recorded events (Jaedicke et al., 2009).

Starting from all the consideration explained above, this thesis did not take advantage from the Norwegian database of landslide because it falls outside the feasible tools for the realisation of a susceptibility map for the limited areas of *Førde* and *Jølster* municipalities.

4.1.1.2. Geological and geomorphological setting of Førde and Jølster Municipalities

Førde and *Jølster* municipalities are part of *Sogn og Fjordane* which is a county located in Western Norway. For the most part of the study area, the available bedrock geologic map is at scale 1:250 000, which could provide just a regional overview. Geologic maps at a scale of 1:50 000 are available only for some section of the Norwegian territory.

In *Figure 19* the bedrock map is shown. Some remarks can be made:

- The study area is mostly composed by metamorphic bedrock, in particular by Precambrian dioritic to granite gneiss and migmatite.
- Second, the most Eastern part of *Jølster* municipality and few and small areas on the Southern part of *Førde*, the bedrock is composed by monzonite and quartz

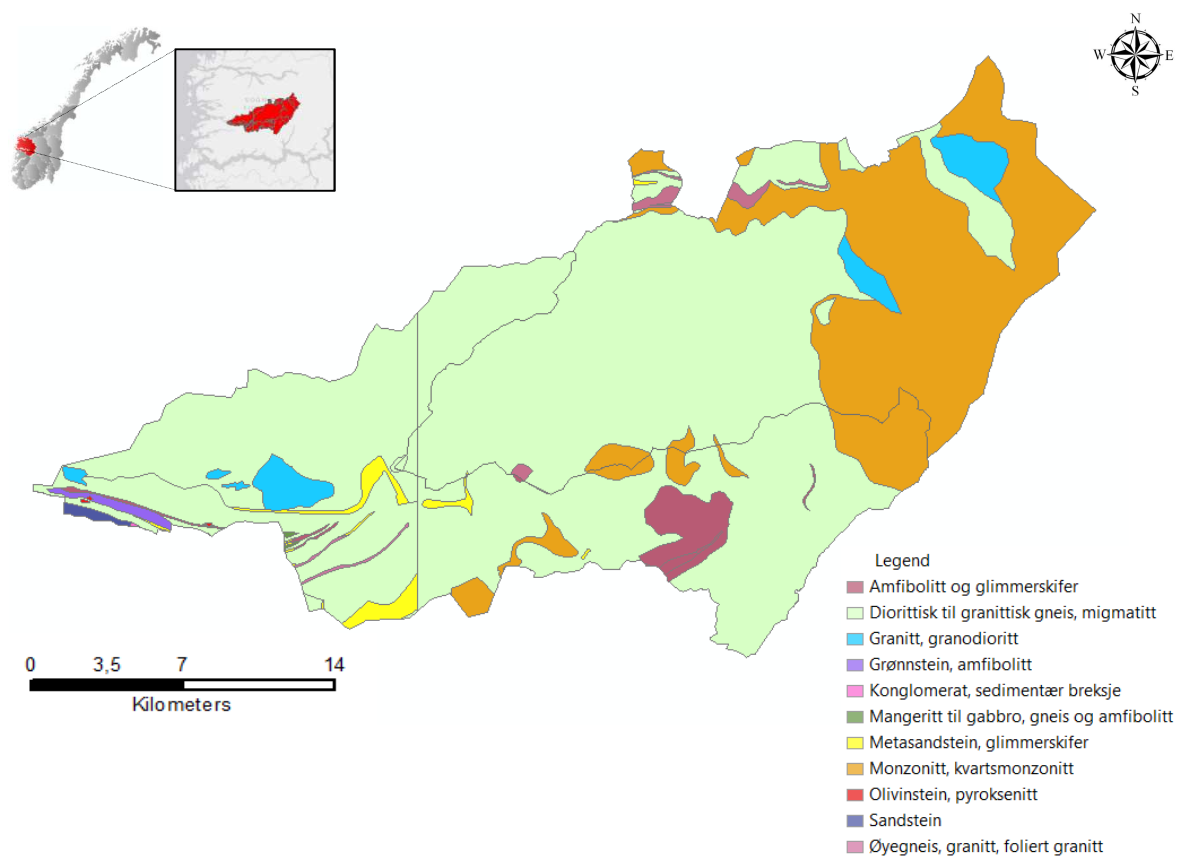


Figure 19. Bedrock geologic map of *Fjørde* and *Jølster* municipalities at a scale 1:250 000. (source: ngu.no)

monzonite with coarse grain while locally eye gneiss is present. Approximately, this bedrock formed 1031 Ma.

- Ultimately, some spots of the study area present granite and granodioritic bedrock. Eye gneiss with large feldspar porphyroblasts (2-5 cm) can be found within this bedrock.

Fjørde and *Jølster* municipalities are characterized by numerous fjords and valleys surrounded by high mountain sides. The steep mountain sides have led to several large rockslides and rock avalanches since the last glaciation. According to the national mass movement inventory (Jaedicke et al., 2009) rockfalls, snow avalanches and slide in soil and debris are the most reported events within the study area. Heading from the western part (*Fjørde*) to the eastern part (*Jølster*) the mountain elevation tends to increase, as well as the slope gradient (*Figure 20*). In accordance with this tendency toward East, *Jølster* municipality territory exhibit more recent paraglacial and periglacial signs than the areas settled in *Fjørde* municipality (the actual *Jostedalsglacier* is closer to the eastern edge of *Jølster*). This results in slightly different geomorphologic features due to local diversification of the environment: the transitory character of landscape and slope activity is more enhanced moving from the coast to the inland (from *Fjørde* to *Jølster*). However, steep rock faces resulting from the past and deep glacial erosion of the Last Glacial

Maximum are present throughout the study area.

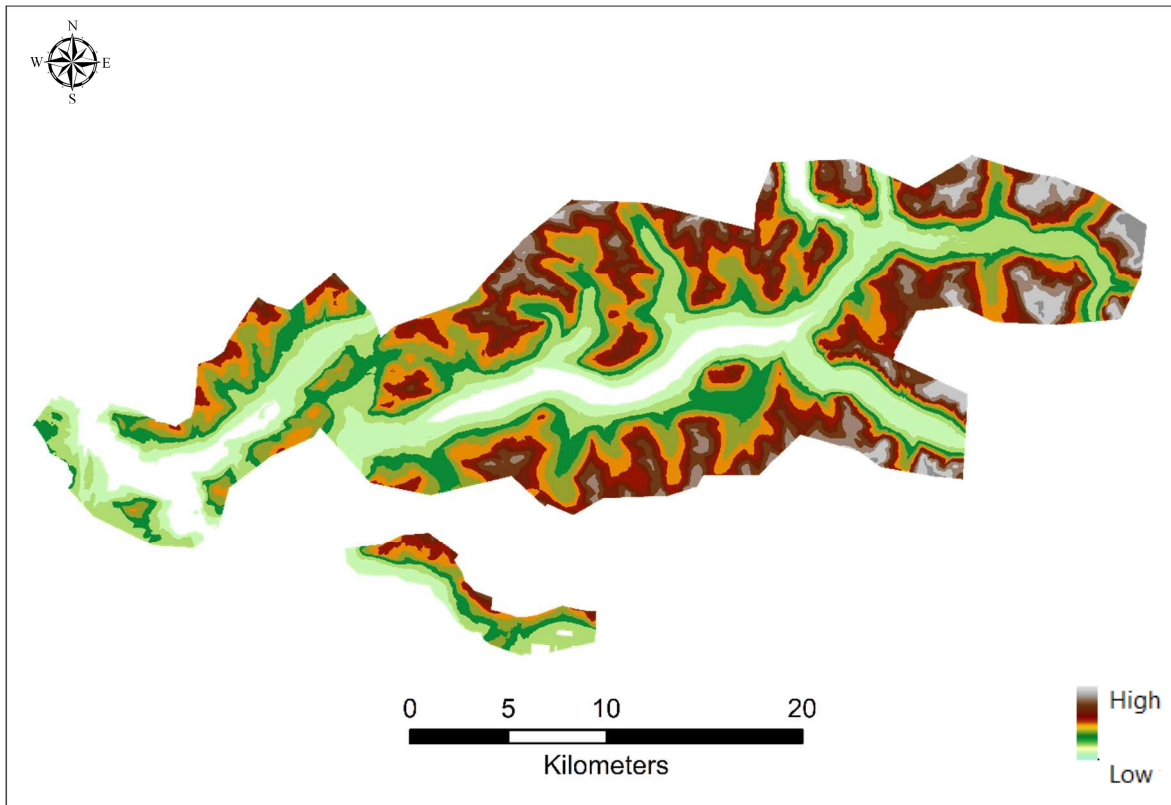


Figure 20. Map showing digital elevation models covering the most part of *Førde* and *Jølster* municipalities. Mountains tend to increase in elevation from East to West.

4.1.2. Field survey

4.1.2.1. Field methods

Field survey usually requires the involvement of qualified personnel, onerous instruments and a lot of time. For this research a minimalist approach was the only possible choice.

The guiding principle of this fieldwork was to gather conciseness and comprehension, in order to observe and record the main aspects of the targeted phenomena.

The digital elevation models and the aerial photographs were examined carefully before planning the field survey. This preliminary phase is always essential when the time allocated to the survey is limited.

All of the most accessible areas in the study area were explored and, when required, some arduous spots were reached. The data collected consist of notes, photographs and GPS points. All the efforts were addressed to the identification of recent and less recent debris flow and debris slide and to the comprehension of their magnitude, triggering mechanism and visual geomorphologic features. This could be accomplished by evaluating the visible characteristics of deposition zones, flow tracks and release zones (*Figure 21*) and by using a multidisciplinary approach: morphology, interpretation of quaternary deposits (*Figure 22*) and the vegetation appearance were some of the different perspectives taken in account. In

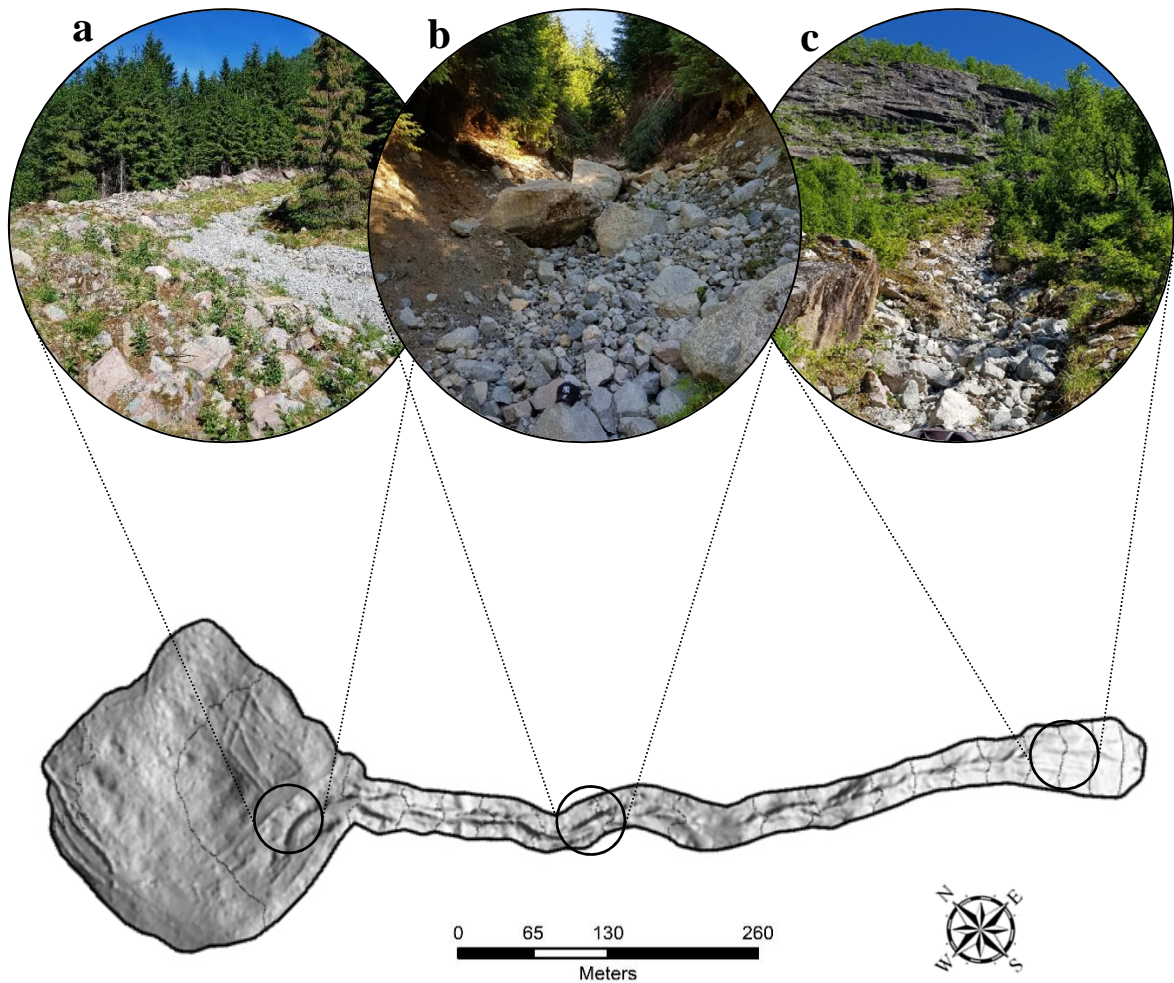


Figure 21. Field survey still constitutes a precious step in detecting the qualitative and quantitative features of the natural phenomenon which is intended to be analysed. In combination with remote sensing, field survey is necessary to get a real comprehension of the object of study. For this thesis, it was conducted a preliminary evaluation of the digital surface models which helped to locate areas likely to have produced debris flow in the past. The most evident (and recent) events were then observed in their entirety, with greater attention paid to three geomorphological units of (a, b, c) deposition zone, flow track and initiation area.

this sense, the evaluation of the shape of the front deposits (*Figure 22*), lateral deposit structure (*Figure 22*) and trees growing on such deposits helped to recognize the nature of the mass movement and to make a coarse estimate of the probable time of activity. In some cases, there were conducted interviews to local people living nearby suspected susceptible zones, as this was considered useful to collect additional historical informations on the hazardous events.

Regardless of few cases, the main part of the observed events needed to be deduced with the help of digital elevation models, as the signs of debris flow deposits and tracks were often concealed by new vegetation or obliterated by man.

4.1.2.2. Debris flow categories and detected features



Figure 22. Photographs taken during the field survey conducted in *Førde* territory. The first (a) shows the deposit structure of lateral confinement banks in a debris flow channel, where clasts surrounded by matrix grow in size upwardly. The second photograph (b) shows the terminal part of a debris flow track declining in the deposition zone, where only large boulders and clasts are visible.

Førde and *Jølster* Municipalities showed many evidences of debris flow activity, which can be generally considered as non-recent. The larger part of the events was not documented within the above-mentioned national landslide inventory because it does not take remote areas in account. In order to better comprehend the studied phenomena, all the recorded events were stored into four different categories which are defined in accordance with two comparative terms: primarily, the deduced triggering mechanism and secondary, the geomorphological features. As stated in the previous chapter, debris flows can alternatively start as shallow slides or with enhanced channel bedload erosion. The higher percentage of the recorded occurrences were observed to be triggered under the conditions of the latter mechanism; on the other hand, about one-third of the events were observed to initiate as translational slides affecting the thin soil cover.

Within the first mechanism (channel-bed erosion), three different geomorphological categories with repeatable features are highlighted in this study:

1. Channelized or unconfined (usually at early stages) debris flows with short flow tracks, small deposition volumes and weathered release zones strictly bounded to steep, small and impermeable bedrock catchments (*Figure 23*); the latter are capable to provide enough strength to the descending water flow so that it can erode and entrain loose material. They usually gather in clusters, which cut through an open slope. Those kind of debris flows might be affected by snow avalanches and even coexist together.

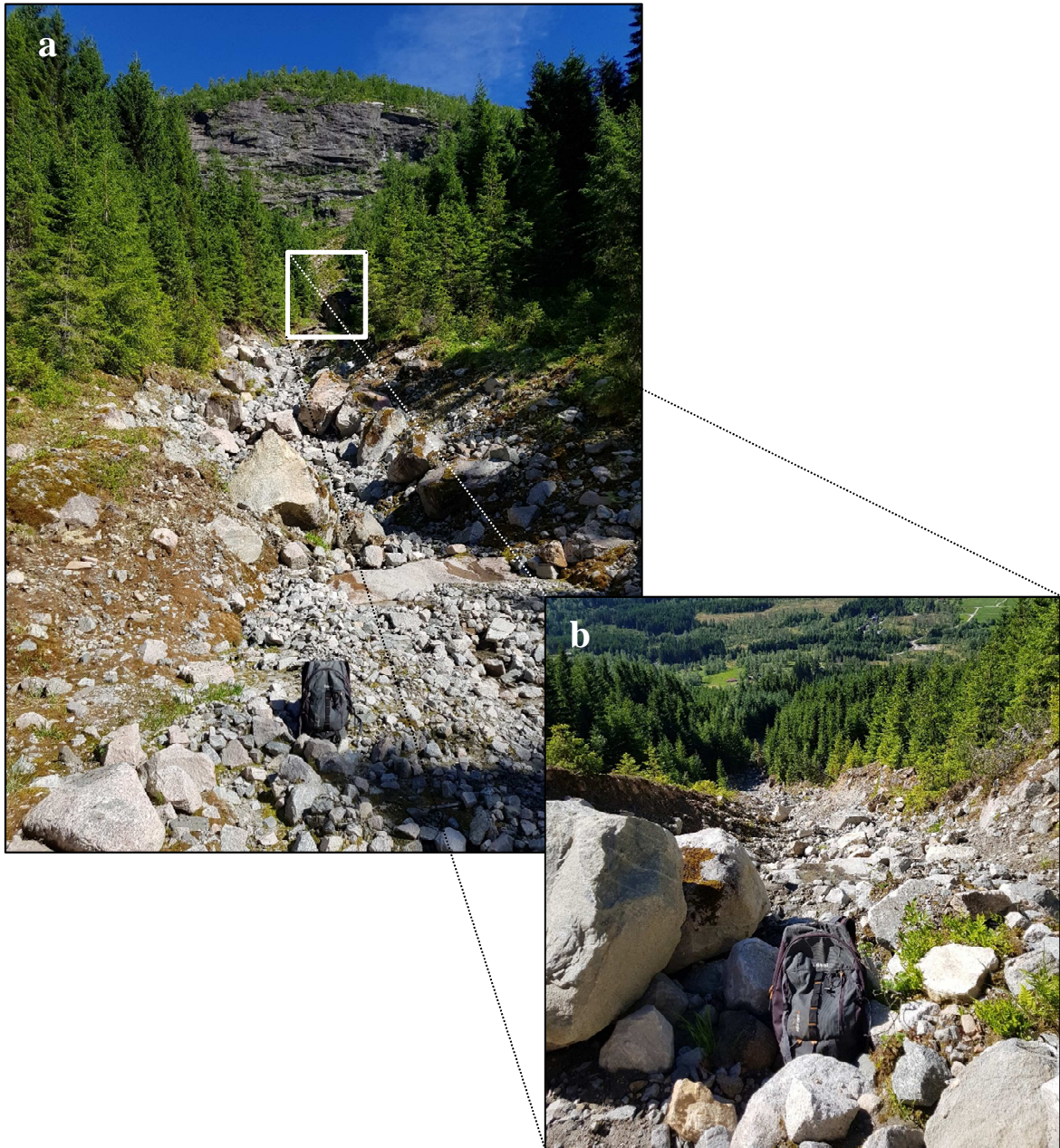


Figure 23. Photographs taken during the field survey. Here is documented the no. 1 category. The main visible features are (a) the steep and flat rock face, (a, b) the erodible debris tied to the catchment, (a, b) the debris flow track.

2. Channelized debris flow characterized by deep incised gullies in bedrock (*Figure 24*). Other distinctive characteristics are the large deposition volumes (debris fans) and wide, hinged release zones which are cirque-shaped and deeply excavated.
3. Channelized debris flow characterized by enhanced erosion of large glaciofluvial deposits. Release zones are usually established along river lengths or in periglacial/paraglacial conditions and are topographically favourable for sediment storage (the slope is usually gentle). High and sudden water inflows might be the responsible of debris discharges and consequently, of both alluvial and debris fans deposits.

Only one geomorphological category was described for the second triggering mechanism:



Figure 24. Photographs taken during the field survey. Here is documented the no. 2 category. The main visible features are (a) the deep incised gully and the large volume of debris and boulders in (b) the deposition zone.

4. Channelized or unconfined (usually at early stages) debris flows with short flow tracks, small deposition volumes and small release zones always triggered by thin soil or debris slips over the underlying bedrock (*Figure 25*); the latter might act as an impermeable layer favouring the water sub-flow and, thus, causing the regolith cover instability. The release areas of this debris flow-type are usually not bounded to any steep rock faces, excluding the chance of any erosional triggering conditions. This category includes debris slides that may turn in debris avalanches.

The third category is composed by few elements and is mainly deducted from aerial photographs, while the others were documented through field investigations. For a schematic and concise representation of the followed conceptual procedure see *Table 1*.

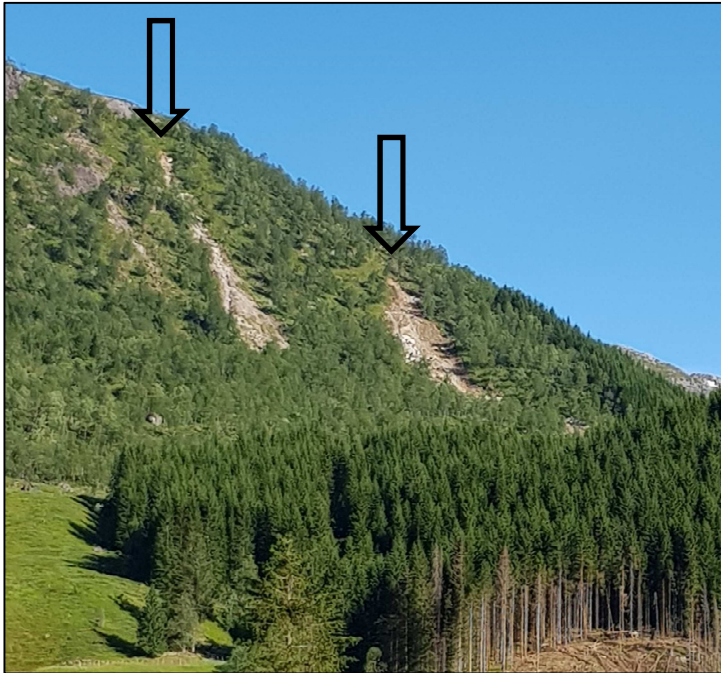


Figure 25. Photograph taken during the field survey. Here is documented the no. 4 category. The main visible features are the lack of a rock wall above the initiation debris slide and the unconfinement of the mass moving downward.

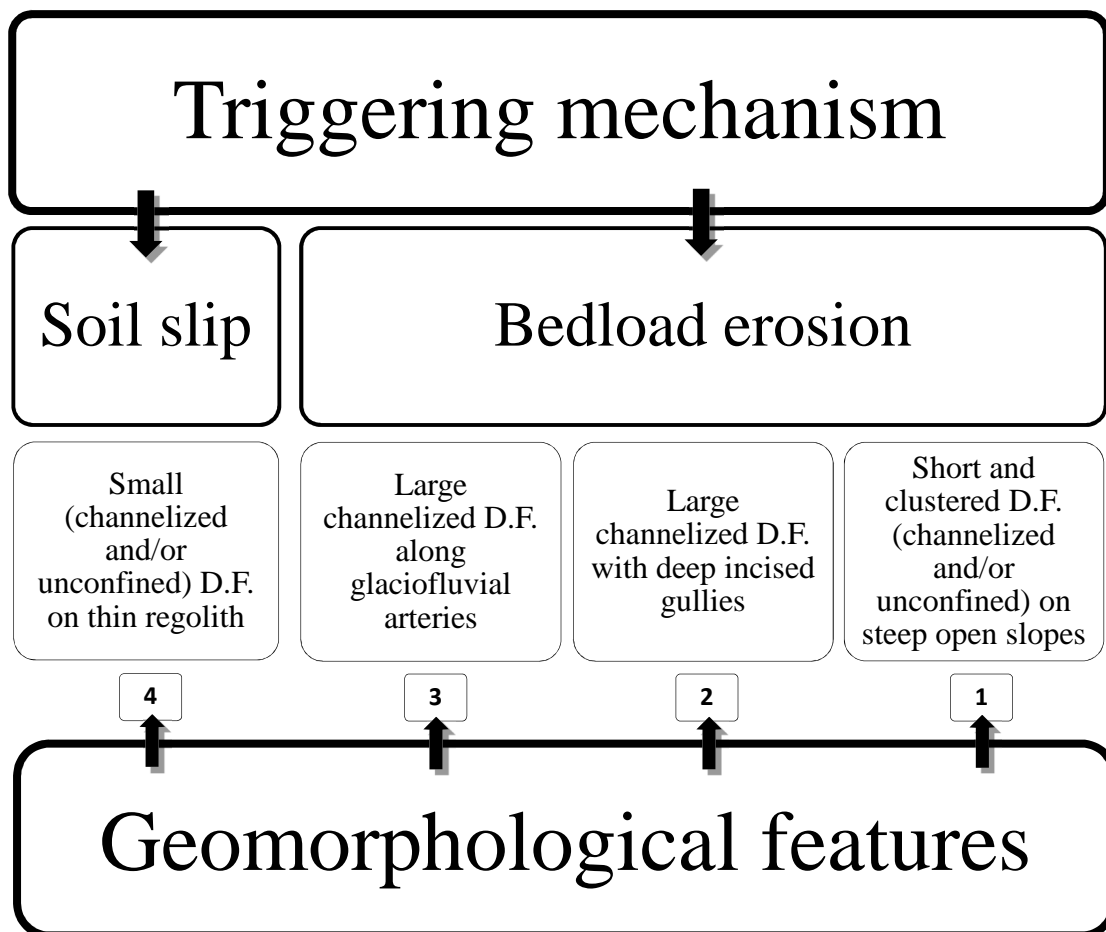


Table 1. Subdivision of the recorded events in 4 different categories based on triggering mechanism and geomorphological features.

4.1.3. Debris flow inventory

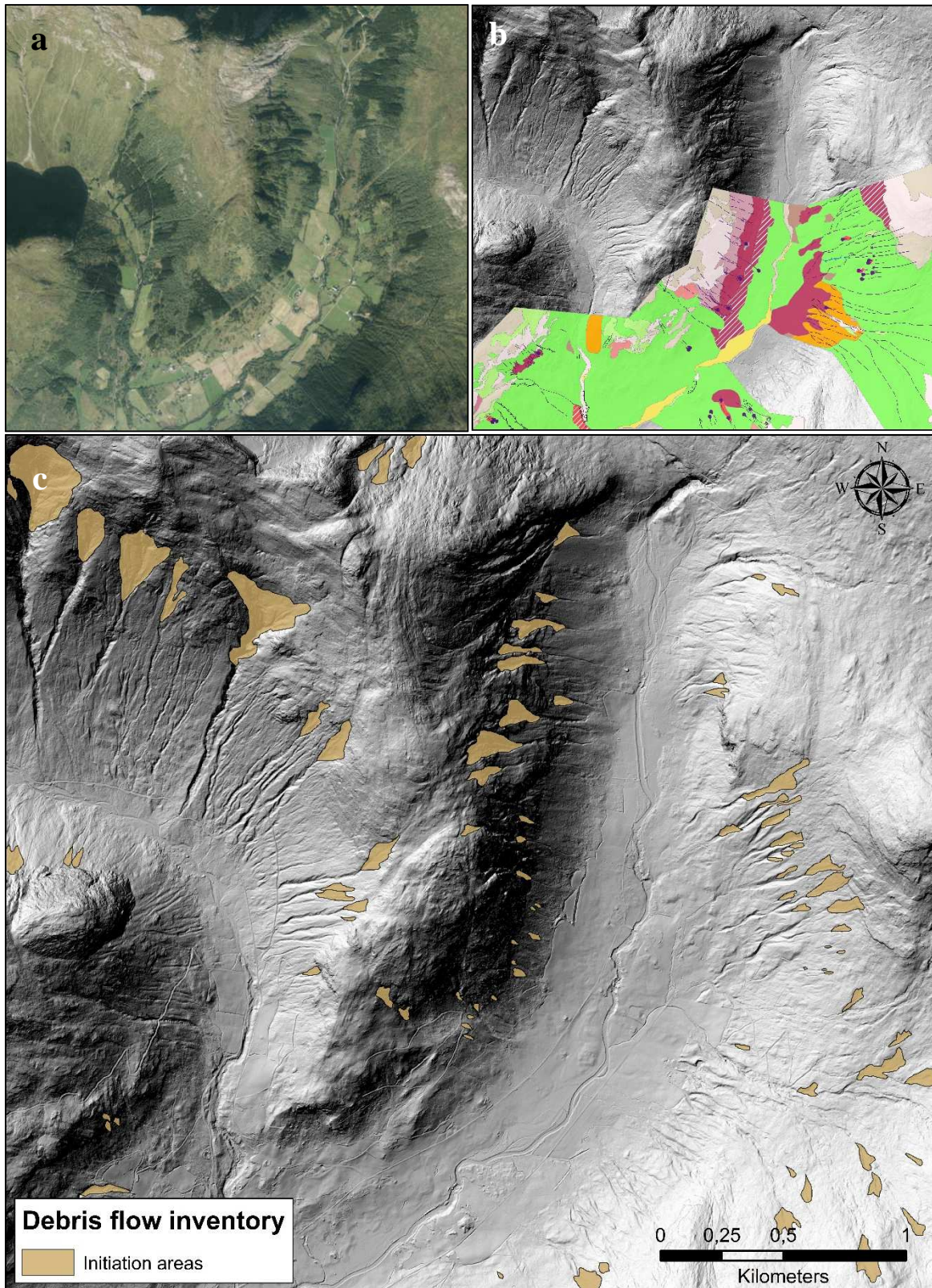


Figure 26. For the realization of the (c) new debris flow inventory, it was indispensable the joint use of (a) aerial photographs and (b) locally available quaternary maps.

Starting from the preliminary study of 1 m x 1 m terrain models (available on <https://www.hoydedata.no>) and from the validation accomplished through the field survey, a new inventory map for all debris flow initiation areas was compiled for Førde and Jølster territories. Other useful and indispensable maps were used for this goal: aerial photographs (available on <https://www.norgebilder.no>), quaternary maps (available on <https://www.ngu.no>) and the national mass movement inventory (available on <http://www.skrednett.no/>). The aerial photographs cover the Norwegian territory with different time spans and different resolutions throughout the country: the oldest satellite imageries are dated 1939 while the most recent ones are dated 2018 and have a resolution of 0.08 meters.

Quaternary maps realized by the Norwegian Geological Society (NGU) were locally available: they consist of shapefiles (polygons, lines, points) delineating sediments, soil and loose rock deposits which were formed during the past 2.6 Ma. Quaternary maps were of primary importance to delineate areas susceptible to initiate debris flows, despite the limited availability throughout the study area.

The national mass movement inventory includes more than 33 000 documented entries (Jaedicke et al., 2009) distributed among the country regions. Despite the large number of recorded events, only 710 entries are classified as debris flows. Several drawbacks are associated with this inventory: the records consist of points which can both indicate transition or deposition; the technical expertise responsible for the documentation of the reported events is various and split between different institutes, thus producing temporal and spatial inaccuracies; registrations of mass movements are usually restricted to accessible and populated areas. Considering the characteristics and the drawbacks, this inventory was regarded as unfitting for the scope of this study.

The new debris flow inventory consists of initiation areas (*Figure 26*), as the present research addressed the definition of a susceptibility map related to the initiation conditions of debris flows within the study area. On the other hand, the identification of landslide deposits was an important step in inferring the related initiation area. The inventory consists of 1105 polygons, where every element is stored in one of the previously mentioned categories (which are defined with respect to the triggering mechanism and geomorphological features). The location and the spatial extent of every release zone is well defined; the temporal occurrence of the mapped events is missing because of the lack of certain and detailed chronological records. The great number of events has to be imputed to the small and detailed scale analysis, the examination of remote areas and the fragmentation of single-event initiation areas in different polygons (to better define the effective release zone). The completion of the whole inventory was accomplished manually using ArcMap 10.1, in order to obtain an accurate dataset for post-processing analysis. Possible sources of errors are linked to the bad interpretation of the mass movement and, therefore, to the delineation of false initiation areas. In addition to that, some events could be unnoticed and not reported within the present inventory, cause slope failures can be easily (and rapidly) obliterated by other mass movements, erosional processes, growth of vegetation, and human actions (Reichenbach et al., 2018).

4.1.4. Statistical evaluation of terrain data

One further aim of this research was to assess the statistical significance and data distribution of the terrain topographic variables (slope, flow accumulation, curvature and roughness are

explained in detail in section 5.1.1) within the mapped release areas and the related upper portion of the catchment.

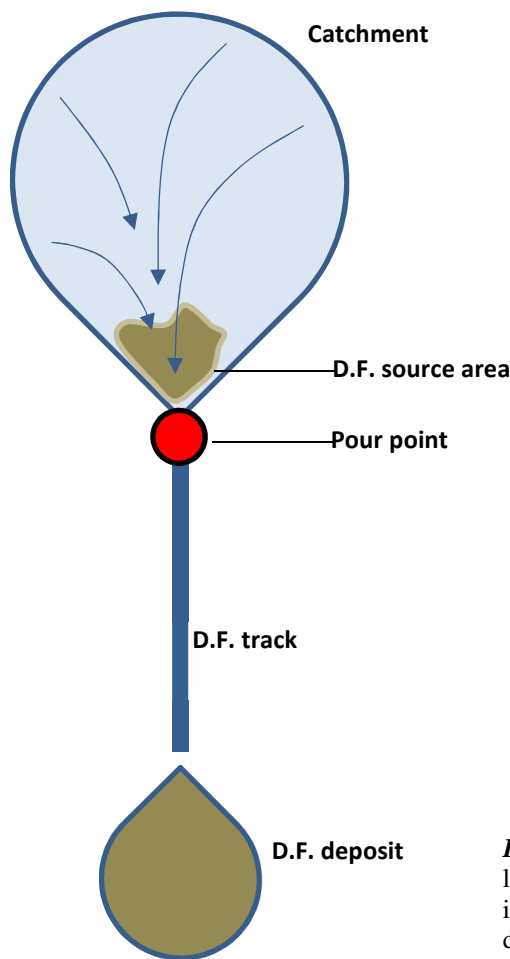


Figure 27. Conceptual scheme representing the location of a pour point. The key issue of this operation is the distinction of the initiation and the transport domain.

The choice of studying the latter object arises from the need of evaluating the hydrogeological conditions under which the observed debris flows initiate. This was possible by determining the number of contributing cells insisting on the mapped initiation areas. As the source areas were fully determined with the completion of the inventory, the catchments had to be circumscribed (*Figure 29*): this has been made possible by identifying the pour points located between the debris flow initiation domain and the transport domain (*Figure 27*). In this way, only the area contributing to the defined pour point was delineated. This was accomplished by using ArcGIS 10.1., with which the flow accumulation rasters were calculated from the available DEMs of the study area and both Snap pour point and Watershed tools of Spatial analyst toolboxes were employed: the pour points were manually placed on the cell of highest flow accumulation between the initiation and transport domain and the watershed related to every catchment was calculated.

The last step concerned the mean and standard deviation values which were derived with the tool Zonal statistics as table (ArcGIS 10.1) which was helpful to determine statistics within source area polygons and catchment polygons. Once again, source areas and related catchments were assigned to one of those four category which were determined during the field survey (based on triggering mechanism and geomorphological features of the observed debris flow).

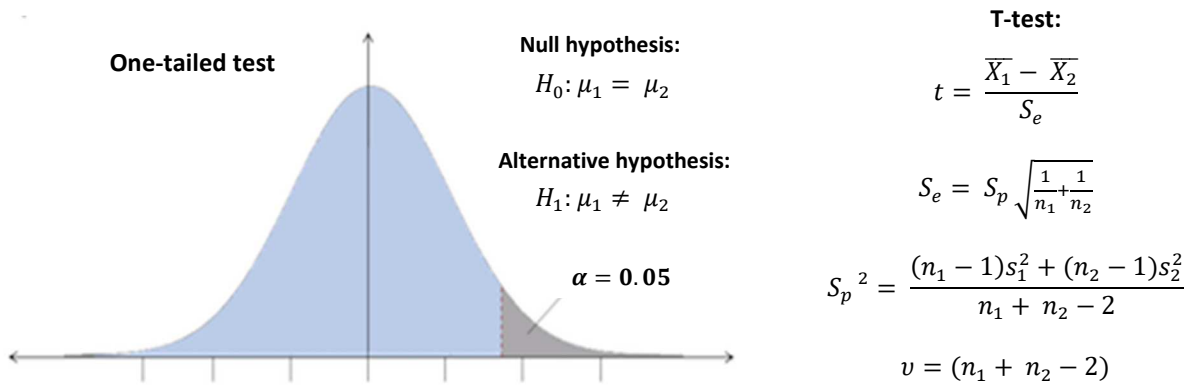


Figure 28. Explanatory image and formulas used for the performed one-tailed T-tests, where S_e is the standard error, S_p is a *pooled* estimate of the standard deviation, found by combining the sample variances of the two data sets, v stands for the degrees of freedom, while \bar{X}_i and n_i refer to sample mean and sample number of elements.

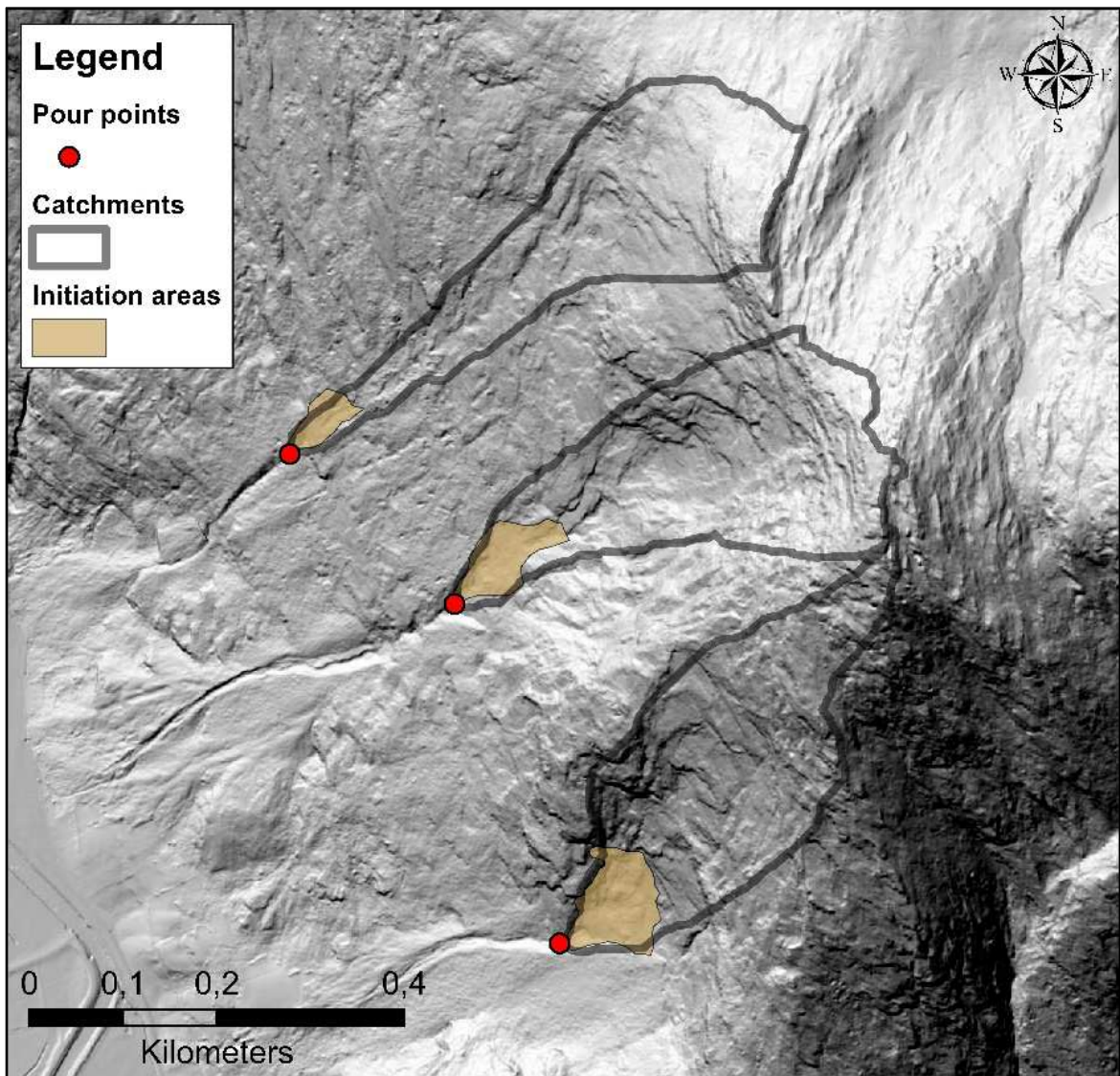


Figure 29. Example of how the catchments (related to every source area) are extracted from the detected pour points.

Ultimately, F-tests and one-tailed Student's T-tests (*Figure 28*) were performed, considering data belonging to every category as different samples, where the comparison terms were the sample variance (F-test) and the mean value (T-test). T-test could be accomplished where the F-tests were positive (a critical assumption is that the tested sample variances need to be equal) and because the populations from which the samples were drawn are normally distributed (another required assumption to perform the tests).

Statistical tests were referred to:

- Spatial extension of catchments (flow accumulation).
- Slope gradient and curvature within source areas and catchments.
- Roughness within the only source areas.

All these topographic parameters were derived from digital elevation models of 1 m x 1 m resolution using the Arc Toolbox functions of ArcGIS 10.1. The choice of the terrain variables to be tested fall on the most common and pertinent parameters which are clearly linked to the assessment of the debris flow initiation susceptibility. In this thesis, curvature and roughness, are considered as proxies for the quantification of the slope morphology which in turn are linked to erosion, run-off processes and sediment availability.

Every category (considering source areas and catchments separately) was tested pair-wise for the equality of the sample means (H_0) with a 5% level of significance ($\alpha = 0.05$), implying that it is acceptable to have a 5% probability of incorrectly rejecting the null hypothesis.

All the calculations were performed using Microsoft Excel.

4.2. Results

In the following sections the results of the statistical analyses performed over the mapped debris flow source areas (contained within the inventory) and the related upper catchments are reported, where special attention is given to the subdivision in categories.

4.2.1. Statistical comparison between source areas categories

	Source areas									
	Categories									
	1		2		3		4		tot	
	<i>mean</i>	<i>std</i>	<i>mean</i>	<i>std</i>	<i>mean</i>	<i>std</i>	<i>mean</i>	<i>std</i>	<i>mean</i>	<i>std</i>
Slope (°)	37.3	6.6	47.1	8.0	25.5	6.3	30.6	5.5	35.9	8.2
Curvature (m^{-1})	-2.15	1.94	-4.07	2.53	-0.92	0.58	-2.34	1.88	-2.31	2.01
Roughness (<i>M</i>)	0.08	0.03	0.16	0.14	0.05	0.01	0.06	0.01	0.08	0.05

Table 2. Mean and standard deviation calculated for terrain data distributions within the mapped initiation area polygons.

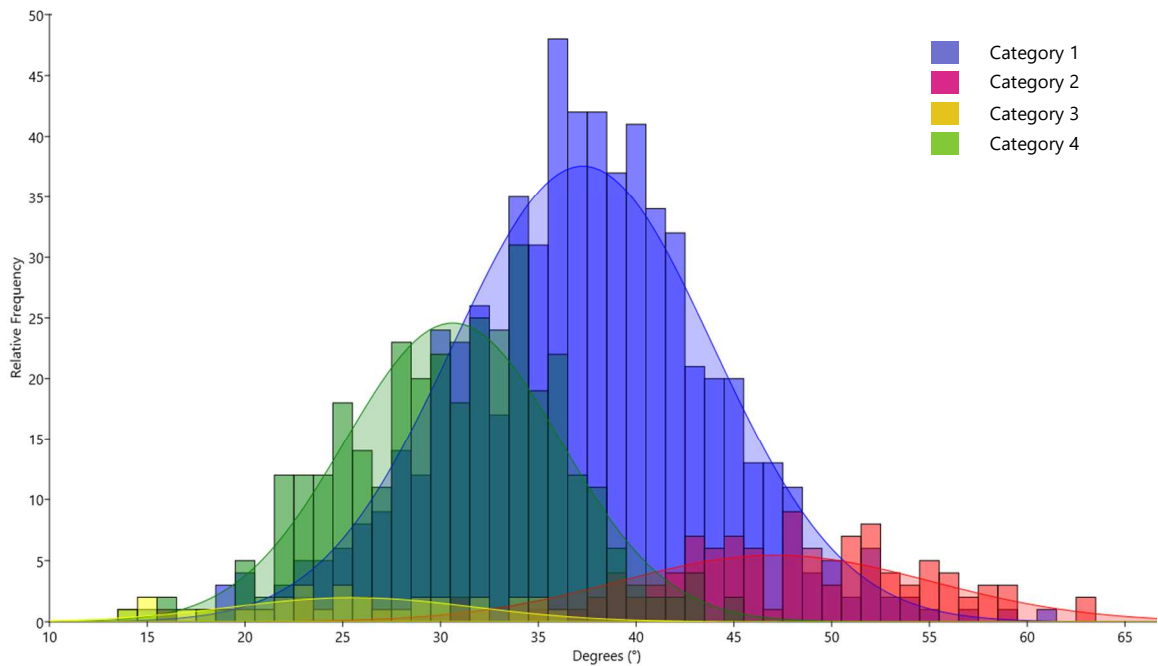


Figure 30. Frequency distribution of the mean slope values within all source area polygons, considering the subdivision in categories. Bin width = 1°.

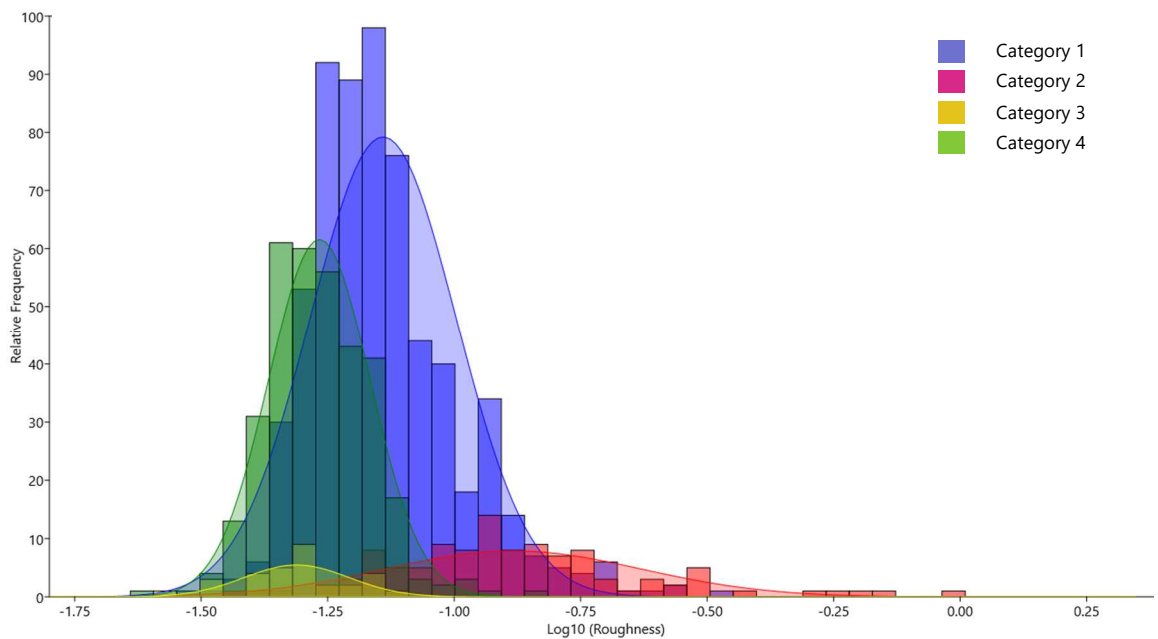


Figure 31. Frequency distribution of the mean roughness values within all source area polygons considering the subdivision in categories. The graph shows log-transformed values. Bin width = 0.04.

The performed F-tests and T-tests over the mean values of the terrain data variables of slope, curvature and roughness gave all negative results. All sample distributions within source areas polygons were obtained by subdividing the terrain distribution data (statistical populations) among the respective terrain categories (based on triggering mechanism and geomorphological features of the observed debris flow). Every tested sample was found to be statistically different from the others (*Figure 30, 31, 32*). The four categories were tested pair-wise for each topographic parameter and every possible combination between them was

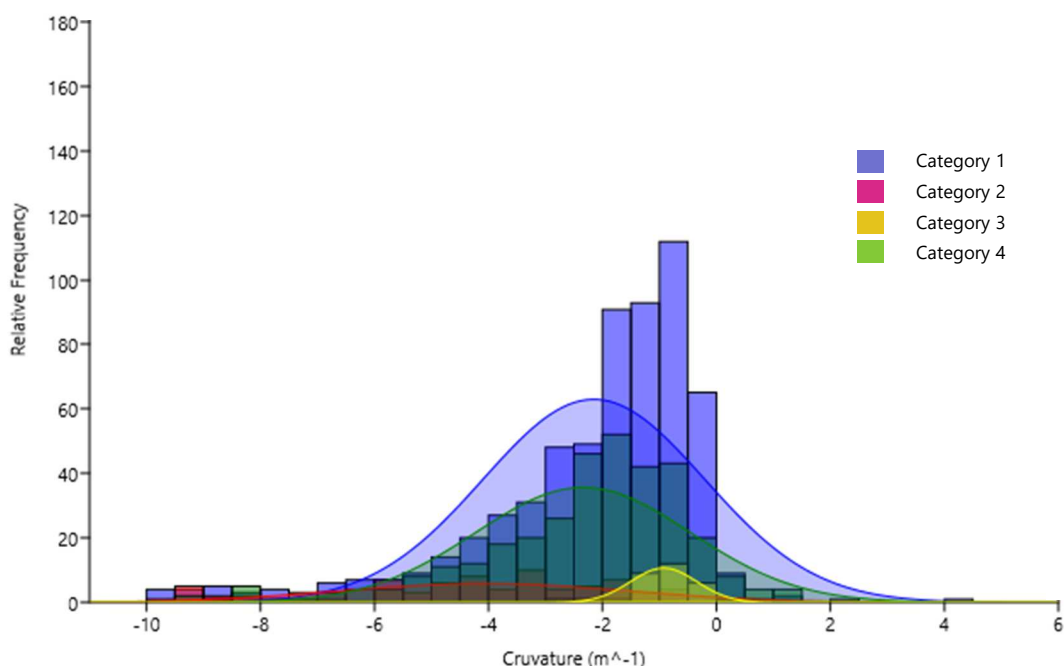


Figure 32. Frequency distribution of the mean curvature values within all source area polygons, considering the subdivision in categories. Bin width = 0.5 m^{-1} .

performed. Where some of the combinations resulted in positive F-tests, the following T-tests gave negative responses in every case.

Within all source areas, the average value of slope gradient is 35.9° , curvature is -2.31 m^{-1} and roughness is 0.08 m .

For what the data distributions within the categories (*Table 2*), some observations can be made:

- The second category (debris flows with deep incised gullies) shows the greatest mean value of slope (47.1°), curvature (-4.07 m^{-1}) and roughness (0.16)
- The third category (debris flows set along glaciofluvial channels) has the lowest mean values (slope: 25.5° , curvature: -0.92 m^{-1} , roughness: 0.05 m).
- The two remaining categories show values closer to the totality of the source areas, with the first one (short and clustered debris flows on open slopes) relatively steeper (37.3°) and with a bigger value of mean roughness (0.08 m).
- The fourth one (which relates to debris flows initiating as shallow soil slips) holds a gentler slope and a smaller value of roughness (slope gradient: 30.6° ; roughness 0.06 m) than the first category.

Generally, the standard deviation of the mean values distributions is large for each terrain variable.

4.2.2. Statistical comparison between catchments categories

For what concerns the upper catchments related to the detected debris flow source area in *Førde* and *Jølster* territories, the performed F-tests and T-tests over the mean values of the

terrain data variables of catchment contributing area, slope and curvature gave all negative results. All sample distributions within the catchment polygons were obtained by subdividing the terrain distribution data among the respective terrain categories (*Figure 33, 34, 35*) and were tested pair-wise considering every possible combination between the different topographic variables.

The calculated total mean areal extension is 0.04 km²; the mean value of slope is 33.6° while, on average, curvature is estimated to be about 0.01 m⁻¹.

	Catchments									
	Categories									
	1		2		3		4		tot	
	<i>mean</i>	<i>std</i>								
Area (km²)	0.04	0.04	0.11	0.14	0.25	0.24	0.02	0.04	0.04	0.07
Slope (°)	35.3	7.3	37.3	9.5	25.1	3.9	29.6	5.1	33.6	7.6
Curvature (m⁻¹)	0.01	0.14	-0.01	0.08	0.00	0.02	0.00	0.18	0.01	0.15

Table 3. Mean and standard deviation calculated for terrain data distributions within the catchment polygons related to every mapped source area.

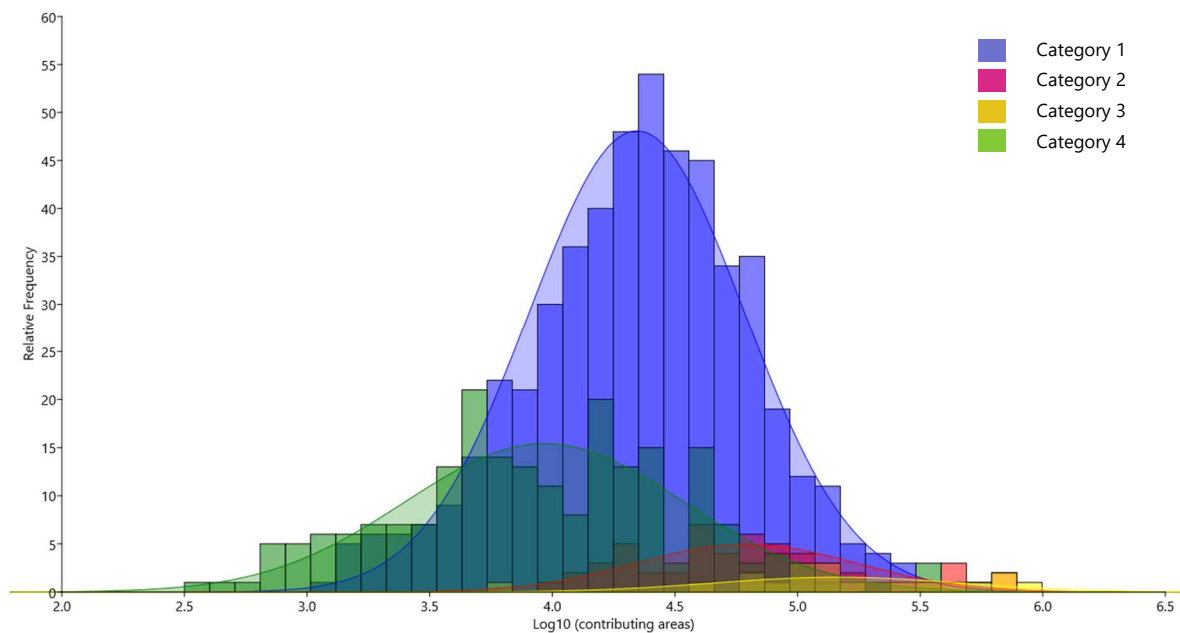


Figure 33. Frequency distribution of the mean areal values of the catchment polygons, considering the subdivision in categories. The graph shows log-transformed values. Bin width=0.16.

The data distribution within the categories is shown in *Table 3*:

- The third-category catchment shows the largest areal value (0.25 km²) and the lowest mean slope value (25.1°).

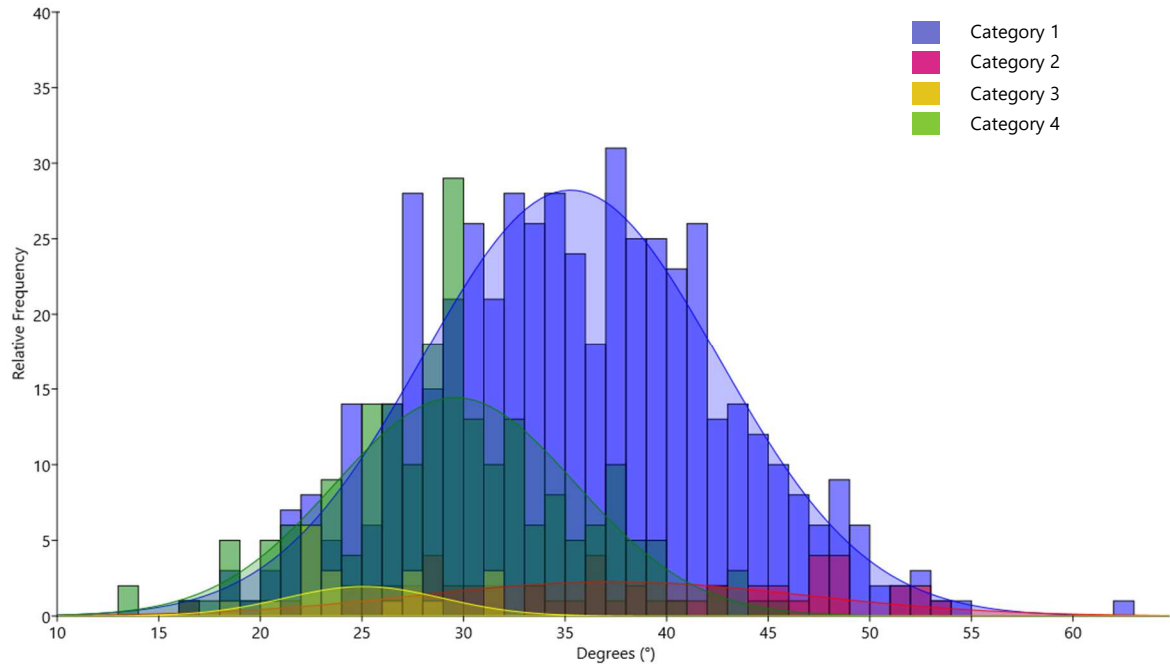


Figure 34. Frequency distribution of the mean slope values calculated within the catchment polygons, considering the subdivision in categories. Bin width = 1°.

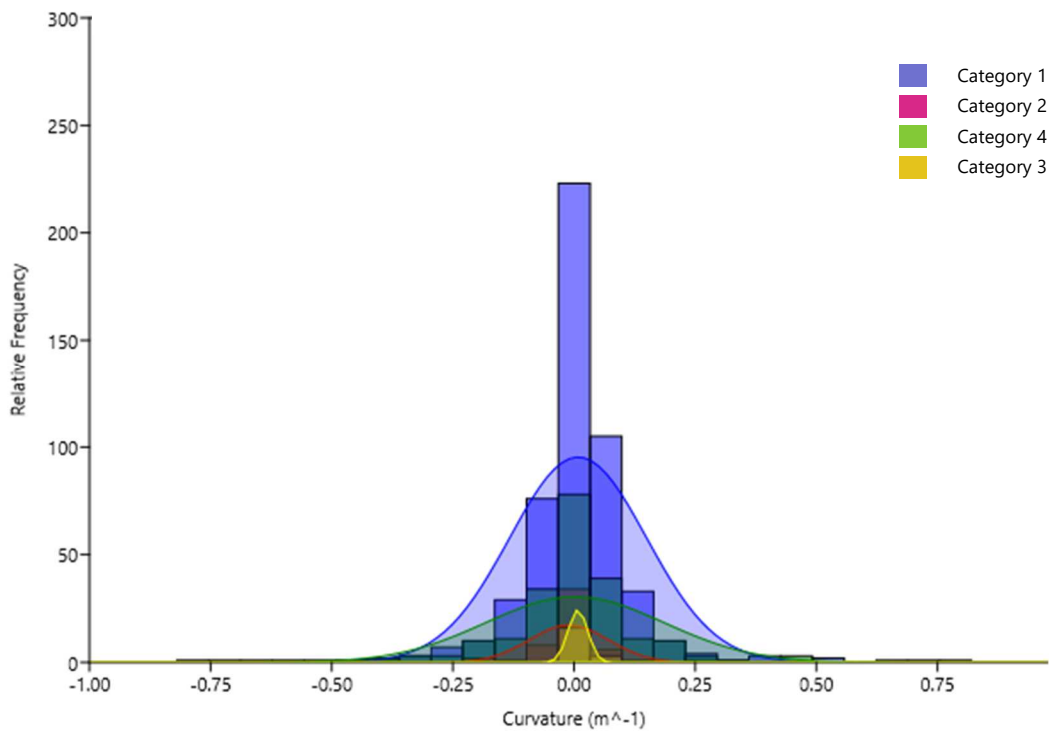


Figure 35. Frequency distribution of the mean curvature values calculated within the catchment polygons, considering the subdivision in categories. Bin width ~ 0.06 m⁻¹.

- The fourth category consists of catchments provided with very small areal values (0.02 km²) and with a mean slope value of 29.6°.

- The second catchment type, on average, is relatively vast (0.11 km²) and steep (37.3°).
- The first category shows values which are the most pertinent considering the totality of the catchments.

Higher values of standard deviation arise from the estimation of curvature, as well as from the distribution of the areal extent of the catchments (*Table 3*).

4.2.3. Discussion

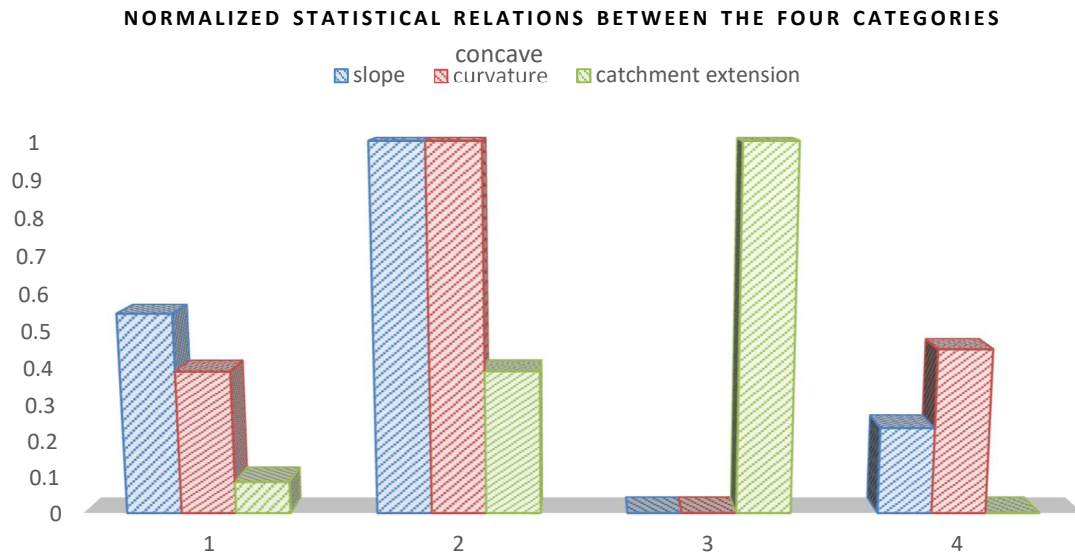


Figure 36. For a better and relative comparison between the data distribution of the 4 categories, the values are adjusted from 0 to 1, with 0 corresponding to the lowest value between the categories and 1 to the largest. Curvature is referred to negative values (see *Table 3*), which in turn represents a measure of surface concavity.

The relations (in terms of the most representative terrain data) between the different categories are schematized in *Figure 36*: slope and curvature within the source areas and areal extension of the upper catchments are normalized from 0 to 1 for relative comparisons between the ranging values of the four categories. Every category weighted differently in data distribution assessment: the first category is 56% of the totality, the second is 10%, the third is 3%, the fourth is 31%.

Considering the totality of the mapped elements, the results show that within the study area, average values of slope calculated for all initiation areas are comprised between 26° and 47°, while upper catchments mean extensions fall between the interval 0.02 – 0.25 km². These values are comparable to the thresholds referred to the Norwegian territory reported by Fischer et al. (2012) and by Meyer et al. (2013).

On the basis of the informations collected during the field work and of the conducted statistical analysis, some statements concerning the different categories can be made:

- The standard deviation of the topographic parameter distributions within both mapped source areas and related catchments is generally large. The mean values of slope, curvature, roughness and contributing area are spread out over a wide range, indicating a great variability of the quantitative terrain features linked to the observed debris flows within the study area.
- The majority of the mapped debris flows are channelized, have a short track, usually cut through open slopes and start with bedload erosion (category 1), otherwise they can be triggered by shallow slips of the weathered soil covering the bedrock (category 4); despite channelized debris flow with wide and deep incised gullies (category 2) constitutes only 10% of the totality, they have a relevant impact on the landscape with their vast deposition fans. Category no. 3 is statistically irrelevant as it constitutes only 3% of the investigated initiation areas.
- Debris flows belonging to category no. 2 hold very steep and very concave initiation areas and the catchment extension insisting on the debris flow source zone is large as well. Under these conditions, those catchment type may direct great amounts of water into the prominent deep channels filled with weathered material. The availability of coarse debris and large boulders found in the deposition zones may be explained with a relatively higher average value of roughness within the source areas (see *Table 2*). The enhanced runoff can explain the large volumes and deposit fans of these debris flow-type, with which are generally associated. Debris flows of this kind are more easily detectable and monitored for their visible physical

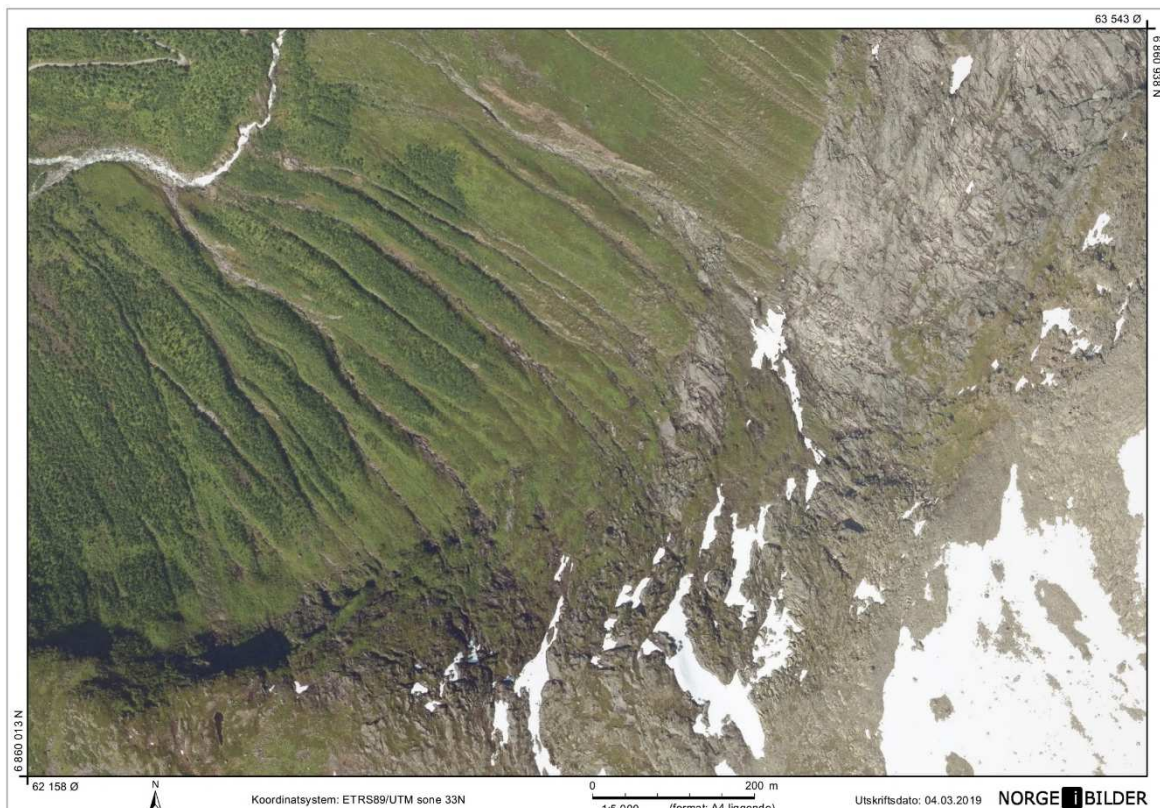


Figure 37. Aerial photograph (taken from Jølster municipality) showing debris flows mapped as belonging to the first category. It is discernible the steep and flat rock face insisting on the initiation zones, the numerous and dense flow tracks which coexist alongside and the absence of a well-defined fan. Enhanced run-off derived by intense rainfalls or snow melts may be the responsible for triggering debris flows of this kind, while debris slides or soil slips seem to be unrelated to the triggering mechanism of those type of phenomenon. (image source: norgebilder.no)

characteristics; however, they are not very widespread throughout the study area if compared to the first and fourth categories.

- Events related to the first (*Figure 37*) and fourth categories are strongly present in the study area. Even though they are linked to smaller areal extents of deposition zones and to smaller deposition volumes, the observed territory showed many signs of their recent and less recent activity (*Figure 37*). Given that these kind of mass movements usually trigger on steep and flat hillslope and given the presence of a favourable landscape throughout the study area (and throughout Western Norway), their spatial spreading is extremely difficult to predict. The two categories show similar curvature values. The source areas belonging to both categories show comparable “measures of concavity” thus indicating that the slope may concentrate similar amounts of surface runoff and subsurface groundwater flow. However, for what concern mean slope gradient values, the first category seems to occur in relatively more steep hilly areas. Interesting considerations can be made for debris flow belonging to the fourth category, where a relative low slope angle (mean value of 31°) is not counterbalanced by a larger contributing area (upper catchment mean value of 0.02 km^2). Possible reasons may be ascribed to undetected groundwater flow patterns of adjacent catchments or to the prominent role of direct infiltration during rainstorms.

5. Susceptibility modelling

5.1. Methods

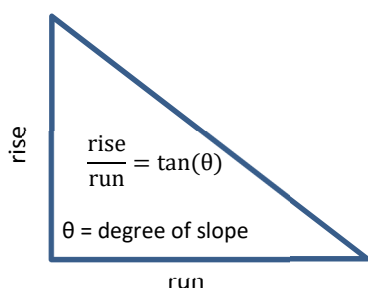
The contents of the following sections seek to outline the required steps to get the necessary data to be used in a susceptibility model for debris flow initiation assessment. For this study, the Weights of Evidence method is employed.

5.1.1. Terrain data and thematic layers

After the above-mentioned analysis (see chapter 4.2) of the functional relationships between known or inferred instability factors (slope, upslope contributing area...) and the past and present distribution of debris flows, this study aimed at exploiting the statistical method of WofE (Weights of Evidence) for landslide susceptibility modelling.

Debris flow source areas were considered as clipping masks for those terrain parameters and thematic maps which are regarded as important informative factors in statistical debris flow susceptibility modelling. The idea behind this is to find the conditions which have been critical in the past and extrapolate them in space to identify other potential debris flow source areas not affected yet. According to Van Westen et al. (2003), many statistical models relate debris flow inventories to the environmental surrounding conditions, as the main underlying assumption is that the initiation of future debris flows will occur under the same conditions as in the past. Here, few topographic parameters were considered as proper preparatory variables able to affect the slope stability:

- ❖ Slope gradient.
- ❖ Flow accumulation.
- ❖ DEM elevation.
- ❖ Total curvature.
- ❖ Roughness.



High degree of slope and high upstream contributing area are two aspects widely linked to increasing probability of mass wasting.

Slope is calculated as the ratio of the vertical rise and the horizontal run. It can be expressed in two type of units, degrees or percentage. For this thesis, slope degree (*Figure 40*) was directly calculated from the available DEMs of the study area (*Figure 38*) by using the Slope tool of Spatial Analyst toolbox (ArcGIS 10.1).

The flow accumulation (*Figure 39*) is a measure of the number of the accumulated cells flowing into each downslope cell. This parameter is of primary importance for hydrogeological calculations. For this thesis, flow accumulation rasters were obtained from different DEMs by performing the Fill tool (useful to remove small sinks and imperfections in the DEMs), Flow direction tool (which creates a raster of flow direction from each cell to its steepest downslope neighbour) and Flow accumulation tool of Spatial Analyst toolbox (ArcGIS 10.1).

Curvature (*Figure 40*) is calculated as the second derivative of the surface (unit of measure: m^{-1}). It can be regarded as a helpful parameter to estimate how water flows across the topographic surface, to understand erosion and runoff processes, to estimate the physical characteristics

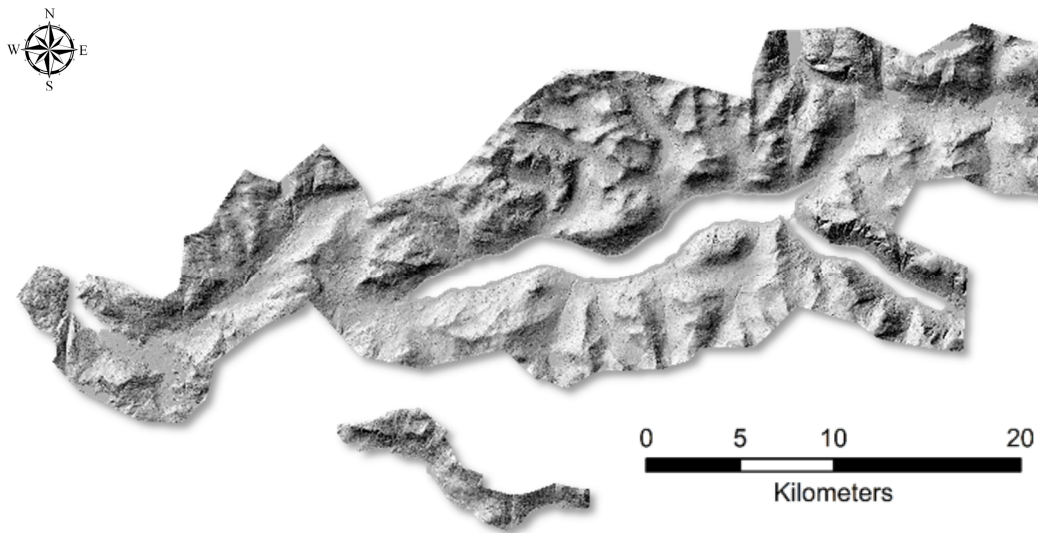


Figure 38. Digital elevation models of the study area.

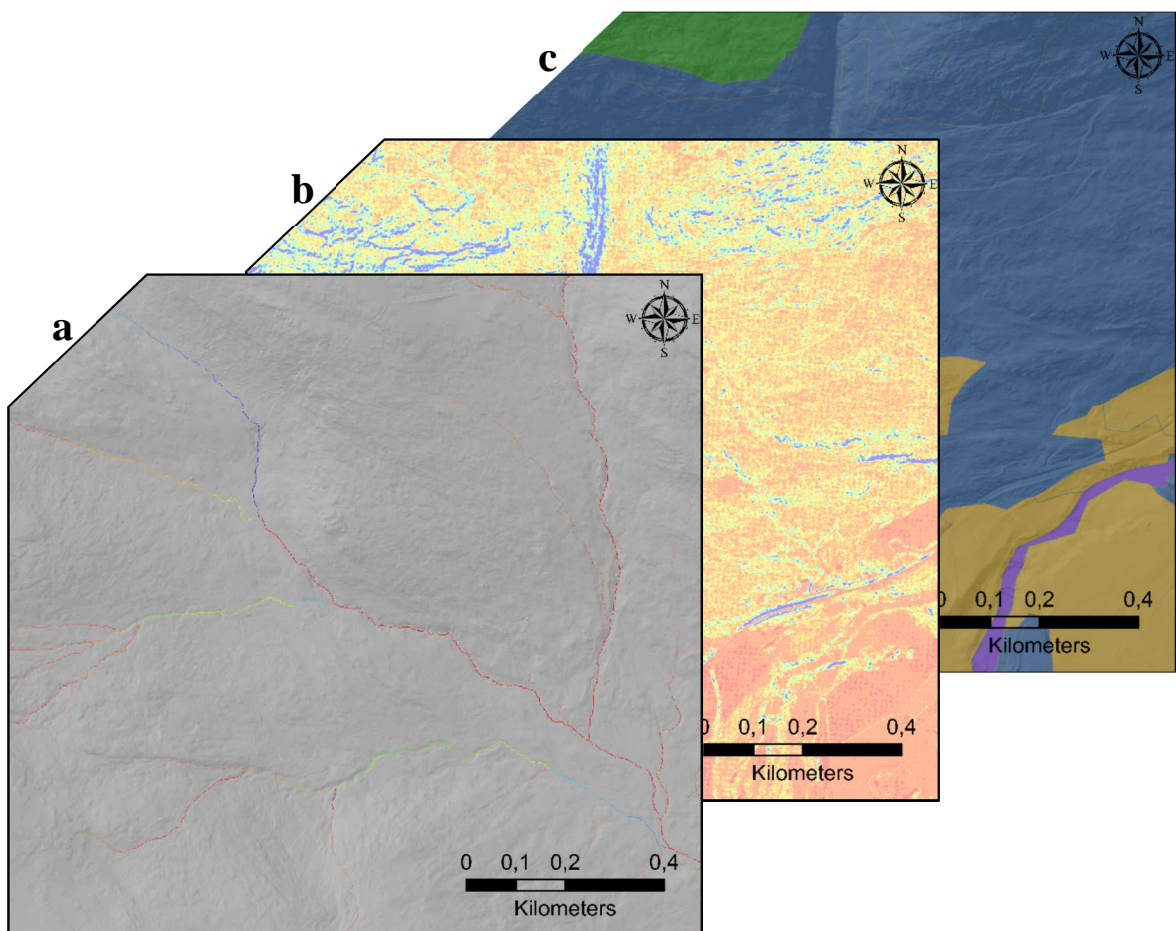


Figure 39. Some examples of the terrain data layers and the thematic layers used: (a) flow accumulation, (b) roughness and (c) AR50.

of a drainage basin and deduce where greater thicknesses of soil gather. Total curvature is the combination of two orthogonal normal sections of the terrain surface (which are called the profile and the plan curvature) and describes the topographic surface curvature, regardless of slope direction. Negative values of curvature indicate that the surface is upwardly concave at that cell, while positive values indicates convexity. Total curvature is here calculated through the Curvature tool of Spatial Analyst, as it need a DEM as input.

Roughness is defined as a measure of the local surface topographic variability, where high values are related to high fraction of finely spaced micro-irregularities on the surface texture. Topographic roughness may be based on standard deviation of slope, standard deviation of elevation, slope convexity, variability of plan convexity, or some other measure of topographic texture. Terrain roughness (*Figure 39*) is here derived by calculating the standard deviation of the subtraction between a DEM and the same smoothed elevation model (unit of measure: *m*). This could be accomplished with the joint use of Focal Statistics tool (using a 3 x 3 calculation window) and Raster Calculator tool of Spatial Analyst toolbox. The resolution of the roughness map corresponds to the resolution of the DEM used for the extraction.

Apparently, the DEM elevation is not directly related to slope instability. For this thesis it is taken into account as it has been successfully applied to landslide modelling in many cases (Reichenbach et al., 2018).

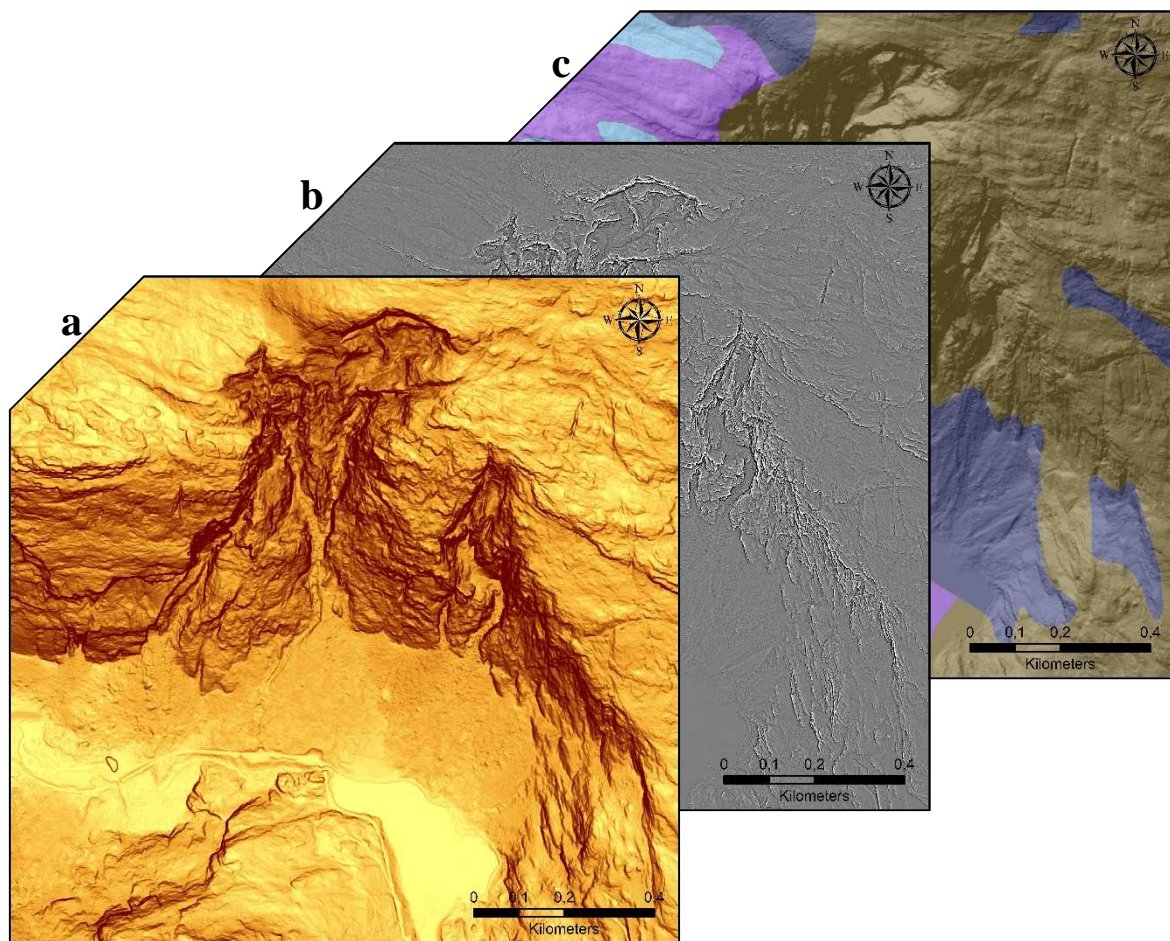


Figure 40. Some examples of the terrain data layers and the thematic layers used: (a) slope, (b) total curvature and (c) Løsmasser N50.

Curvature and roughness are the only variables whose value range is directly correlated with the cell size of the used DEM, with bigger ranges associated to elevation models with smaller cell size.

In addition to the above-mentioned continuous variables, categorical datasets were chosen to be included in susceptibility modelling. It is commonly acknowledged that some geolithological types, some types of quaternary sediments, vegetation and human activity may influence debris flow initiation.

Two thematic layers were here considered:

- *Løsmasser N50* (Figure 40), which is the map of the main soil types and superficial deposits covering the bedrock surface, with data mapped in scale 1:50 000 or finer (available on <https://www.ngu.no>).
- *AR50* (Figure 39), which is literally the areal resources map. It can be regarded as the land use map, with data represented in scale 1:50 000 or finer (available on <https://www.nibio.no>).

The first thematic map mainly shows the distribution of moraine deposits, landslide deposits, fluvial deposits, glaciofluvial deposits, organic deposits and exposed bedrock.

The second thematic map consists of a multi-layer map. For this study, the layer referred to as “Arealtype” was used. This layer partitions the study area in arable land, farmland, swamp zones, forest, anthropogenic areas, areas covered by scrub and low forest vegetation, areas permanently covered by ice or snow, river/lake, sea.

The reason related to the employment of the above-mentioned terrain continuous variable is explained: all the parameters that were judged ambiguous or inconsistent with the associated problem are here avoided. For what concerns the thematic layers, the choice was made because of the restricted availability of such products (e.g. the scale of the only available bedrock map was too coarse).

5.1.2. D.F. initiation susceptibility

5.1.2.1. Weights of Evidence

This research aimed at coupling direct and indirect detailed mapping of debris flow source areas with statistical modelling. The first aspect is usually related to small scale studies, while the second is typical of regional-scale studies. The decision of correlating a set of environmental indicators with a debris flow inventory is common. This approach inevitably derives from the lack of spatially distributed physical parameters such as soil depth or slope hydrology, which are the only unambiguous data related to slope instability. Nevertheless, landslides and their occurrence are controlled by physical laws that can be analysed empirically, statistically, or deterministically. Conditions that cause landslides (i.e., the instability factors), directly or indirectly linked to slope failures, can be collected and used to build predictive models for landslide spatial occurrence (Hutchinson, 1988). Statistical susceptibility maps (which show the spatial proneness to landslide without quantifying any probability) still remain powerful and reliable objects able to exploit terrain and categorical variables which approximate the landslide-preparatory factors (Dai et al., 2002; Van Westen et al., 2005) and to quantify their influence; in this way, the explanation of the exact relation between slope and landslide occurrence is overcome.

Debris flows need a steep slope, availability of unconsolidated sediment and sufficient water supply: slope gradient, flow accumulation, curvature, roughness, superficial deposit type,

land use and bedrock type can be regarded as direct and indirect factors affecting the spatial likelihood of debris flows.

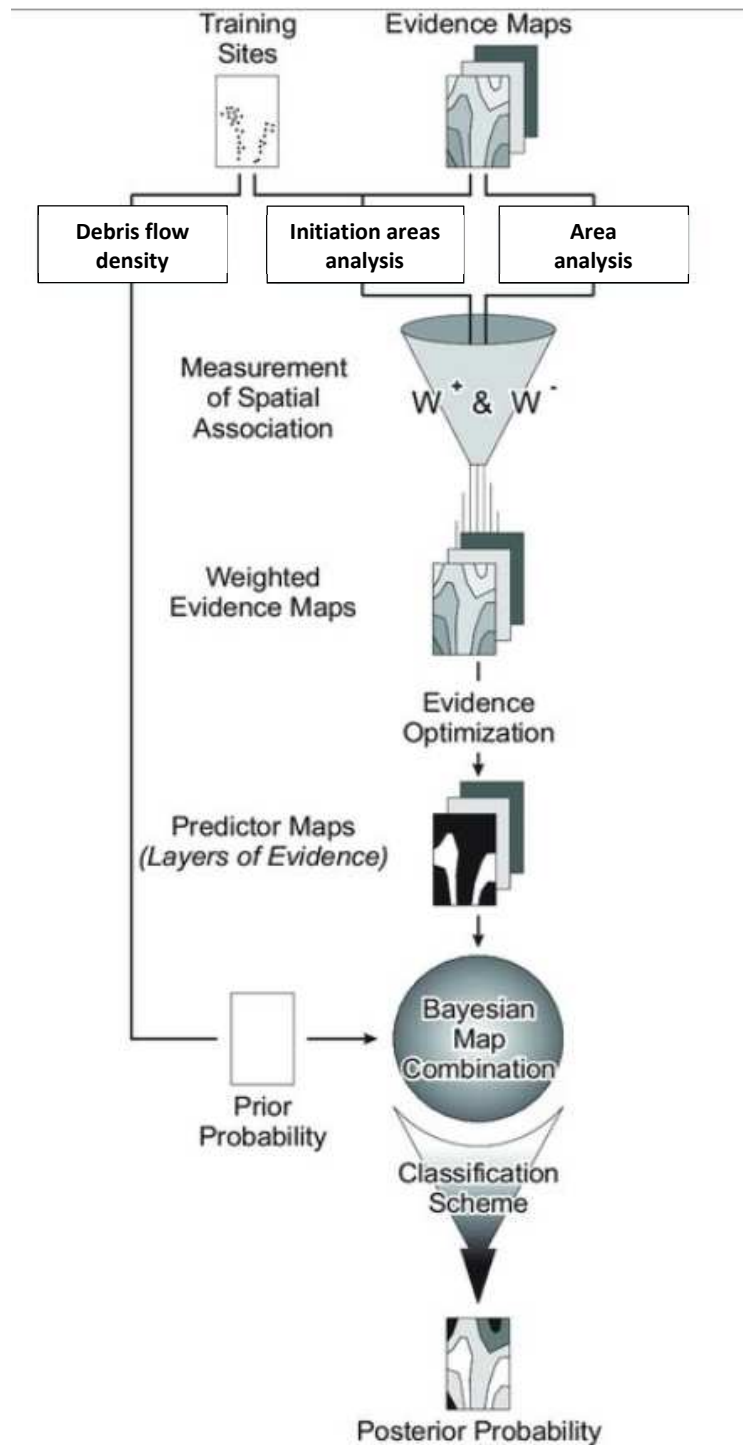


Figure 41. Flow chart illustrating the Weights of Evidence modelling method. (source: Leonard et al., (2002), modified).

A Weights of Evidence method (Figure 41) was here chosen to couple the above-mentioned predictor variables. WofE is a data-driven statistical bivariate method using a log-linear form

of Bayes' theorem to determine the weight of importance of every single factor (Bonham-Carter, 1994). To apply WofE, the first step is to compute the prior probability of landsliding. This task is accomplished by using the training data set (Figure 42), which corresponds to the inventory of debris flow initiation areas in the study area (Figure 41). The spatial density of the reported events is then used to compute the odds, which is the ratio of debris flow occurrence probability to the probability that it will not occur:

$$P_{\text{priori}} = \frac{N_{\text{pix}(\text{landslide})}}{N_{\text{pix}(\text{total})}}$$

$$O_{\text{priori}} = \frac{P_{\text{priori}}}{1 - P_{\text{priori}}} = \frac{N_{\text{pix}(\text{landslide})}}{N_{\text{pix}(\text{total})} - N_{\text{pix}(\text{landslide})}}$$

where $N_{\text{pix}(\text{landslide})}$ is the number of raster cells containing mapped debris flow source areas, while $N_{\text{pix}(\text{total})}$ is the total number of every cell in the study area.

WofE method is a binary classifier system and it can only operate with discrete predictor variables: while land use and superficial deposits maps are already categorical data, values of slope, flow accumulation, curvature, elevation and roughness needed to be reclassified in defined classes consisting of small ranging values. The underlying principle of this method is the evaluation (in terms of pixels) of the presence or absence of the predictor variable classes within debris flow source areas and the consequent attribution of their relative weight. WofE is based on the measurement of the spatial association of every reclassified predictor variable.

According to Bayes' theorem, the frequency of a variable can be used to estimate its probability. In this way, for j classes related to i variables, positive weights (W_{ij}^+) and negative weights (W_{ij}^-) can be computed as follows:

$$W_{ij}^+ = \log_e \frac{\frac{N_{\text{pix}(1)}}{N_{\text{pix}(1)} + N_{\text{pix}(2)}}}{\frac{N_{\text{pix}(3)}}{N_{\text{pix}(3)} + N_{\text{pix}(4)}}}; W_{ij}^- = \log_e \frac{\frac{N_{\text{pix}(2)}}{N_{\text{pix}(1)} + N_{\text{pix}(2)}}}{\frac{N_{\text{pix}(4)}}{N_{\text{pix}(3)} + N_{\text{pix}(4)}}}$$

***j*th class of *i*th variable**

Debris flow source area	<i>presence</i>	<i>absence</i>
<i>presence</i>	$N_{\text{pix}(1)}$	$N_{\text{pix}(2)}$
<i>absence</i>	$N_{\text{pix}(3)}$	$N_{\text{pix}(4)}$

where, with $W_{ij}^+ > 0$ the predictor variable class is positively correlated with debris flow occurrence; with $W_{ij}^+ < 0$ the predictor variable class is negatively correlated; no correlation exists if $W_{ij}^+ \sim 0$. Conversely with $W_{ij}^- > 0$ the predictor variable class is negatively correlated with debris flow occurrence; with $W_{ij}^- < 0$ the predictor variable class is positively correlated; no correlation exists if $W_{ij}^- \sim 0$.

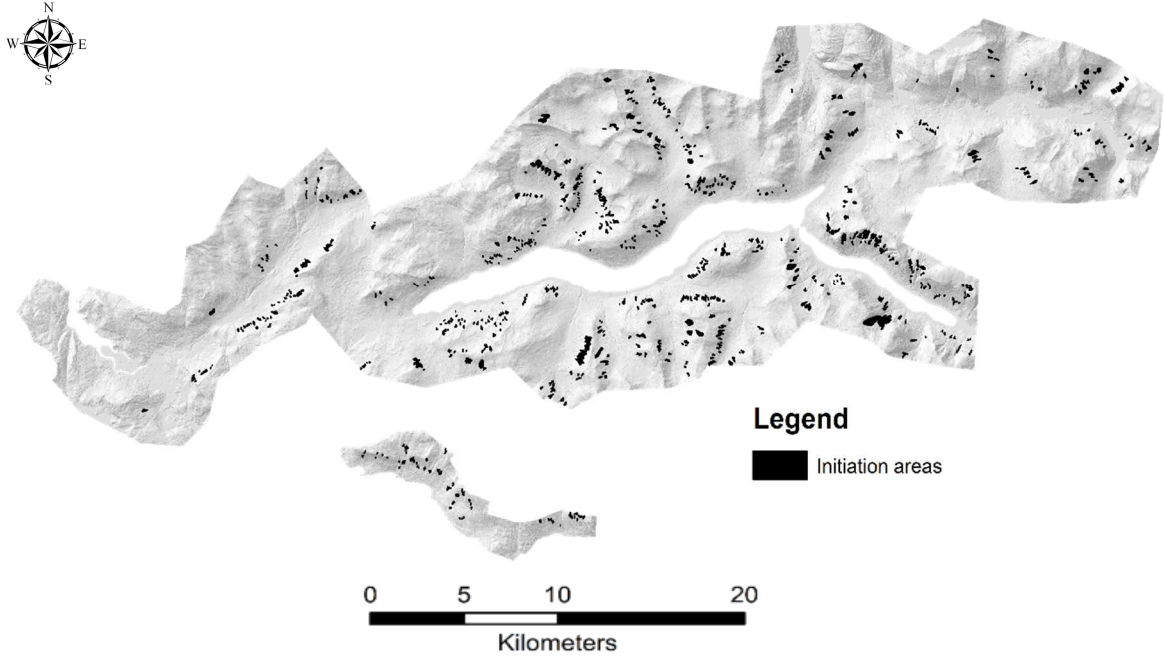


Figure 42. Overview of the inventory map related to debris flow initiation areas. For this thesis, this object was used as the training data set for WofE modelling. It was reclassified (with ArcGIS 10.1) in a binary raster map to differentiate the presence or absence of debris flow source areas.

At first sight, the contrast C , which is the difference between W_{ij}^+ and W_{ij}^- , gives the rate of correlation of a determined variable class with the landslide occurrence.

$$C = W_{ij}^+ - W_{ij}^-$$

Positive weights and negative weights retain the same importance in computing the proneness of a certain variable class to initiate debris flows.

All the weighted values obtained are then overlaid and combined in order to obtain the posterior probability, which is in turn calculated from the posterior odds as follows:

$$\text{Log}_e O_{posterior} = \sum_{i=1}^n \sum_{j=1}^m W_{ij}^{\pm} + \text{log}_e O_{priori}$$

$$P_{posterior} = \frac{O_{posterior}}{1 + O_{posterior}}$$

The posterior probability is the landslide susceptibility index (LSI) and can be regarded as an updating of the prior probability. Through the informative layers it has added additional evidence (in terms of landslide occurrence probability) to those terrain units (raster cells) which contemporary belong to predictors classes positively associated with debris flow initiation and don't belong to classes negatively associated with debris flow source areas. The final product of the WofE modelling is a raster map reclassified to the posterior probability (LSI), where the raster values owning higher values corresponds to higher probabilities of landsliding. Where the value of LSI exceeds the prior probability, there is a

positive correlation with the targeted phenomena; in the event that the posterior probability equals the prior probability, no further predictive information is gained.

An implicit assumption in the Bayes' theorem is the conditional independence of the different predictor variables employed. Bonham-Carter (1994) points out that all classes of every predictor have to be tested pair-wise and the contingency table must include a χ^2 value for all possible combinations of the classes of two predictor variables. Both the assumption and the conditional independence test are, in practice, difficult to respect and to accomplish (given the huge number of possible combinations between the different classes). For this reason, in order to directly reduce the effects related to the possible conditional dependence, some of the predictor variables could be alternatively omitted in the computation of the posterior probability; this can result in an enhanced fitting between the susceptibility map and the landslide inventory.

All the steps necessary to run the WofE model were accomplished through to the joint use of ArcGIS 10.1 and MATLAB R2018b, where the first was used for converting rasters to ASCII files and vice versa (achieved by using the Conversion toolbox), and the second was used as the environment for computing the Weight of Evidence method.

5.1.2.2. Model performance

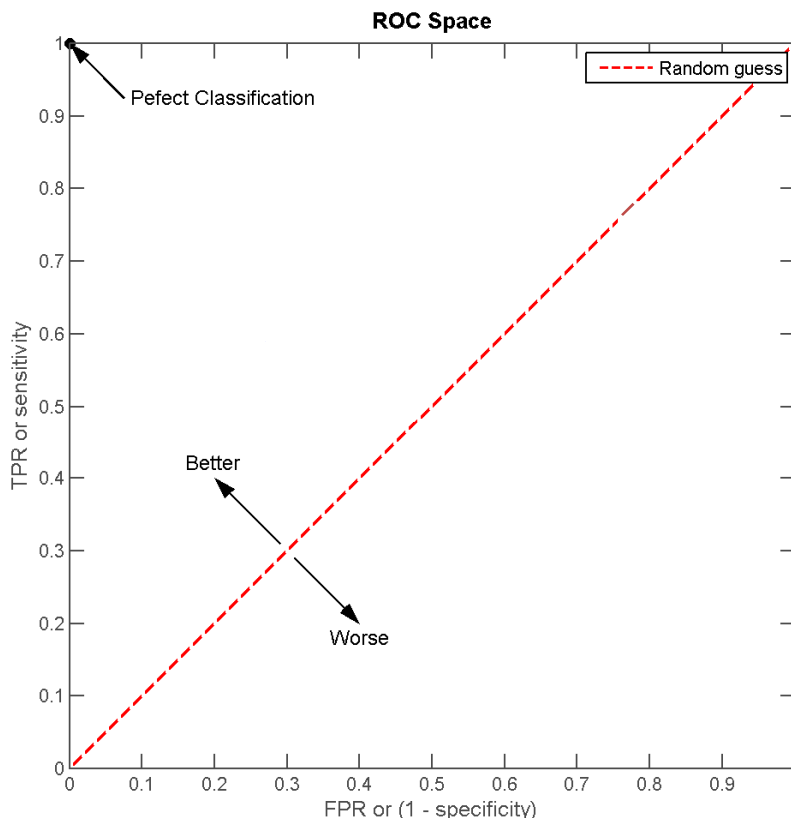


Figure 43. The ROC space. (source: Wikipedia, modified)

The landslide susceptibility map obtained by using the WofE method needed to be tested for its reliability. The receiving operating characteristic (ROC) curve is one of the most

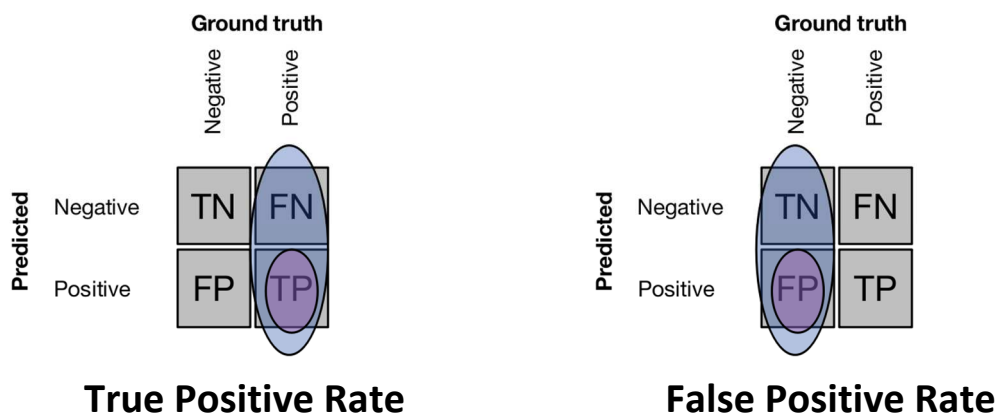
commonly used metrics in the literature to evaluate the model fitting performance and the model prediction performance. In combination with the ROC curve, which is used to visualize the performance of a binary classifier, the AUC (Area Under Curve) value can be regarded as the best way to summarize the model performance in a single number. Generally speaking, the higher the area under the ROC curve the better the model at distinguishing terrain units which are susceptible to initiate a landslide from those which are not susceptible.

The ROC curve and the respective AUC value are related to classification problems at various thresholds settings. The ROC curve is plotted with True Positive Rates (TPR) against the False Positive Rates (FPR) where TPR is on the y-axis and FPR is on the x-axis. TPR (or Sensitivity) is the probability of detection of correctly classified debris flow cells (True Positives) within the mapped source areas (condition positive); FPR is the probability of finding falsely classified debris flow cells (False Positives) within the mapped source area (condition positive). FPR can also be calculated as $1 - \text{Specificity}$, where specificity is the ratio of True Negatives to the sum of true negatives and false positives (FP). In a binary classification system like WofE, there are four possible outcomes: in addition to the ones which are mentioned above (TP and FP), a True Negative (TN) occurs when a raster cell is correctly classified as stable (it falls outside debris flow source area), while a False Negative (FN) is falsely classified as instable.

$$TPR = \frac{TP}{TP + FN}$$

$$\text{Specificity} = \frac{TN}{TN + FP}$$

$$FPR = 1 - \text{Specificity} = \frac{FP}{TN + FP}$$



Sensitivity and Specificity are inversely proportional to each other. When the decision threshold of LSI (Landslide Susceptibility Index) is decreased, this would result in more True Positives and less True Negatives thus there is an increasing of the TPR (Sensitivity). Similarly, when the threshold is increased, this would result in fewer False Positives and more False Negatives thus, we obtain lower FPR (Figure 44).

It can be deduced that the guiding principle of ROC curves concerns the analysis of the probability distributions for both detection and false alarm. The rate of “separability” (the

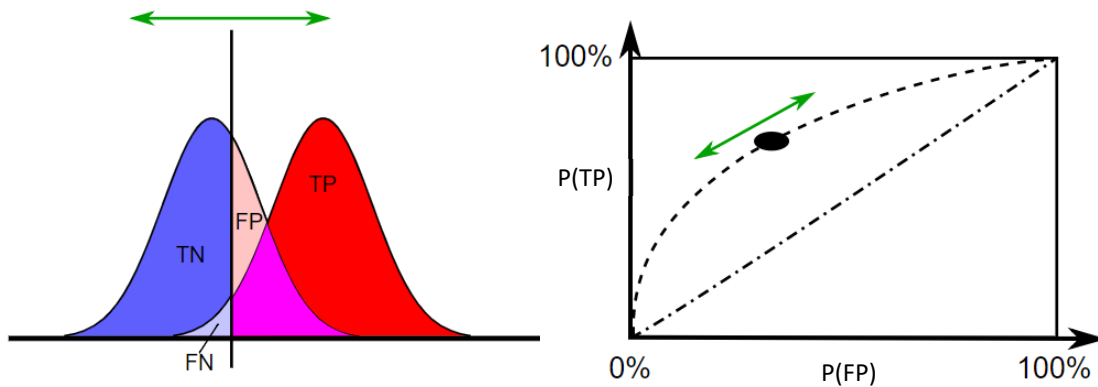


Figure 44. By varying the decision threshold, the value of TP, TN, FP, FN changes. The increase of the threshold corresponds to a leftward movement in the ROC space; the decrease of the threshold corresponds to a movement to the right. (source: Wikipedia, modified)

overlap between the two distributions) determines the shape of the curve and thus how capable the model is to distinguish between the truly predicted raster cells and the false alarms. The best-case scenario would be when the two distributions do not overlap; vice versa, type 1 (false positive findings) and type 2 (false negative findings) statistical errors are introduced (*Figure 44*). By varying the decision threshold, they can be minimized or maximized.

FPR and TPR respectively depicts relative trade-offs between True Positives (benefits) and False Positives (costs). In our case, the best balance is accomplished by varying the decision threshold (Cut-off value) of LSI value over the whole range for a fixed number of times. ROC analysis provides tools to select possibly optimal models and to discard suboptimal ones, where the decision making is independently from (and prior to specifying) the cost context or the class distribution. The area under the curve (AUC) shows values that state the spatial accuracy assessment for the model. The best possible prediction method would result in a point in the upper left corner of the ROC space (*Figure 43*), representing 100% Sensitivity (no False Negatives) and 100% Specificity (no False Positives). A random sampling would give a point along a diagonal line from the left bottom to the top right corner (*Figure 43*).

When computing the AUC, its value is usually expressed with decimal numbers (e.g. a value of 0.75 means that there is 75% probability that the model will be able to distinguish between cells positively and negatively associated with debris flows initiation areas).

For this study, the ROC curves method is used to estimate the classification model's performance in terms of success rate. No prediction rate has been taken in account also because multi-temporal data are not available. The procedure for the generation of a predictive rate is similar to that of the success rate, with the main difference that a more recent landslide inventory map is used to check if the landslides have indeed occurred in the areas indicated as highly susceptible. While the success rate measures a goodness of fit (since it indicates how well the mapped source areas fit in the susceptibility zones), the prediction rate provides the validation of the predictions. However, the success rate by itself is also a useful indicator for the quality of the produced susceptibility map. The drawback is that it doesn't show how good the resulting weight scores can explain the input landslide inventory that was used to calculate them (Chung & Fabbri, 1999; Van Westen et al., 2003).

The discretization scheme of the continuous variables (slope, elevation, flow accumulation, curvature, roughness) and the different combination (and omission) of the totality of the predictor variables (considering also *AR50* and *Løsmasser N50*) are reasons of different performances of the WofE model. The discretization is an important step to evaluate, since subjective choice of the number of classes entails a trade-off between retaining high information content and obtaining statistically significant results (Meyer et al., 2013). In this sense, different cases scenarios were tested and, thus, different AUC values were obtained and compared in order to evaluate the best combination of predictors.

5.2. Results

The sections comprised in this chapter illustrate the main findings issued from debris flow susceptibility modelling with the WofE method. Emphasis is given to the results linked to the model which fits better to the training data set used to generate it.

5.2.1. Weights of the predictor variables

The DEM and all the terrain data layers (rasters) were reclassified to 5 x 5 meters resolution in order to reduce the computation time.

As the categorical variables (*Løsmasser N50*, *AR50*) were already provided with standalone classes, only the continuous predictors needed a partitioning.

Two different manual classifications were performed:

1. The first consists of a dense and equally distributed subdivision of slope, flow accumulation, curvature and roughness between the rasters extreme values.
2. The second, based on the data distribution analysis illustrated in the chapter 4.2, consists of a manual greater refinement of statistically consistent intervals, while more extreme values were retained in wider classes.

As the largest errors are tied to classes covering only small portions of the study area and containing few debris flow cells, in both cases they were merged to the neighbouring classes to prevent erroneous weighting scores.

The results of the two classification scheme were compared on an equal footing on terms of predictors. By changing the amount of predictors used for modelling and by testing different combinations of predictors, the first classification scheme was never associated to models with relative larger fitting rates when compared to the models produced by the second partition scheme. However, just a slight improvement could be appreciated for the second classification scheme since the AUC values showed a modest enhancing of the fitting rate. The models based on the second discretization scheme, compared to the ones which were employed in the first discretization scheme, increased its performance by 1% at best. Starting from these considerations, from here on out, this thesis will refer only to the second classification scheme of the predictor variables, since it showed better reliability.

The continuous predictor of slope gradient is based on a classification of 12 classes; the bin width varies from 5° for middle values to 15° for extreme values. The same applies for DEM classification which consists of 58 variable classes, as more resolution was required for central intervals. Roughness and contributing area are divided based on a logarithm scale, which are respectively 15 and 19 classes of variable width. Total curvature is partitioned in

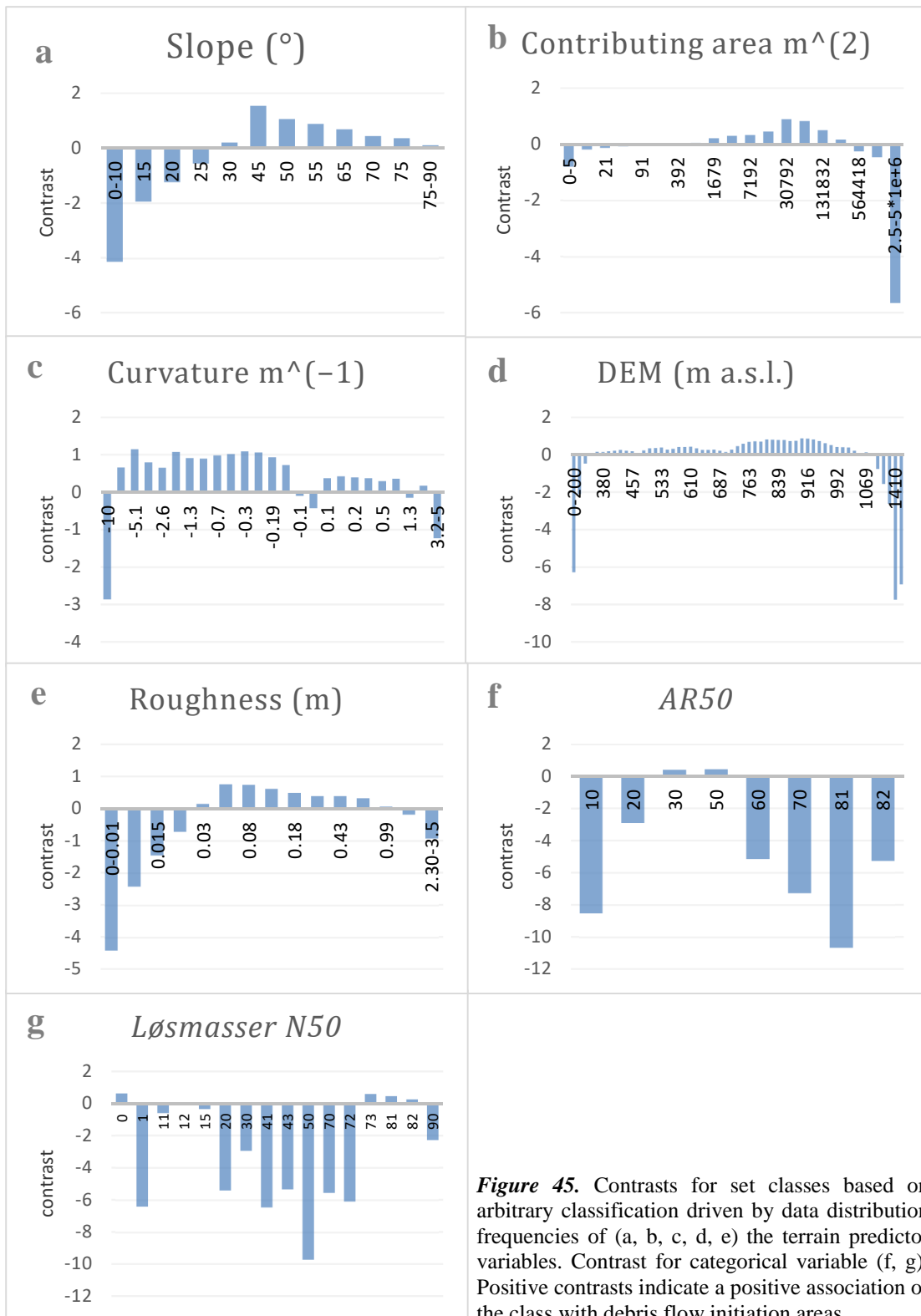


Figure 45. Contrasts for set classes based on arbitrary classification driven by data distribution frequencies of (a, b, c, d, e) the terrain predictor variables. Contrast for categorical variable (f, g). Positive contrasts indicate a positive association of the class with debris flow initiation areas.

26 classes where smaller and more numerous bins are set around 0 and negative values (surface upwardly concave).

The contrast values, computed using the WofE method, are represented in *Figure 45*. Positive association with source areas are found within the following intervals:

- Slope angles between 25° and 75°.

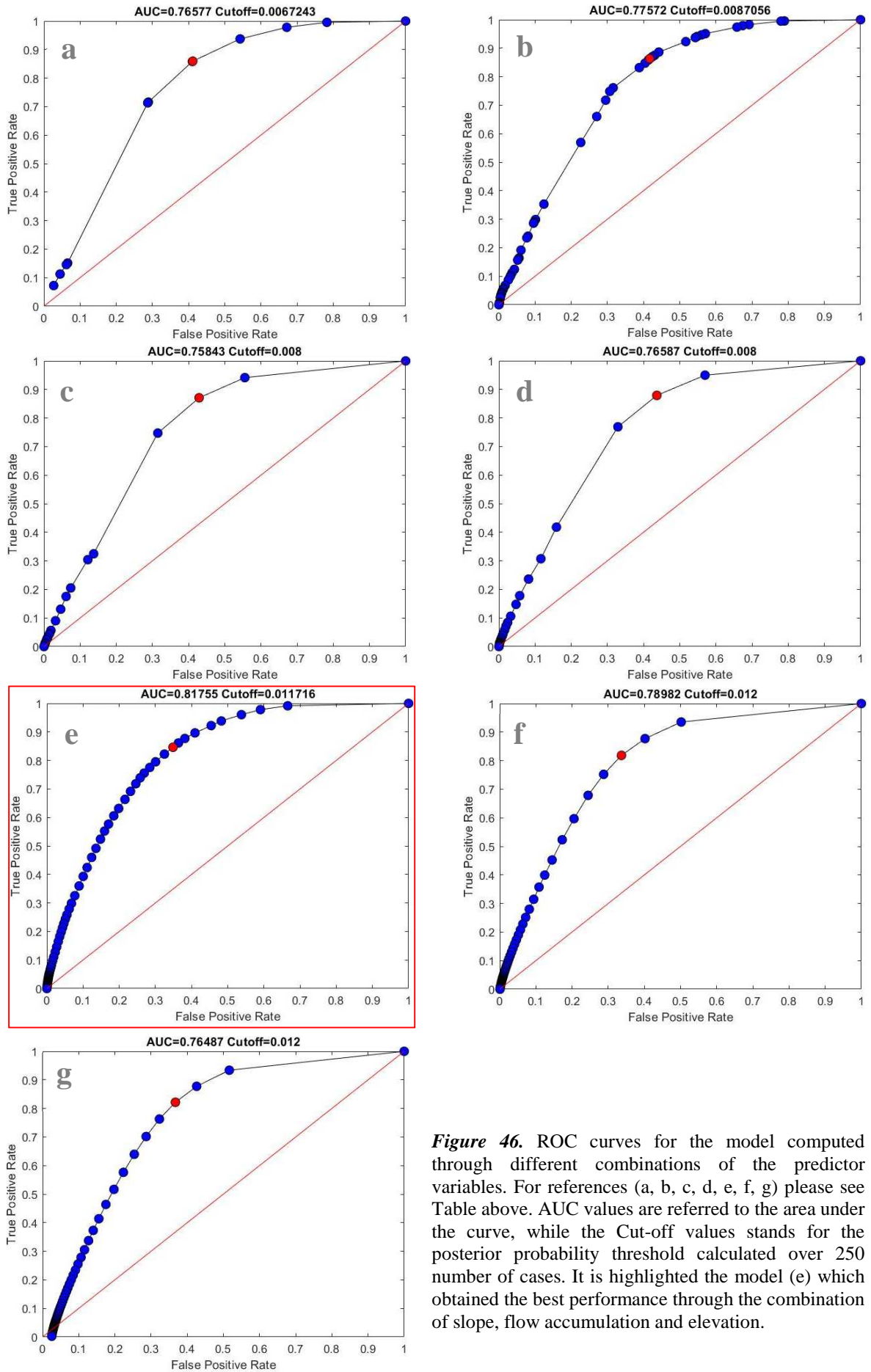
- Flow accumulations of 800 to 250 000 m² (0.008 km²- 0.25 km²).
- Curvature between -7 and -0.1 m⁻¹ and between 0.1 and 0.8 m⁻¹.
- DEM (elevation) between 370 and 1050 m a.s.l.
- Roughness of 0.03 to 0.10 m.
- AR50 classes of 30 and 50, which stand for forested areas and lower canopy covers.
- Løsmasser N50 classes of 0, 73, 81, 82, which stand respectively for bare mountain areas, weathering material (stone and block rich), landslide material (continuous cover with great power), landslide material (incoherent or thin cover over the bedrock).

For what concerns the highest positive contrast scores, the interval of slope comprised between 30° and 45° showed the best correlation with the targeted phenomenon (debris flow initiation), as well as contributing areas ranging from 0.015 to 0.065 km². There is only a slight distinction between all the negative values of curvature (ranging from -7.1 and -0.13), which roughly hold the same amount of (positive) contrast. In the study area, elevation values comprised between 775 m a.s.l. and 935 m a.s.l. and values of roughness comprised between 0.03 m and 0.08 m seem to have a better correlation with the debris flow initiation. Ultimately, the land use map and the map of the superficial deposits showed expected positive associations with areas marked as covered by low scrubs and low forest vegetation, weathered and loose material, landslide material. However, unexpected positive associations are related to forested areas and bare rock areas, which should theoretically fall outside of the landslide initiation domain. The reason of that may be ascribed to the representative scale of the used maps, which is large if compared to the spatial extent of the mapped release areas. In this way, the categorical thematic maps may be misleading and deceptive. The observed values of positive contrast, which is calculated as $C = W_{ij}^+ - W_{ij}^-$, are generally low as they do not overcome the threshold value of 2, while negative contrasts are larger.

5.2.2. Models performances for different combinations of predictors

Models performances								
	Slope	Flow accumul.	Curvature	DEM	Roughness	AR50	Løsmasser N50	Success rate
a	•							77%
b	•	•						78%
c	•		•					76%
d	•	•	•					77%
e	•	•		•				82%
f	•	•	•	•	•			79%
g	•	•	•	•	•	•	•	76%

Table 4. Model success rates resulting from different combinations of predictor variables.



Since the variation of the classification scheme doesn't yield any relevant consequence, the model performance is tested in response to different combination of the used predictors. The prior probability of debris flow initiation is 0.010 throughout the study area. All the pixels with a value of posterior probability (which is the LSI index) greater than the prior probability should be considered as susceptible to initiate an event.

The model performance is evaluated through the correspondent AUC values obtained by varying the decision threshold 250 times. Terrain data are first considered singly and then in association with the others. In *Table 3* the most important results are reported:

- The success rate for the only slope model is 77% with 45% of the entire area exceeding the LSI value of 0.010.
- The success rate of slope and flow accumulation is 78% with 48% of the entire area estimated as susceptible.
- The success rate of slope and total curvature is 76% with 45% of the totality estimated as susceptible.
- Slope, flow accumulation and curvature model show a success rate of 77% with 43% of the study area covered.
- Slope, flow accumulation and elevation model show a success rate of 82% with 39% of the study area estimated as susceptible.
- Slope, flow accumulation, curvature, roughness and elevation model (all the terrain predictor variables are considered) show a success rate of 79% with 39% of the study area estimated as susceptible.
- The model with the totality of the predictor considered (*AR50* and *Løsmasser N50* in addition to the terrain variables) show a success rate of 76% with the 48% of the entire study area estimated as susceptible.

The ROC curves and the corresponding AUC values underline the better overall performance of the WofE model using the combination of slope, flow accumulation and elevation (*Figure 46*) and a cut-off value of 0.012.

For this susceptibility map (*Figure 47*), with a resolution of 5 x 5 m, posterior probabilities values range from 0 to 0.325 and 5 susceptibility classes are defined according to standard deviation data classification technique as follows: *very low*, *low*, *medium*, *high*, *very high*, which cover 43%, 31%, 16%, 7%, 3% of the study area.

<i>Susceptibility class</i>	<i>% of area covered</i>	<i>% d. f. pixels</i> <i>% area covered</i>
Very low	43	0.1
Low	31	0.8
Medium	16	2.0
High	7	3.0
Very High	3	4.7

Table 5. Percentage of area covered by every susceptibility class and ratio of the percentage of debris flow source area pixels captured to the percentage of area covered.

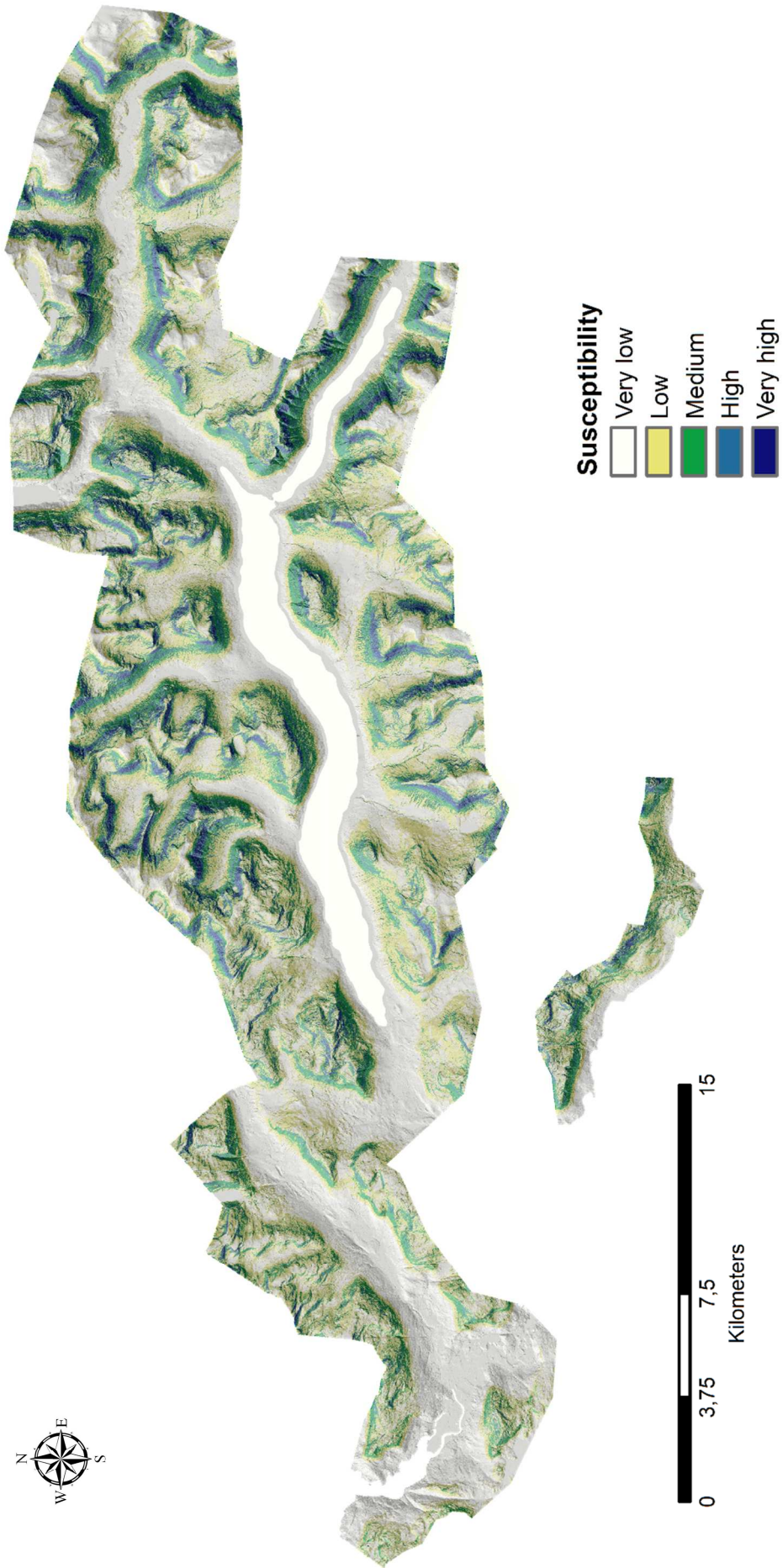


Figure 47. Susceptibility map derived from the model with the best success rate. Five different classes indicate *very low*, *low*, *medium*, *high*, *very high* susceptibility.

The ratio of the percentage of source areas cells seized by every class to the percentage of the area covered by the same class is a good indicator of debris flow initiation susceptibility: the ratio is remarkably larger for the zone classified as very high susceptible (*Table 5*).

5.2.3. Discussion

This study dealt with the development of a debris flow susceptibility map for initiation areas. The study area is restricted to the main part of the territories of *Førde* and *Jølster* Municipalities. This could be accomplished by using the WofE method and a new debris flow inventory specially made for the above-mentioned goal. The latter object served for a further aim, which is the analysis of the terrain data distribution within debris flow source areas in order to better investigate the different debris flow-types encountered during the field survey.

The higher success rate (82%) in susceptibility modelling was here achieved through an arbitrary classification driven by the previous assessment of data distribution frequencies and through the combination of slope, flow accumulation and DEM as the only predictor variables (*Figure 46*). Based on the result of this study, terrain data predictors such as curvature and roughness are related to slightly lower success rates models (79%), while the worst performance (76%) is tied to the joint use of both the totality of terrain and categorical (*AR50* and *Løsmasser N50*) data layers (*Figure 46*).

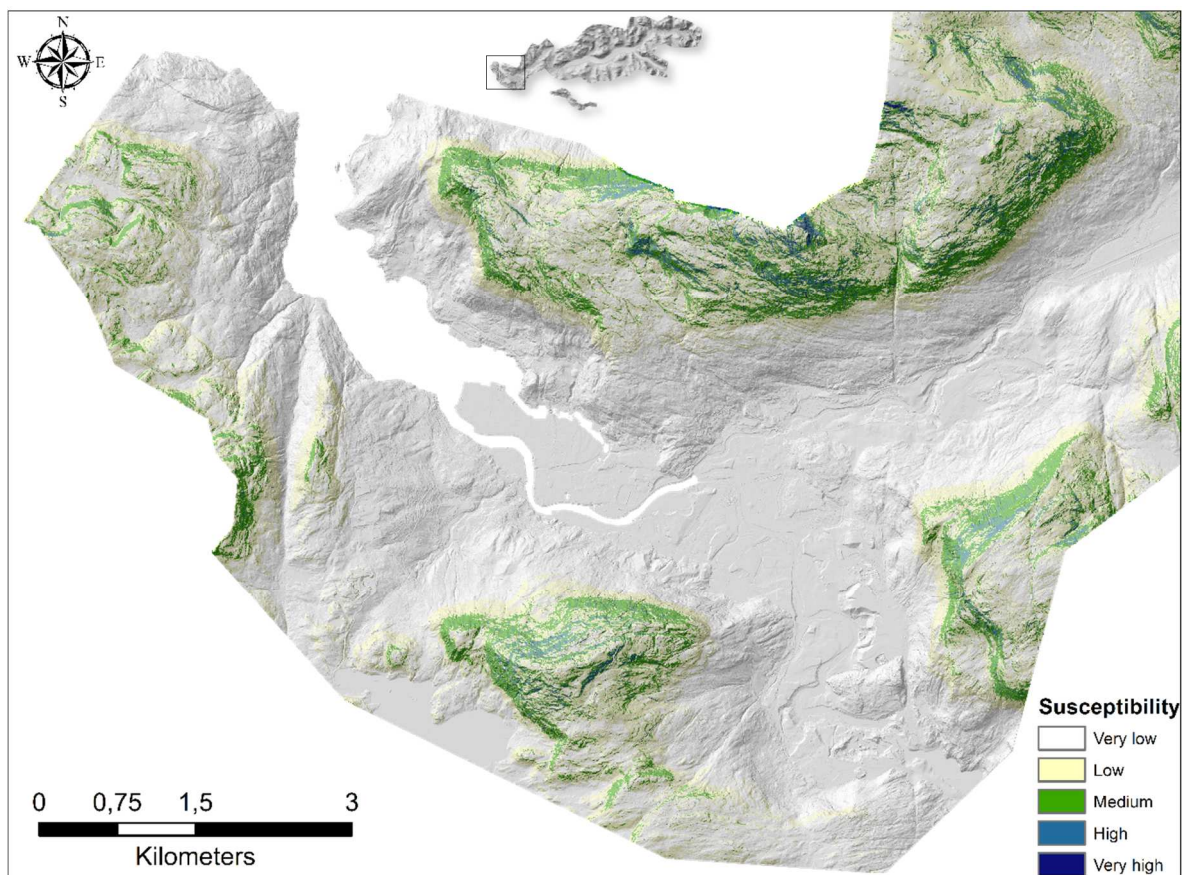


Figure 48. Magnification of the susceptibility map within Førde municipality (part one).

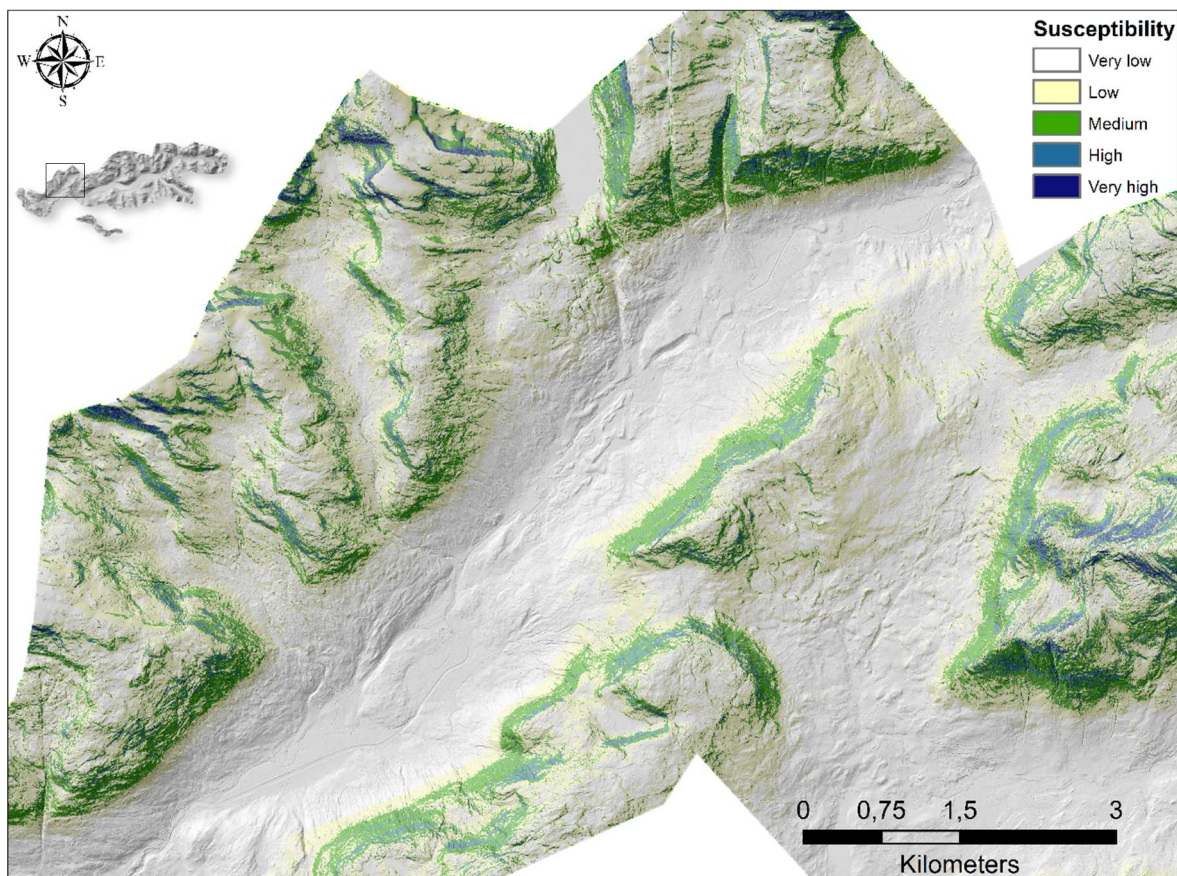


Figure 49. Magnification of the susceptibility map within Førde municipality (part two).

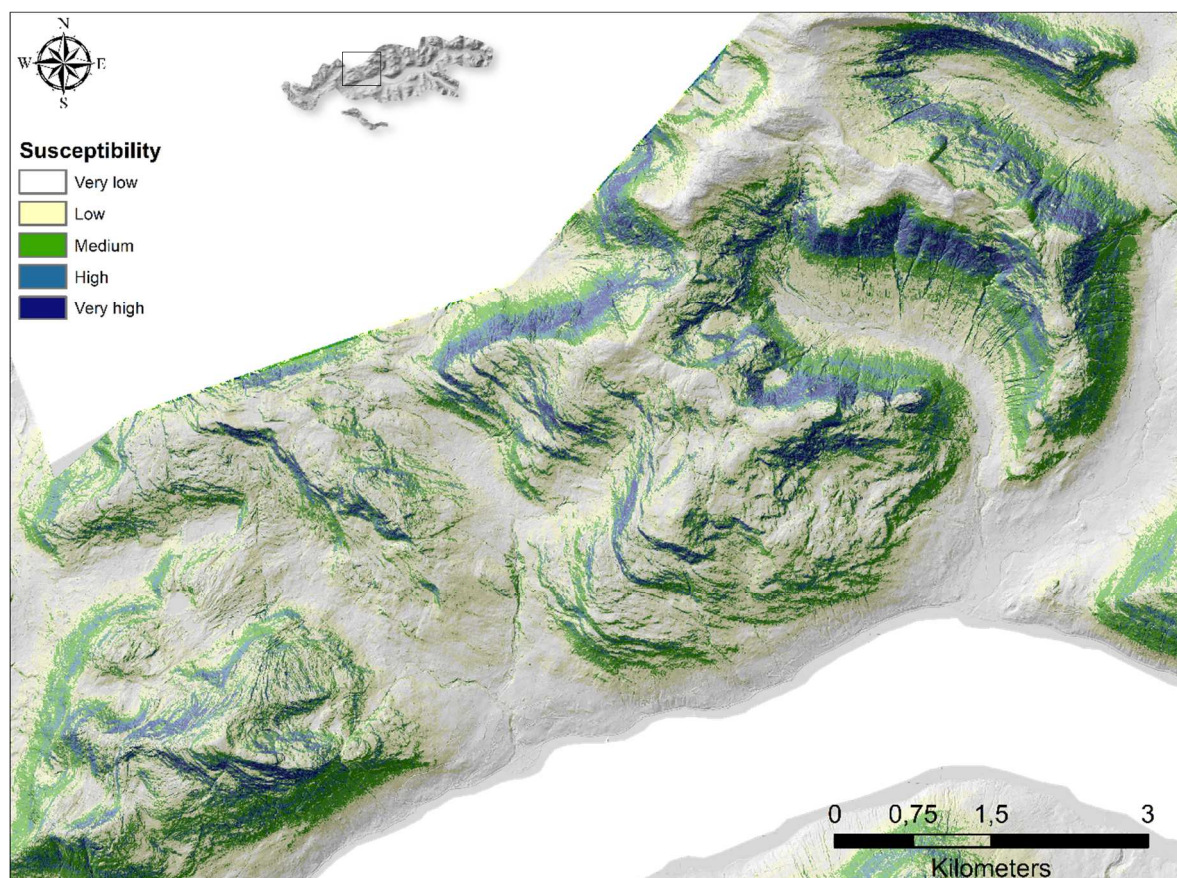


Figure 50. Magnification of the susceptibility map within Jølster municipality (part one).

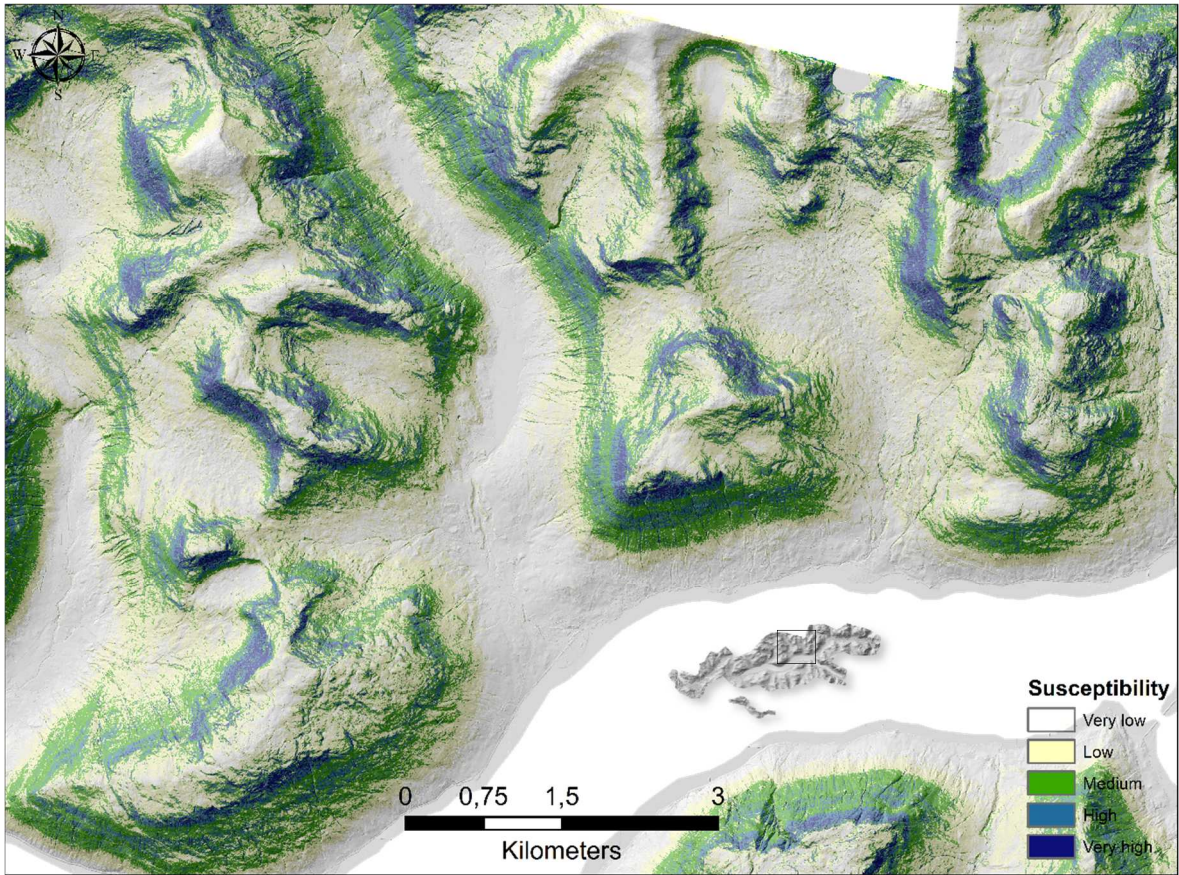


Figure 51. Magnification of the susceptibility map within Jølster municipality (part two).

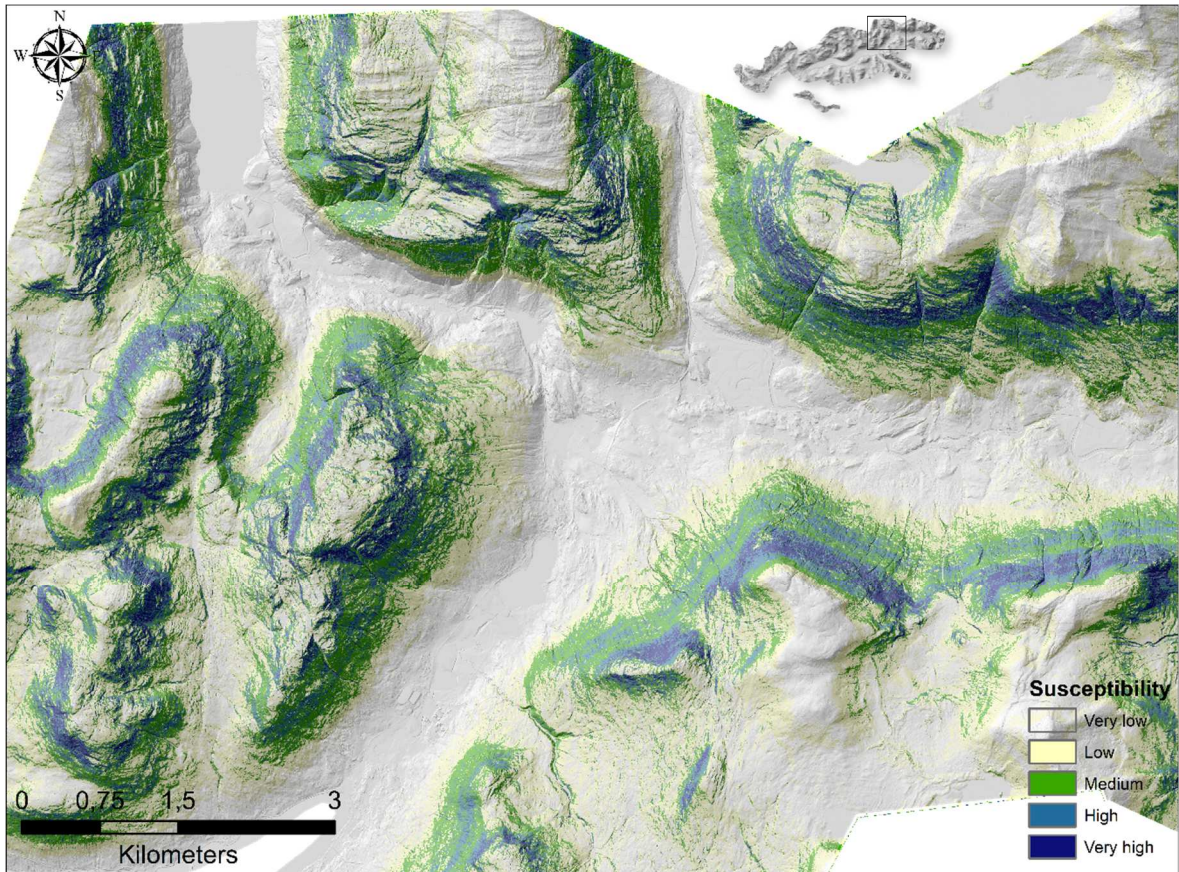


Figure 52. Magnification of the susceptibility map within Jølster municipality (part three).

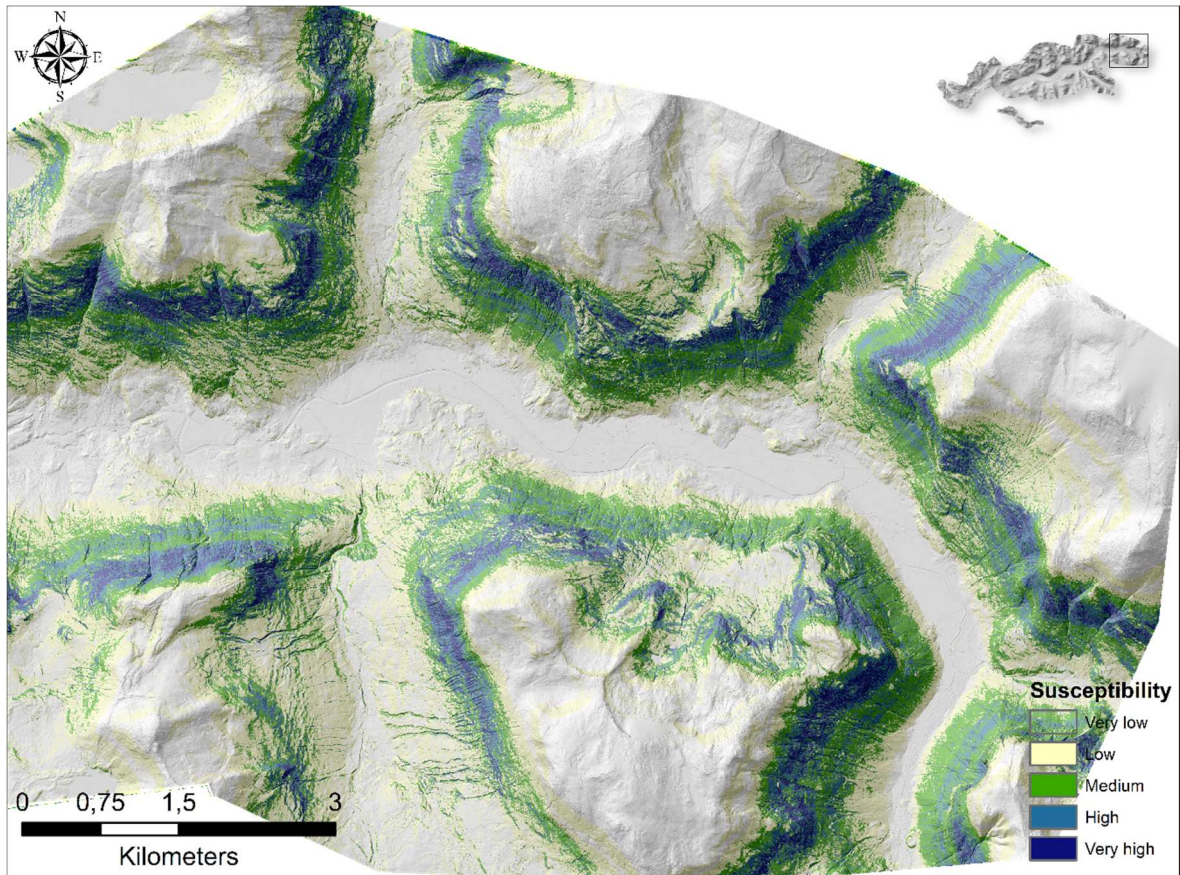


Figure 53. Magnification of the susceptibility map within Jølster municipality (part four).

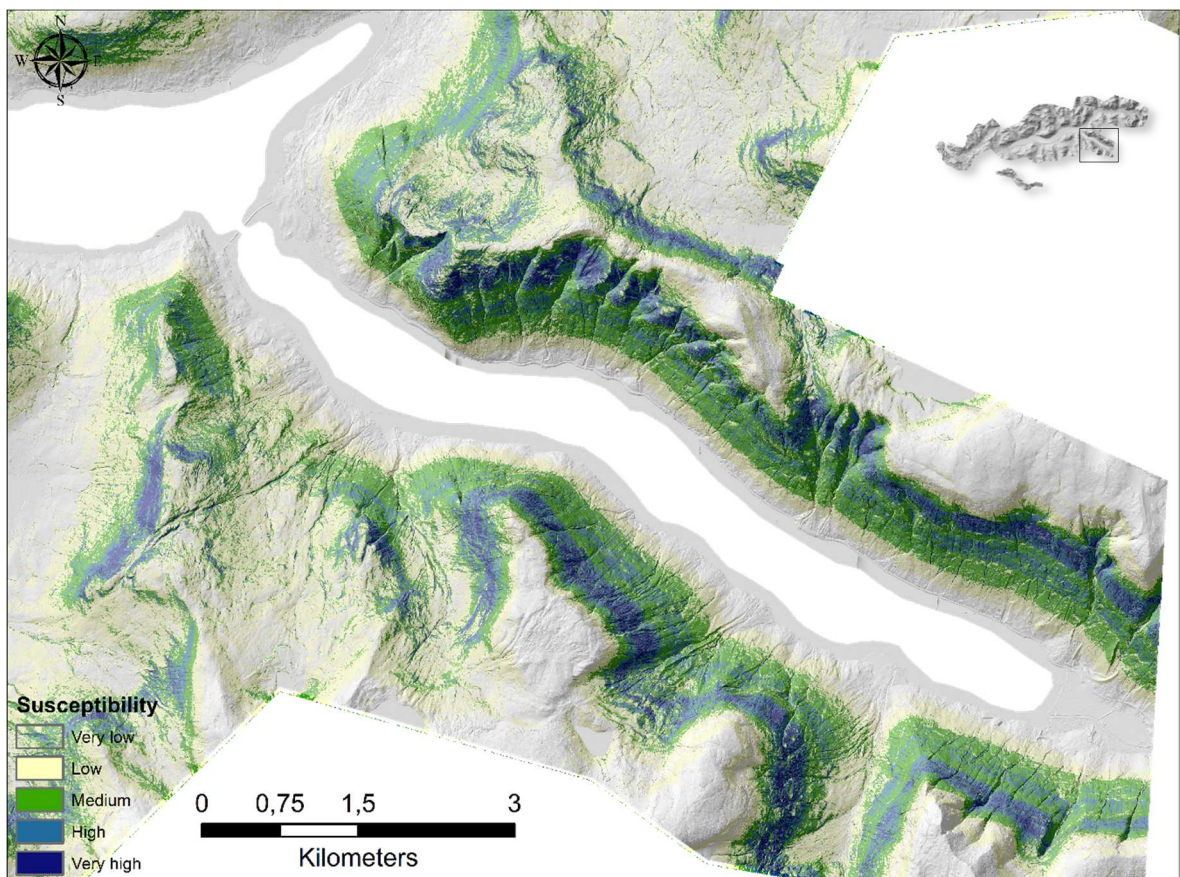


Figure 54. Magnification of the susceptibility map within Jølster municipality (part five).

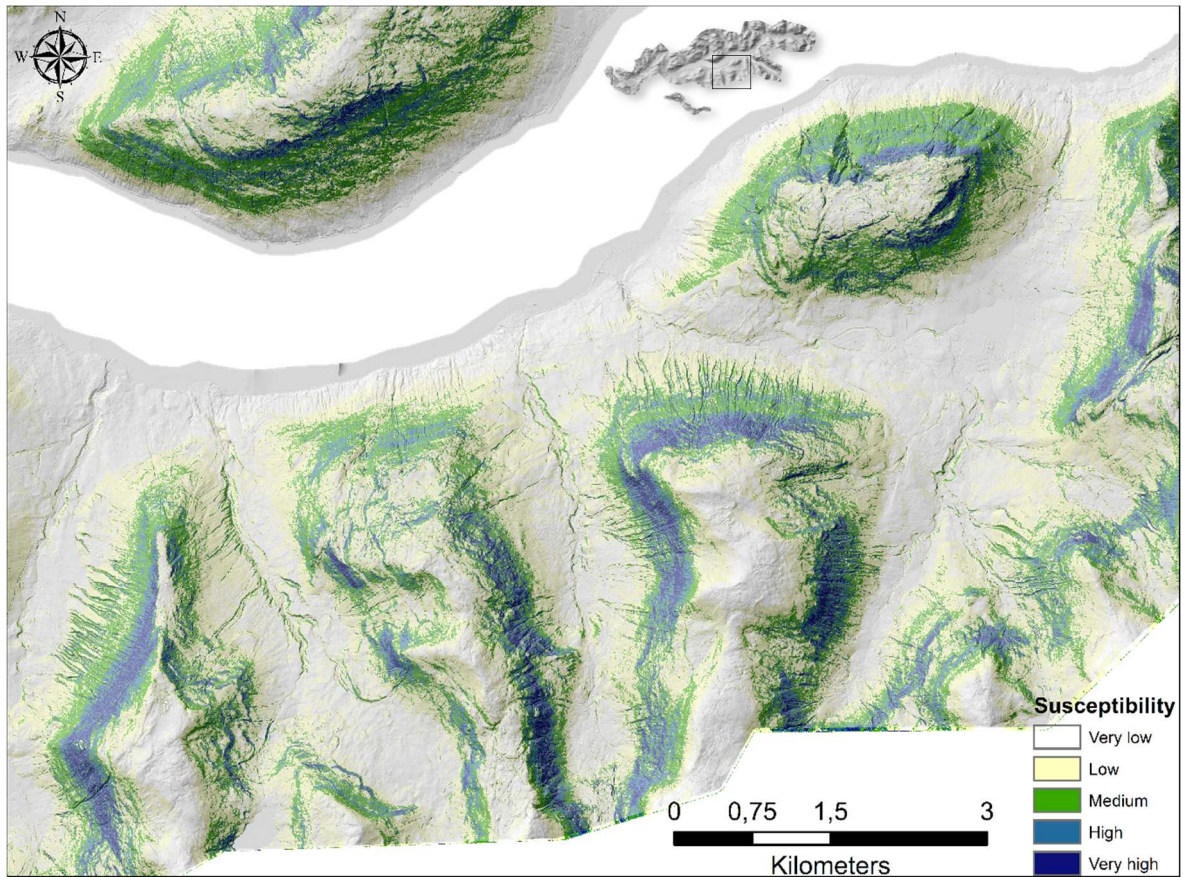


Figure 55. Magnification of the susceptibility map within Jølster municipality (part six).

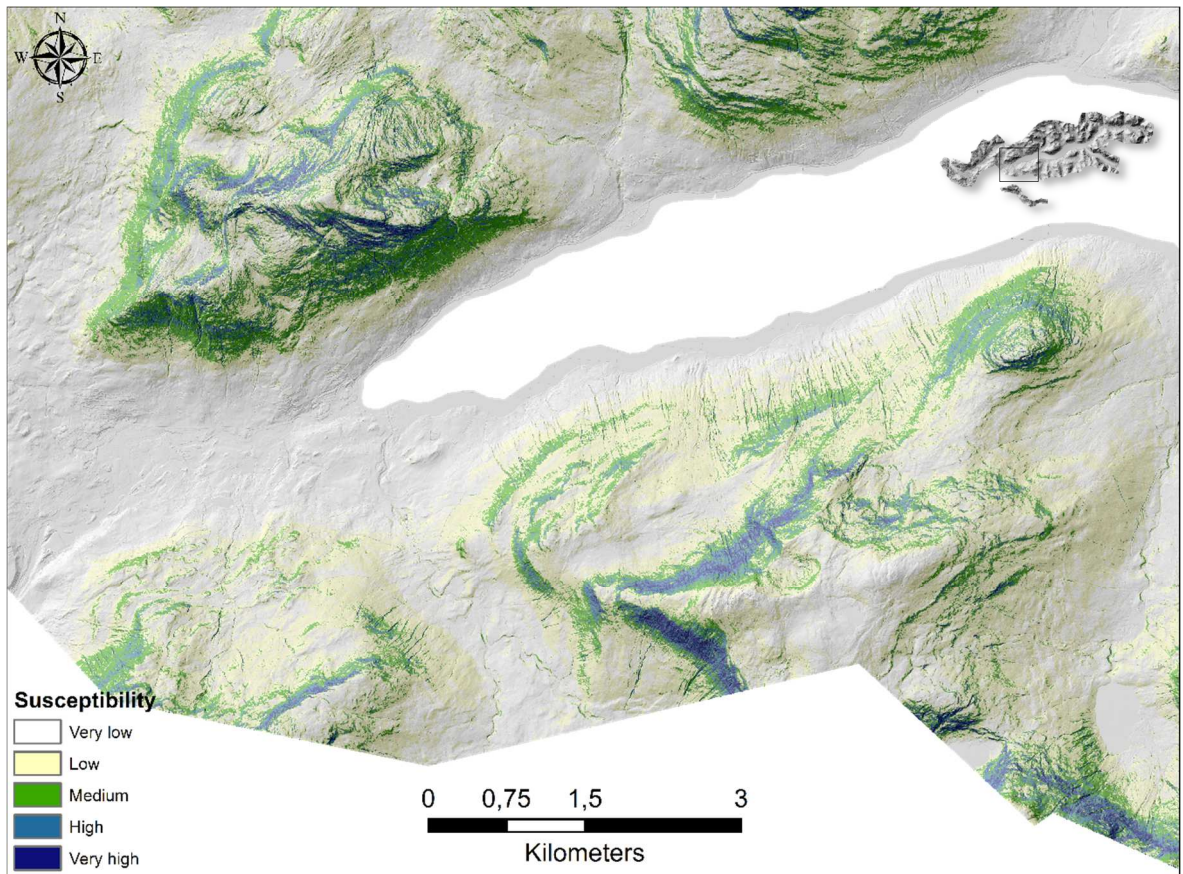


Figure 56. Magnification of the susceptibility map within Jølster municipality (part seven).

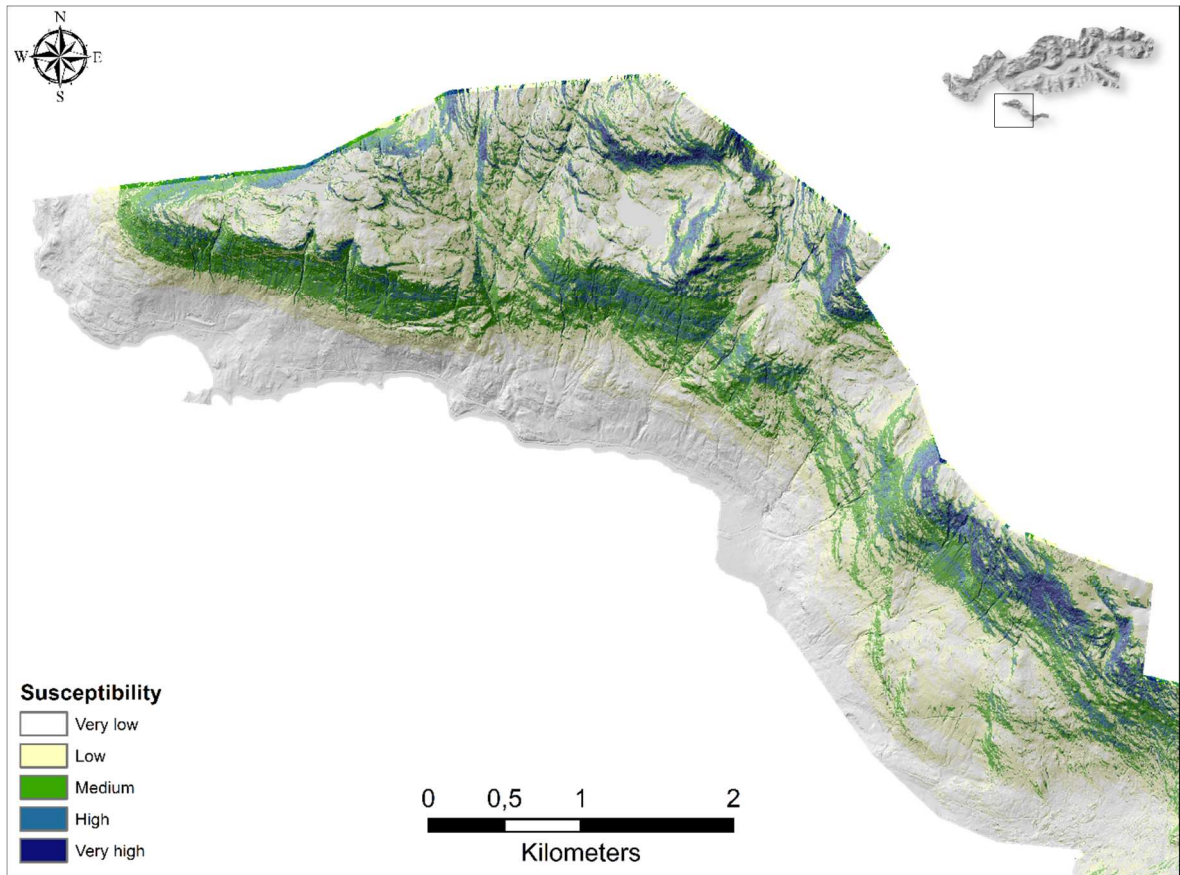


Figure 57. Magnification of the susceptibility map within Førde municipality (part four).

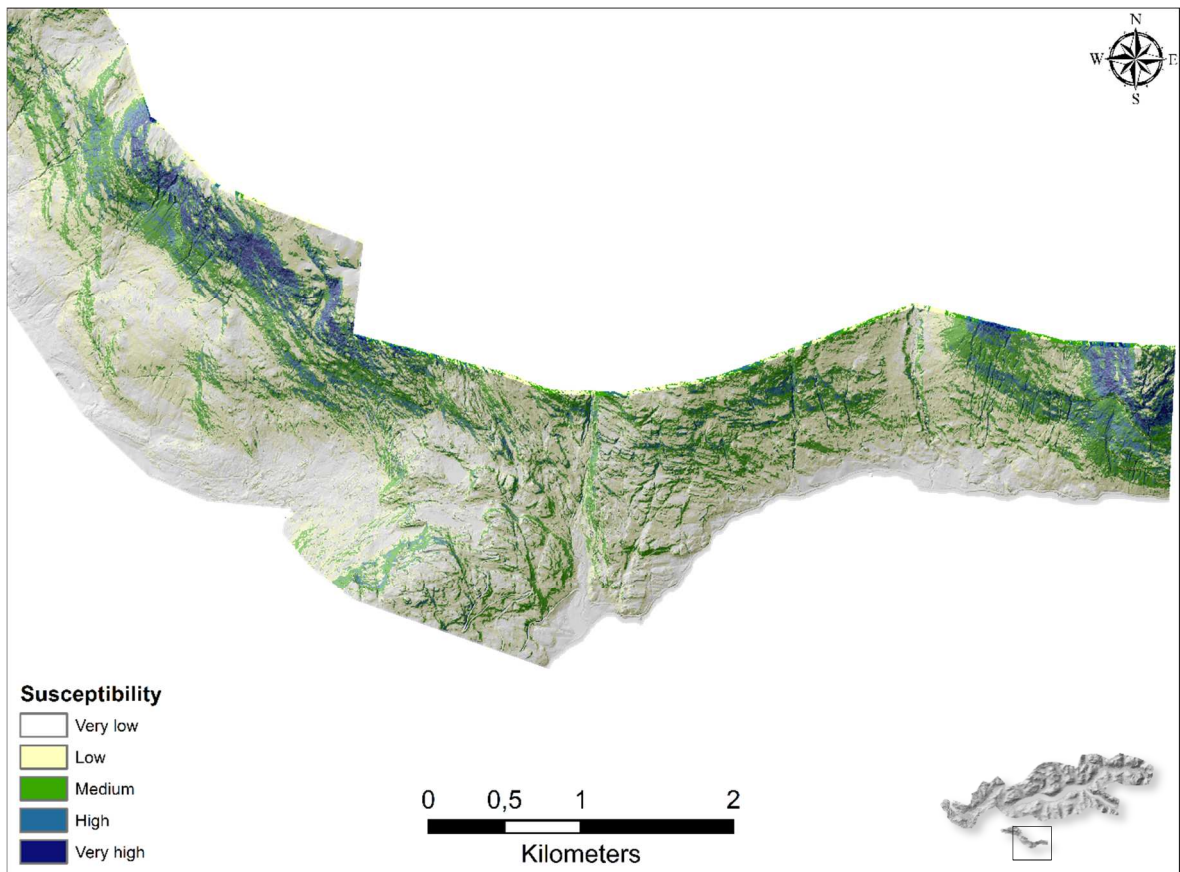


Figure 58. Magnification of the susceptibility map within Førde municipality (part five).

This may suggest the impracticability of the two thematic layers in locating the areas susceptible to initiate debris flow, as it may be indicated by the low positive contrast values distributed among only few classes (*Figure 46*). Here, the proper use and combination of pertinent predictor variables seems to influence AUC values much more than the choice of the discretization scheme; however, further tests are required.

When considering the susceptibility map with the best fit (*Figure 47*), estimated very high and high susceptible areas seems to be more concentrated where the landscape shows a steeper slope gradient and where the average elevation is higher (which corresponds to the eastern part of the study area). More details can be observed in *Figure 59*. Generally, the upper parts of the slope, coinciding with those catchments insisting on well-defined channels, are marked as highly susceptible zones. The same applies for the same channels, which seem to be favourable zones for debris flow initiation regardless for the relatively lower values of slope gradient and elevation: this may be ascribable to the “weight” of the flow accumulation predictor.

Some pitfalls, which were not considered in this study, could be linked to the presented

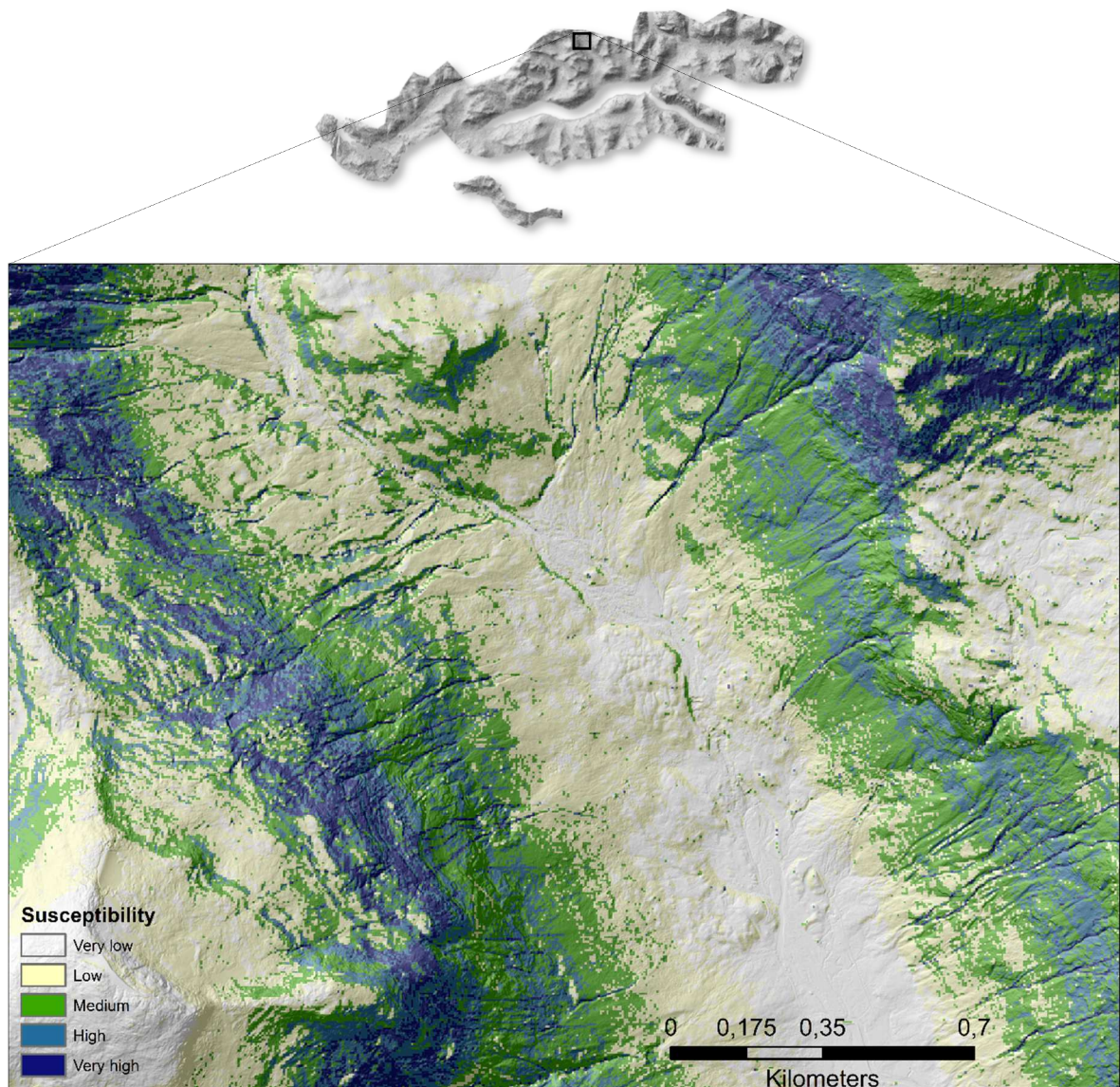


Figure 59. Magnification of the susceptibility map within Jølster municipality. The larger channels and their relative upper part of the basin retain high concentrations of very high and high susceptible cells.

susceptibility model:

- Conditional independence of variables classes.
- Uncertainties related to the weighting score of the different classes.
- Biased estimation and evaluation of the spatial extent of the mapped source areas thus determining errors tied to susceptibility modelling.
- Absence of a multi-temporal test dataset, and thus the neglected estimation of a real predictive rate capable of revealing the model performance in prediction of future landslides.
- A model with a large AUC has a better statistical performance than a different model with a lower AUC. However, the second model may be more meaningful from a geomorphological perspective than the first model (Reichenbach et al., 2018).

One further outstanding question may concern how the model performances would be influenced by considering only a subset of the inventory based on the debris flow types (categories). In this sense, the percentage of the study area calculated as susceptible to debris flow initiation (posterior probability exceeding the prior probability) might be decreased.

For a better spatial comprehension of the calculated proneness to initiate debris flow and debris slides within the study area, please refer to *Figures 48, 49, 50, 51, 52, 53, 54, 55, 56, 57, 58, 59*.

Although the success rate of the presented susceptibility model (*Figure 46*) is good compared to those reported from literature, it remains a general indicator of slope areas which may be prone to future failure, without any possible prediction in terms of time and damage extent. The validation of landslide susceptibility mapping and its usefulness depends on the maintenance of appropriate records indicating the frequency and magnitude of on-going landslide activity and its relationship with terrain and triggering conditions (Dai et al., 2002).

References

- Berthling I., Etzelmüller B., 2011. The concept of cryo-conditioning in landscape evolution. *Quaternary Research* 75 (2), 378-384.
- Bjordal H., Helle T.E., 2011. Skred og flom på veg. SVV report, 5 (in Norwegian).
- Bonham-Carter G.F., 1994. *Geographic Information Systems for Geoscientists, Modelling with GIS*. Pergamon.
- Carrara A., Cardinali M., Guzzetti F., Reichenbach P., 1995. GIS Technology in Mapping Landslide Hazard. In: Carrara A., Guzzetti F. (Eds), *Geographical Information Systems in Assessing Natural Hazards*. Kluwer Acad. Publ., the Netherlands, 135-176.
- Cavalli M., Crema S., Trevisani S., Marchi L., 2017. GIS tools for preliminary debris-flow assessment at regional scale. *Journal of Mountain Science* 14 (12).
- Cepeda J. M., 2009. *Characterisation and Risk Management of Rainfall-Induced Landslides: a thesis presented for the degree of Philosophiae Doctor (Ph.D.) at the University of Oslo*, Oslo: Universitetet i Oslo.
- Chung F.C., Fabbri A., 1993. The representation of geoscience information for data integration. *Nonrenewable Resources* (2), 122-139.
- Chung C. F., Fabbri A., 1999. Probabilistic prediction models for landslide hazard mapping, *Photogrammetric Engineering & Remote Sensing* 65 (12), 1389-1399.
- Chung C. F., Fabbri A., 2003. Validation of Spatial Prediction Models for Landslide Hazard Mapping. *Natural Hazards* (30), 451-472.
- Costa J.E., 1984. *Physical Geomorphology of Debris Flows. Developments and applications of geomorphology* (10).
- Crosta G., Hermanns R., Frattini P. Valbuzzi E., Valagussa A., 2014. Large Slope Instabilities in Northern Chile: Inventory, Characterization and Possible Triggers. In: Sassa K., Canuti P., Yin Y. (Eds), *Landslide Science for a Safer Geoenvironment: Volume 3: Targeted Landslides*. Springer International Publishing, 175-181.
- Cruden D.M., 1991. A simple definition of a landslide. *Bulletin of the International Association of Engineering Geology* (43), 27-29.
- Cruden D.M., Varnes D.J. (1996). *Landslides Types and Processes*. In: Turner A.K., Schuster R.L. (Eds), *Landslides: Investigation and Mitigation*. Transportation Research Board Special Report 247. National Academy Press, WA, 36-75.
- Dai F.C, Lee C.F, Ngai Y.Y., 2002. Landslide risk assessment and management: An overview. *Engineering Geology* (64), 65-87.

- Fischer L., Rubensdotter L., Sletten K., Stalsberg K., Melchiorre C., Horton P., Jaboyedoff M., 2012. Debris flow modeling for susceptibility mapping at regional to national scale in Norway.
- Guinau M., Vilajosana I., Vilaplana J. M., 2007. GIS-based debris flow source and runout susceptibility assessment from DEM data – a case study in NW Nicaragua. *Nat. Hazards Earth Syst. Sci.*, 7, 703-716.
- Guzzetti F., Reichenbach P., Ardizzone F., Cardinali M., Galli M., 2006b. Estimating the quality of landslide susceptibility models. *Geomorphology* (81), 166-184.
- Guzzetti F., Mondini A.C., Cardinali M., Fiorucci F., Santangelo M., Chang K.T., 2012. Landslide inventory maps: new tools for an old problem. *Earth-Sci. Rev.* 112 (1), 42-66.
- Hanssen-Bauer I., Drange H., Førland E.J., Roald L.A., 2009. Klima i Norge 2100. Bakgrunnsmateriale til NOU klimatilpasning. Norsk Klimasenter, Oslo (in Norwegian).
- Hanssen-Bauer I., Førland E., Haddeland I., Hisdal H., Lawrence D., Mayer S., Nesje A., Nilsen J. E., Sandven S., Sandø A., Sorteberg A., Ådlandsvik B., 2017. Climate in Norway 2100.
- Highland L., Bobrowsky P., 2008. The Landslide Handbook – A Guide to Understanding Landslides. U.S. Geological Survey Circular 1325.
- Hungr O., Leroueil S., Picarelli L., 2013. The Varnes classification of landslide types, an update. *Landslides* 11 (2), 167-194.
- Hungr O., Evans S.G., Bovis M.J., Hutchinson J.N., 2001. A review of the classification of landslides of the flow type. *Environmental and Engineering Geoscience*, 7 (3), 221-238.
- Hürlimann M., Copons Llorens R., Altimir J., 2006. Detailed debris flow hazard assessment in Andorra: A multidisciplinary approach. *Geomorphology* (78), 359-372.
- Hutchinson J.N., 1988. Morphological and geotechnical parameters of landslides in relation to geology and hydrogeology. In: *Proceedings of the 5th International Symposium on Landslides*. Lausanne, Switzerland, 3-35.
- IPCC, 2012. Managing the risks of extreme events and disasters to advance climate change adaptation (SREX). Summary for Policymakers. Special report of the First Joint Session of Working Groups I and II.
- Iverson R.M., 1997. The physics of debris flows. *Reviews of Geophysics* 35 (3), 245-296.
- Jakob M., Hungr O., 2005. Debris-flow Hazards and Related Phenomena.
- Jaedicke C., Lied K., Kronholm K., 2009. Integrated database for rapid mass movements in Norway. *Natural Hazards & Earth System Sciences*, 9(2), 469-479.

Kalsnes B., Nadim F., Hermanns R., Hygen H., Petkovic G., Dolva B., Berg H., Høgvold D., 2016. Landslide risk management in Norway. In: Ho K.K.S., Lacasse S., Picarelli L. (Eds), Slope Safety Preparedness for Impact of Climate Change, CRC Press, 215-252.

Leonard S.C., Mihalasky J.M., Peters S., 2002. CHAPTER 6 Weights-of-Evidence Modeling of Sedimentary Rock-Hosted Au Deposits, P.R. China. In: Peters S.G. (Ed), Geology, Geochemistry and Geophysics of Sedimentary Rock-Hosted Au Deposits in P.R. China. USGS Open-File Report: 02-131.

Lidmar-Bergström K., Ollier C.D., Sulebak J.R., 2000. Landforms and uplift history of southern Norway. *Global and Planetary Change* 24(3), 211-231.

Lorenzini G., Mazza N., 2004. Debris flow: Phenomenology and Rheological Modelling. WIT Press, Southampton, Boston.

Meyer N.K., Dyrddal A.V., Frauenfelder R., Etzelmüller B., Nadim F., 2012. Hydrometeorological threshold conditions for debris flow initiation in Norway. *Nat. Hazards Earth Syst. Sci.*, 12, 3059-3073.

Meyer N.K., Schwanghart W., Korup O., Romstad B., Etzelmüller B., 2013. Estimating the topographic predictability of debris flows. *Geomorphology* (207), 114-125.

McCall G.J.H., Laming D.J.C., 1990. Geohazards: natural and man-made. *Journal of the Geological Society* 147 (5), 879-881.

Nadim F., Schack Pedersen S.A., Schmidt-Thomé P., Sigmundsson F., Engdahl F., 2009. Natural hazards in Nordic countries. *Episodes* 31 (1), 176-184.

Norem H., Sandersen F., 2012. Flom- og sørpeskred. Project report "Klima og Transport". SVV report 73.

Olsen, L. (2002). Mid and Late Weichselian ice sheet fluctuations northwest of the Svartisen glacier, Nordland, northern Norway. *Geological Survey of Norway Bulletin* (440), 39-52.

Paudel U., Oguchi T., Hayakawa Y.S., 2016. Multi-Resolution Landslide Susceptibility Analysis Using a DEM and Random Forest. *International Journal of Geosciences* (07), 726-743.

Reichenbach P., Rossi M., Malamud D. B., Mihir M., Guzzetti F., 2018. A review of statistically-based landslide susceptibility models. *Earth-Science Reviews* (180).

Sigmond E.M.O., 2002. Geological Map, Land and Sea Areas of Northern Europe, Scale 1:4 million. Geological Survey of Norway, Trondheim.

Stancanelli M.L., Peres D.J., Cancelliere A., Foti E., 2017. A combined triggering-propagation modeling approach for the assessment of rainfall induced debris flow susceptibility. *Journal of hydrology* (550), 130-143.

Strom K. M., 1948. The Geomorphology of Norway. *The Geographical Journal* (112), 19-23.

Van Westen C. J., Rengers N., Soeters R., 2003. Use of geomorphological information in indirect landslide susceptibility assessment. *Natural hazards* 30(3), 399-419.

Van Westen C.J., Van Asch T.W.J., Soeters R., 2005. Landslide hazard and risk zonation; why is it still so difficult? *Bulletin of Engineering geology and the Environment* 65 (2), 167-184.

Van Westen C.J., Castellanos E., Kuriakose S.L., 2008. Spatial data for landslide susceptibility, hazard, and vulnerability assessment: An overview. *Engineering Geology*, (102), 112-131.

Varnes D.J., 1978. Slope movements: types and processes. In: Schuster R.L., Krizek R.J. (Eds), *Landslide Analysis and Control*. National Academy of Sciences, Special Report 176 Transportation Research Board, Washington D.C., 11-33.

Varnes D.J., 1984. *Landslide Hazard Zonation: a Review of Principles and Practice*. UNESCO, 1-63.

Yalcin A., Reis S., Aydinoglu A.C., Yomralioglu T., 2011. A GIS-based comparative study of frequency ratio, analytical hierarchy process, bivariate statistics and logistics regression methods for landslide susceptibility mapping in Trabzon, NE Turkey. *Catena* (85), 274-287.